

Diss. ETH No. 19373

**Refinement and Standardization of Small Animal PET Scanning
Experimentation and Data Analysis**

A dissertation submitted to

ETH ZURICH

for the degree of

DOCTOR OF SCIENCES

presented by

MARIANNE ISABELLE KEHL

Dipl. Naturwissenschaftlerin, ETH Zurich

born April 5th, 1982

citizen of Rebstein SG, Switzerland

accepted on the recommendation of

Prof. Dr. P.A. Schubiger, examiner

Prof. Dr. S.M. Ametamey, co-examiner

Dr. M. Honer, co-examiner

2010

Acknowledgements

First of all, I would like to thank Prof. Dr. Pius August Schubiger for giving me the opportunity to perform my Ph.D. thesis in his research group. Further thank goes to Prof. Dr. Simon Mensah Ametamey for accepting to be a co-referent of this thesis.

Special thank goes to Dr. Michael Honer, my direct thesis supervisor, for his excellent support and advice during my experimental and evaluative work, as well as to Claudia Keller for her patience and support with her profound know-how of *in vivo* PET studies and animal handling.

Furthermore, I'm very grateful for the *in vivo* and *ex vivo* experimentation support by Sabine Baumann, namely in the field of dissection, tissue slicing, autoradiography and histochemical staining of tissue, and for fruitful discussions with Dr. Volkmar Uhlendorf about basic principles of PET and PET physics. Additional thank goes to Malte Alf for his help with Matlab evaluation of performance evaluation data.

My sincere thank is also going to Prof. Dr. Tobias Ross for his patience and support in teaching me [¹⁸F]-labelling of [¹⁸F]fallypride as well as his friendship and all the assistance at BBQs ☺.

Moreover, I would like to thank PD Dr. Stefanie Krämer, Dr. Alexander Hohn and Dr. Viviane Mumprecht for fruitful discussions about compound degradation, performance evaluation and microradiography; as well as to Dr. Markus Kalisch from the “Statistischer Beratungsdienst” of ETH and Markus Küpfer from the “Zentralwerkstatt HCI” of ETH.

Many thanks go to all the people from the Schubiger group for their help and the nice atmosphere in the lab and for their friendship; particularly I would like to thank Phoebe Lam, Miray Demirer, Mathias Nobst, Cindy Fischer, Dr. Svetlana Selivanova, Dr. Linjing Mu, Monica Langfritz and Dr. Jessica Becaud.

Finally, I would like to thank all my friends for their support and encouragement. Many thanks go to Reto Baumann for his strong encouragement especially during the starting phase of this thesis, to Roman Haefeli for entertainment and distraction ☺, to Nathan Schmid and Stefan Christen for many lively discussions ☺ ☺, as well as to Andrea Huber and Irene Romer for their friendship in any situation.

My very special thank goes to my parents, my brother and sister for their support and to (Dr.) Miljen Martić for encouraging and bearing me at all times ☺.

Table of Content

List of Abbreviations	6
Summary.....	10
Zusammenfassung.....	14
1. Introduction.....	18
1.1. Positron Emission Tomography.....	18
1.2. Radiopharmaceuticals	19
1.2.1. [¹⁸ F]FDG	19
1.2.2. [¹⁸ F]Fallypride.....	20
1.3. Detection of Gamma Rays	20
1.3.1. Gas-filled Detectors	21
1.3.2. Scintillation Detector	21
1.3.3. Autoradiography using Phosphor Imager Plates.....	22
1.3.4. Small Animal PET	22
1.4. Animal Models in Translational Research.....	25
1.5. Refinement and Standardization of Small Animal PET Experimentation.....	26
1.6. Aims of the Thesis	28
1.7. References.....	29
2. Performance Evaluation of the Dedicated Small Animal PET/CT Tomograph eXplore Vista According to the NEMA NU4-2008 Standards	37
2.1. Introduction.....	37
2.2. Material and Methods	37
2.2.1. Spatial Resolution	38
2.2.2. Axial Sensitivity Profile and Absolute Central Point Source Sensitivity (ACS).....	38
2.2.3. Scatter Fraction and Count Rate Performance.....	39
2.2.4. Image Quality.....	40
2.2.6. Activity Outside of the Field of View.....	41
2.3. Results.....	42
2.3.1. Spatial Resolution	42

2.3.2. Sensitivity	44
2.3.3. Scatter fraction and Count Rate Performance.....	45
2.3.4. Image Quality.....	47
2.3.5. Activity Outside of the Field of View.....	50
2.4. Discussion.....	52
2.5. Conclusion	56
2.6. References.....	57
3. Comparison of Standardization and Heterogenization Approaches Towards	
Reproducible Small Animal PET Data.....	60
3.1. Introduction.....	60
3.2. Materials and Methods.....	61
3.2.1. Animal Preparation	61
3.2.2. Radiotracer Application.....	62
3.2.3. Small Animal PET Imaging.....	63
3.2.4. Quantification of <i>ex vivo</i> Tissue Uptake.....	64
3.2.5. Measurement of Physiological Parameters.....	64
3.2.6. Assessment of Test-Retest Variability of [¹⁸ F]FDG Whole Brain and [¹⁸ F]Fallypride Striatum Uptake	64
3.2.7. Influence of Experimental Parameters on [¹⁸ F]FDG and [¹⁸ F]Fallypride Biodistri- bution	65
3.2.8. Analysis of Standardization vs. Pseudo-Heterogenization	65
3.2.9. Statistical Analysis.....	67
3.3. Results.....	67
3.3.1. Test-Retest Variability of [¹⁸ F]FDG Brain Uptake and Striatal Uptake of [¹⁸ F]Fallypride.....	67
3.3.2. Impact of Experimental Parameters on [¹⁸ F]FDG and [¹⁸ F]Fallypride Tissue Distribution	70
3.3.3. Standardization vs. “Pseudo-Heterogenization”	73
3.4. Discussion.....	75
3.5. Conclusion	77
3.6. References.....	78

4. Characterization of Retro-ocular PET Tracer Accumulation in Rodents	82
4.1. Introduction.....	82
4.2. Material and Methods	84
4.2.1. Animal Preparation	84
4.2.2. Radiotracers	84
4.2.3. Radiotracer Injection.....	84
4.2.4. Measurement of physiological parameters	85
4.2.5. PET imaging / <i>ex vivo</i> biodistribution	85
4.2.6. <i>In vitro</i> Autoradiography using [¹⁸ F]Fallypride.....	87
4.2.7. Histology.....	87
4.2.8. Statistical Analysis.....	88
4.3. Results.....	88
4.3.1. Identification of the Responsible Tissue for Retro-ocular [¹⁸ F]FDG and [¹⁸ F]Fallypride Hotspots	88
4.3.2. Strain Differences in Retro-ocular Tracer Uptake.....	93
4.4. Discussion.....	94
4.5. Conclusion	97
4.6. References.....	98
5. Conclusion and Future Perspectives	104
Curriculum Vitae.....	107
Presentations	108
Scientific Talks	108
Poster Presentations	108

List of Abbreviations

2D	2-dimensional
3D	3-dimensional
A	Ampère
am	ante meridiem
Ar	Argon
ACS	Absolute central point-source sensitivity
ANOVA	Analysis of variance
BaFBr	Barium bromofluoride
Bgr	Background
BN rat	Brown Norway rat
Bq	Becquerel
bpm	breaths per minute
Br	Bromine
BSA	Bovine serum albumin
°C	degree Celsius
C	Carbon
cm	centimeter
CNS	Central nervous system
COV	Coefficient of variation
cps	Counts per second
CT	Computer tomography
D2R	Dopamin-2 receptor
D4R	Dopamin-4 receptor
DMSO	Dimethylsulfoxid
DOI	Depth of interaction
e ⁺	Positron
e.g.	exempli gratia
eV	electron Volt
F	Fluorine

List of Abbreviations

FBP	Filtered back projection
[¹⁸ F]FDEGPECO	(E)-3-(Pyridin-2-ylethynyl)cyclohex-2-enone O-2-(2- [¹⁸ F]fluoro-ethoxy)ethyl oxime
[¹⁸ F]FDG	2-[¹⁸ F]Fluoro-2-deoxyglucose
[¹⁸ F]FECNT	2b-carbomethoxy-3b-(4-chlorophenyl)-8-(2-[¹⁸ F]fluoroethyl)-nortropane
FORE	Fourier rebinning
FOV	Field of view
FWHM	Full width at half maximum
g	gram
G	Giga
GE	General Electric
GluT	facilitative Glucose transporter
GSO	Gadolinium orthosilicate
h	hours
HCl	Hydrochloric acid
HG	Harderian gland
HIDAC	High-density avalanche chamber
i.p.	intra peritoneal
IP	Imager plate
k	kilo
KCl	Potassium chloride
logP	logarithmus of partition coefficient between octanol and water
LSO	Lutetium orthosilicate
LYSO	Lutetium-yttrium orthosilicate
LOR	Line of response
M	Mega
min	minute
MIP	Maximum intensity projection
mm	millimeter
M	molar

List of Abbreviations

mol	mol
[¹¹ C]MPEP	6-[¹¹ C]Methyl-2-(phenylethynyl)-pyridine
μ	micro
n	nano
N	Nitrogen
NaCl	Sodium chloride
NEMA	National electrical manufacturers association
[¹⁸ F]NMe-FHBT	N-Methyl-6-(3-[¹⁸ F]Fluoro-2-(hydroxymethyl)propyl)-5-methylpyrimidine-2,4(1H,3H)-dione
O	Oxygen
OSEM	Ordered subset expectation maximization
P	statistical p-value
p ⁺	Proton
[¹⁸ F]PECMO	(E)-3-((6-[¹⁸ F]Fluoropyridin-2-yl)ethynyl)cyclohex-2-enone O-methyl oxime
PET	Positron emission tomography
pm	post meridiem
p.i.	post injection
PSL	Photo stimulated luminescence
R _{int}	Intrinsic event rate
R _{r+s}	Random and scatter event rate
R _s	Scatter event rate
R _t	True event rate
R _{tot}	Total even rate
RC	Recovery coefficient
ROI	Region of interest
s	second
SD	Standard deviation
SD rat	Sprague Dawley rat
SF	Scatter fraction
SLC2A	Solute-carrier family 2A

List of Abbreviations

S/N	signal to noise ratio
SOR	Spill-over ratio
SSRB	Single slice rebinning
SPECT	Single photon emission computed tomography
SUV	Standardized uptake volume
Tris	Tris(hydroxymethyl)-aminomethan
V	Volt
VOI	Volume of interest

Summary

Positron emission tomography (PET) is an excellent imaging tool to investigate biochemical, physiological and pharmacological processes non-invasively in healthy and diseased individuals. In recent years, the development of dedicated small animal PET scanners with high spatial resolution crucially increased the utility of PET in preclinical research. The non-invasiveness of PET allows longitudinal follow-up studies, where animals can be used as their own controls. Such set-ups are considered to give more reliable results than the traditional approach using control groups. However, the use of small animal PET in preclinical research still bears several challenges and major differences compared to clinical PET. In contrast to clinical PET, preclinical PET requires the anesthetic immobilization of small animals during data acquisition. Experimental parameters, such as the administration of anesthetic agents or general animal handling and keeping might hamper the translatability of preclinical results to the clinical setting. Another major difference between clinical and preclinical PET is that quantification or semi-quantification of data is crucial for small animal PET whereas clinical PET is mainly based on visual inspection of patient scans for diagnostic purposes. Despite the fast development of preclinical tomographs, reliable data quantification remains difficult and it is still hardly possible to directly compare data generated at different institutes.

In this thesis, the challenges of small animal PET scanning were approached from different directions but with the common aim to improve, refine and standardize small animal PET experimentation and data analysis. In the first part of this thesis, a detailed performance analysis of the dedicated small animal PET scanner eXplore Vista PET/CT (GE Healthcare) was carried out. In the second part of the study, experimental parameters with a potential impact on PET data were investigated and it was analyzed whether strict standardization of those parameters needs to be applied in order to achieve reliable and reproducible small animal PET data. In a third part, the phenomenon of high retro-ocular PET tracer uptake observed on small animal PET images was investigated using two exemplary tracers. The responsible tissue for the high accumulation was determined and the uptake characteristics were analyzed in detail.

The eXplore Vista was evaluated according to the national electrical manufacturers association (NEMA) standards for performance measurements of small animal PET tomographs (NEMA NU4-2008). These standards provide detailed guidelines how to determine the performance of

small animal PET scanners in order to achieve direct comparability of different systems available. Additional tests were performed in order to evaluate the impact of radioactivity located outside of the field of view (FOV) on data acquisition. The performance evaluation of the eXplore Vista showed competitive results in terms of spatial resolution ($<1.8\text{mm}$ FWHM in the central 3cm), sensitivity (4.2% ACS), uniformity ($7.4\pm 0.9\%$ SD) and recovery coefficient (RC) compared to similar devices described in literature. The optimal energy window for data acquisition was determined 250-700keV and it was found that optimal image quality can be achieved by reconstructing data with a 2D OSEM algorithm applying scatter and random correction. It seems worthwhile for the future, to determine the benefit of the 3D OSEM reconstruction algorithm on image quality.

In order to determine the impact of experimental parameters on small animal PET data, two representative PET tracers ($[^{18}\text{F}]\text{FDG}$, a glucose analogue, as an example of a metabolic tracer, which is trapped inside the cell and $[^{18}\text{F}]\text{fallypride}$, a dopamine D_2 receptor ligand, as a typical representative of a tracer with reversible binding kinetics) were investigated. Test-retest PET scanning experiments were performed to examine whether using animals as their own control leads to more reliable study outcome. Furthermore, the benefit of standardization on the reliability of results was investigated by studying gender-specific $[^{18}\text{F}]\text{FDG}$ tissue uptake under standardized and heterogenized conditions. Experimental parameters showed minor impact on $[^{18}\text{F}]\text{FDG}$ tissue uptake. $[^{18}\text{F}]\text{FDG}$ brain uptake was only affected by the duration of anesthesia application (27% less brain uptake for animals anaesthetized for 60min compared to 40min). The results indicate that strict standardization of anesthetic protocols and tracer formulation might lead to increased reliability and reproducibility of small animal PET data. However, intra-animal variability of $[^{18}\text{F}]\text{FDG}$ brain uptake proved to be larger than inter-animal variability, suggesting that using animals as their own control does not increase the reliability of study results. Therefore, the performance of group size calculation prior to small animal PET studies is highly recommended. This includes the estimation of the variability of the PET tracer uptake to the target tissue. Furthermore, it was shown that strict standardization might reduce reproducibility of small animal PET results by trend. This finding indicates that in contrast to strict standardization, systematic heterogenization of experimental parameters might be more beneficial for the reliability of study outcome as it tends to increase the external validity of results. Therefore, it is recommended to find the balance between standardization of parameters

with significant impact on PET tracer distribution (such as anesthesia duration) and heterogenization of factors with no crucial impact on study outcome. In the future, the next step should be the performance of studies which involve different small animal PET centers in order to investigate closer on external validity of results.

Finally, the high retro-ocular accumulation of [^{18}F]FDG and [^{18}F]fallypride was characterized by PET scanning, *ex vivo* tissue counting and *ex vivo / in vitro* autoradiography with subsequent eosin and haematoxylin staining of tissue slices. Retro-ocular uptake of [^{18}F]FDG was shown to be due to the Harderian gland (HG), an eye gland present in almost all mammals, with yet unknown function. The strong [^{18}F]FDG accumulation might be explained by a high glucose consumption for lipid synthesis taking place in the HG. In contrast to [^{18}F]FDG, [^{18}F]fallypride accumulation in a similar area could be mainly allocated to the retina. This [^{18}F]fallypride accumulation was exclusively observed *in vivo* in pigmented mice and the administration of a potent dopamine receptor ligand did not show any blocking effect. An explanation for such retro-ocular uptake might be a non-specific accumulation of PET tracers with lipophilic physiochemical properties ($\log P > 1$) to pigmented structures, such as the retina and the porphyrin-containing HG. The closer investigation on the detailed characteristics of retro-ocular PET tracer accumulation in different test animals remains for the future.

Zusammenfassung

Die Positronen-Emissions-Tomographie (PET) ist ein hervorragendes Bildgebungsverfahren zur nicht-invasiven Untersuchung von biochemischen, physiologischen und pharmakologischen Prozessen in gesunden und kranken Individuen. Die Entwicklung von hochauflösenden Kleintier-PET-Tomographen hat in den letzten Jahren zu einem starken Anstieg der präklinischen Nutzung von PET geführt. Dass es sich bei PET um eine nicht-invasive Methode handelt, ermöglicht die Durchführung langfristiger Folgestudien und damit die Nutzung eines Individuums gleichermaßen als Kontroll- und Testsubjekt. Nichtsdestotrotz birgt der Einsatz von Kleintier-PET immer noch zahlreiche Herausforderungen und gravierende Unterschiede zum klinischen PET. Im Gegensatz zum klinischen PET setzt präklinisches PET eine Immobilisierung der Testtiere durch Narkose voraus. Experimentelle Parameter, wie die Verabreichung von Anästhetika, der allgemeine Umgang mit dem Tier und die Tierhaltung könnten die Translationsfähigkeit von präklinischen Resultaten auf die klinische Situation beeinträchtigen. Ein weiterer zentraler Unterschied zwischen klinischem und präklinischem PET ist die Notwendigkeit, mit quantitativen oder semi-quantitativen Kleintierdaten arbeiten zu können, während beim klinischen PET die visuelle Inspektion von Patientenscans für diagnostische Zwecke in der Regel genügt. Trotz der rasanten Entwicklung der präklinischen Tomographen bleibt es schwierig, Daten verlässlich zu quantifizieren und es ist immer noch so gut wie unmöglich, Daten, die an verschiedenen Instituten generiert wurden, direkt miteinander zu vergleichen.

In dieser Dissertation wurden die Herausforderungen von Kleintier-PET von verschiedenen Richtungen her angegangen, allerdings mit dem übergeordneten Ziel, Kleintier-PET-Experimente und -Datenanalyse zu standardisieren und zu verbessern. Im ersten Teil der Arbeit wurde eine detaillierte Leistungsanalyse des Kleintier-PET-Tomographen eXplore Vista PET/CT (GE Healthcare) durchgeführt. Im zweiten Teil wurden dann experimentelle Parameter untersucht, die einen potentiellen Einfluss auf PET-Daten haben könnten und es wurde analysiert, ob eine strikte Standardisierung dieser Parameter nötig ist für die Generierung von verlässlichen und reproduzierbaren Kleintier-PET-Daten. Im dritten Teil wurde die auf Kleintier-PET-Bildern häufig beobachtete retro-okulare Anreicherung von PET-Tracern anhand von zwei

exemplarischen Tracern untersucht. Das verantwortliche Gewebe für diese Anreicherung wurde bestimmt und die Anreicherungscharakteristik wurde analysiert.

Die Leistung des eXplore Vista PET/CT wurde gemäss den Richtlinien der „National Electrical Manufacturers Association (NEMA)“ Standards für die Leistungsmessungen von Kleintier-PET-Tomographen (NEMA NU4-2008) bestimmt. Diese Standards stellen detaillierte Richtlinien dar, wie die Leistung eines Kleintier-PET-Tomographen überprüft werden muss, um einen direkten Vergleich von verschiedenen Systemen zu ermöglichen. Zusätzliche Tests wurden durchgeführt, um den Einfluss von Radioaktivität ausserhalb des Gesichtsfeldes des Tomographen auf die Messung zu untersuchen. Die Leistungsanalyse des eXplore Vista PET/CT führte zu konkurrenzfähigen Resultaten im Hinblick auf die räumliche Auflösung ($<1.8\text{mm}$ FWHM innerhalb der zentralen 3cm des Gesichtsfeldes), Empfindlichkeit (4.2% ACS), Uniformität ($7.4\pm 0.9\%$ SD) und „Recovery Coefficient (RC)“, verglichen mit anderen Systemen, die in der Literatur beschrieben wurden. Als geeignetes Energiefenster bei der Datengenerierung wurden 250-700keV bestimmt und es wurde befunden, dass ein 2D OSEM Algorithmus mit Streuungs- und Zufallskoinzidenzkorrektur zu optimaler Bildqualität führt.

Um den Einfluss von experimentellen Parametern auf Kleintier-PET-Daten zu untersuchen, wurden zwei exemplarische PET-Tracer verwendet ($[^{18}\text{F}]\text{FDG}$, ein Glucose-Analogon als Beispiel eines metabolischen Tracers und $[^{18}\text{F}]\text{Fallypride}$, ein Dopamin D_2 Rezeptor-Ligand als typisches Beispiel eines Tracers mit reversibler Bindungskinetik). Test-Retest PET-Experimente wurden durchgeführt, um zu untersuchen, ob die Verwendung ein und desselben Tieres als Test- und Kontrollsubjekt in höherer Verlässlichkeit des Studienergebnisses resultieren würde. Des Weiteren wurde analysiert, ob die Standardisierung von Testbedingungen vorteilhaft wäre. Dies wurde getestet, indem geschlechtsspezifische Unterschiede in der Gewebeanreicherung von $[^{18}\text{F}]\text{FDG}$ unter standardisierten und heterogenisierten Bedingungen bestimmt wurden. Experimentelle Parameter zeigten nur einen kleinen Einfluss auf die Gewebeaufnahme von $[^{18}\text{F}]\text{FDG}$. Die $[^{18}\text{F}]\text{FDG}$ Hirnaufnahme wurde lediglich von der Dauer der Anästhesie signifikant beeinflusst (27% weniger Hirnanreicherung in Tieren, die über 60min unter Narkose standen, verglichen mit solchen, die über 40min anästhesiert waren). Die Resultate weisen darauf hin, dass eine strikte Standardisierung der Anästhesieprotokolle und Tracerformulierungen zu einer erhöhten Verlässlichkeit und Reproduzierbarkeit von Kleintier-PET-Daten führt. Andererseits erwies sich die intra-individuelle Variabilität der $[^{18}\text{F}]\text{FDG}$ Hirnanreicherung nicht

als geringer verglichen mit der inter-individuellen Variabilität. Dies deutet darauf hin, dass die Verwendung ein und desselben Tieres als Test- und Kontrollsubjekt nicht zu einer erhöhten Studienverlässlichkeit führt. Daher wird empfohlen, immer eine Gruppengrössenberechnung im Vorfeld einer Studie durchzuführen. Eine solche Berechnung würde auch eine Abschätzung der Aufnahmevariabilität des zu untersuchenden PET-Tracers ins Zielgewebe beinhalten. Es wurde ausserdem gezeigt, dass die strikte Standardisierung von experimentellen Parametern tendenziell eine verringerte Reproduzierbarkeit von Kleintier-PET-Resultaten zur Folge hat. Eine systematische Heterogenisierung von experimentellen Parametern könnte daher für die Verlässlichkeit von Studien vorteilhaft sein, da angenommen werden kann, dass die externe Gültigkeit der Resultate dadurch ansteigt. Aufgrund dieser Ergebnisse wird empfohlen, nur solche Parameter zu standardisieren, welche einen signifikanten Einfluss auf die PET-Traceranreicherung haben (zum Beispiel Dauer der Anästhesie) und die restlichen Parameter zu heterogenisieren. In Zukunft sollte eine Studie in Betracht gezogen werden, die verschiedene Kleintier-PET-Zentren einschliesst, um die externe Gültigkeit von Resultaten genauer zu untersuchen.

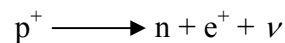
Schliesslich wurde die retro-okulare Anreicherung von [^{18}F]FDG und [^{18}F]Fallypride mittels PET-Scanning, *ex vivo* Gewebemessung, *ex vivo* / *in vitro* Autoradiographie und anschliessender Eosin/Hämatoxilin-Färbung von Gewebeschnitten charakterisiert. Es konnte gezeigt werden, dass [^{18}F]FDG retro-okular hauptsächlich in die Harderdrüse (HD) aufgenommen wird. Diese Drüse findet sich in fast allen Säugern, ihre Funktion ist aber bis heute noch nicht mit Bestimmtheit geklärt. Die hohe HD-Aufnahme von [^{18}F]FDG könnte mit einem hohen Glucose-Bedarf erklärt werden, welcher durch die in der HD stattfindenden Lipid-Synthesen zu Stande kommt. Im Gegensatz zu [^{18}F]FDG wurde die starke [^{18}F]Fallypride-Anreicherung nicht der HD, sondern hauptsächlich der Retina zugeordnet. Diese [^{18}F]Fallypride-Aufnahme wurde allerdings nur *in vivo* in pigmentierten Tieren festgestellt und eine Blockade mittels eines potenten Dopamin Rezeptor-Liganden war nicht möglich. Eine Erklärung für diesen Befund könnte eine unspezifische Anreicherung von Radiopharmazeutika mit erhöhter Lipophilie ($\log P > 1$) in pigmentierten Geweben, wie der Retina oder der porphyrin-haltigen HD, sein. Für die Zukunft erscheint eine genauere Untersuchung der detaillierten Charakteristik dieser retro-okularen PET-Tracer-Anreicherung in verschiedenen Tierstämmen lohnenswert.

1. Introduction

1. Introduction

1.1. Positron Emission Tomography

Positron emission tomography (PET) is a non-invasive functional imaging modality generally used for the clinical diagnostic of cancer and diseases of the central nervous system (CNS) [1]. The principal of PET is based on the decay mechanism of positron emitting nuclides. An unstable nuclide reaches stability by the decay of a proton to a neutron via the emission of a positron and a neutrino.



The emitted positron collides with an electron of the surrounding matter, resulting in an annihilation of the positron and the electron. In this annihilation process energy and momentum are conserved. Therefore, two gamma rays are emitted, each having an energy equal to the rest-mass energy of the electron or the positron ($mc^2 = 511\text{keV}$), which propagate in the opposite direction of each other. The two gamma rays are coincidentally registered by the ring detectors of the tomograph (**Figure 1.1**) [2].

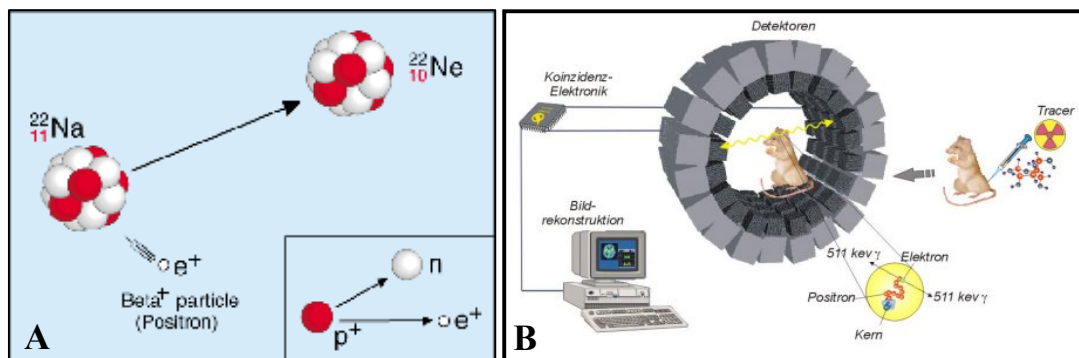


Figure 1.1. A) Positron decay [3] and B) detection principle of PET [4].

In the reconstruction process, the two points of coincidence registration are connected by a virtual line referred to as line of response (LOR). The concentration distribution of the radionuclide in the field of view (FOV) of the tomograph is determined by the LOR intersection density.

1.2. Radiopharmaceuticals

Radioactive compounds used for diagnosis in nuclear medicine are referred to as radiopharmaceuticals or radiotracers. PET radiopharmaceuticals are labeled with a positron emitting nuclide, i.e. ^{11}C , ^{13}N , ^{15}O , ^{18}F or ^{76}Br . Radio-labelling using the first three nuclides provides radiotracers with no effect on their biochemical characteristics. ^{18}F or ^{76}Br are usually introduced as hydrogen substituents [2]. The radionuclides produced on-site at ETH Höggerberg are ^{11}C and ^{18}F . Due to its substantially longer half life (109.8min for ^{18}F vs. 20.4min for ^{11}C) and a shorter positron range [5], ^{18}F is often preferred over ^{11}C .

In the following paragraphs, the two ^{18}F -labelled radiotracers relevant for this work are introduced in more detail.

1.2.1. [^{18}F]FDG

2- [^{18}F]Fluoro-2-deoxy-D-glucose ([^{18}F]FDG, **Figure 1.2**) is a metabolic PET tracer taken up by cells, just like glucose, via facilitative transport across cell membranes mediated by a family of several structurally related proteins (glucose transporters Glut/SLC2A) [6, 7]. Depending on the type of tissue, different transporter subtypes are predominantly responsible for glucose uptake [8]. Transport of the hydrophilic glucose analogue across the blood brain barrier, for example, is facilitated by Glut1. After cell uptake, [^{18}F]FDG is phosphorylated by the enzyme hexokinase to 2- [^{18}F]FDG-6-phosphate. Because 2- [^{18}F]FDG-6-phosphate cannot be metabolized any further in the glycolysis pathway, this ^{18}F -labeled metabolite stays trapped inside the cell as it cannot be transported outside anymore. This leads to an accumulation of radioactivity in tissue cells with high glucose consumption, such as brain, heart or some tumors. [^{18}F]FDG is the most frequently used clinical PET tracer and has also wide applicability in preclinical animal research [9].

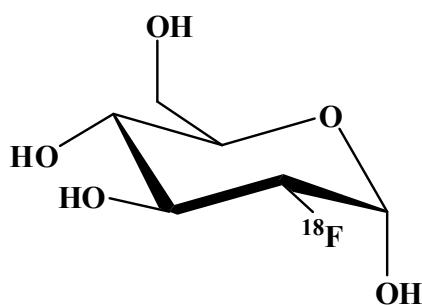


Figure 1.2. Chemical structure of [^{18}F]FDG.

1.2.2. [¹⁸F]Fallypride

(S)-N-[(1-allyl-2-pyrrolidiny)methyl]-5-(3-[¹⁸F]fluoropropyl)-2,3-dimethoxybenzamide ([¹⁸F]fallypride, **Figure 1.3**) was developed as a high affinity dopamine D₂ and D₃ receptor ligand [10]. The D₂ receptor is thought to be involved in a variety of pathophysiologies such as schizophrenia and Parkinson's disease [11, 12].

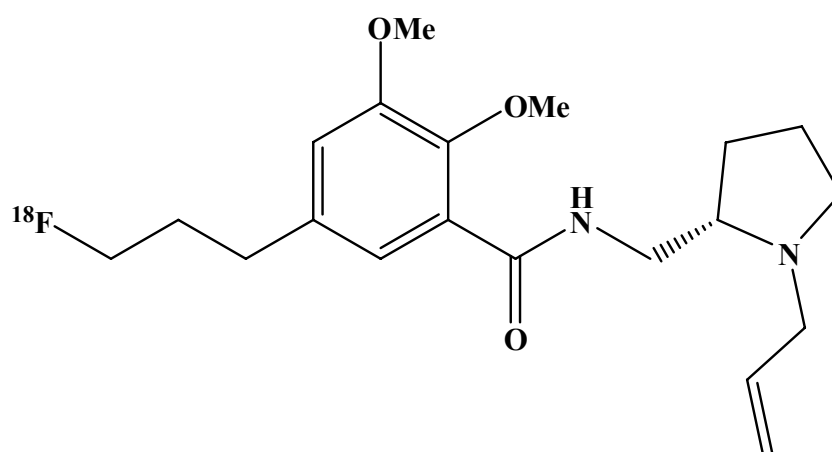


Figure 1.3. Chemical structure of [¹⁸F]fallypride.

These receptors are mainly located in the striatum, however, they can also be found in the frontal cortex, parietal cortex, amygdala, hippocampus, thalamus and hypothalamus [10].

[¹⁸F]Fallypride is a typical representative of PET tracers binding reversibly to their target sites (in this case the D₂ receptor). Its lipophilic physicochemical properties (logP=2.48 [13]) allow it to passively diffuse through the blood brain barrier.

1.3. Detection of Gamma Rays

For the detection of gamma rays and a quantitative or semi-quantitative determination of radioactivity, several methods are available. A description of the ones with most relevancy for this thesis are described in the following sections.

1.3.1. Gas-filled Detectors

The detection principle of gas-filled detectors is based on the ionization of gas molecules by radiation and the subsequent measurement of current. The measured current is proportional to the amount of radiation and the applied voltage between the operating electrodes. There are two main types of gas-filled detectors that are commonly used: ionization chambers (e.g. dose calibrators) and Geiger-Müller counters. The main difference between the two is the operation voltage (ionization chamber: 50–300V, Geiger-Müller counter: around 1000V) [14]. An example of an ionization chamber is the VDC-505 (Veenstra Instrumental) used at ETH Hönggerberg, Zürich. This device is qualified for measuring high activity samples up to 200GBq. The detector consists of argon gas (13bar, overpressure) with the capacity of detecting high energy samples in the range of 25-3000keV. It is surrounded by lead to shield the detector against radioactivity outside of the measuring chamber. The VDC-505 is used for the determination of injected doses or total activities in standard test series or phantom studies due to easy handling and its capacity to measure high amounts of radioactivity [15].

1.3.2. Scintillation Detector

The operation principle of scintillation detectors is based on the interaction of gamma rays with the sodium iodine crystal detector and the subsequent emission of light photons by the crystals, which are striking the photocathode in a photomultiplier tube, where a pulse is generated and further amplified by a linear amplifier. The pulse height analyzer sorts out the pulses by energy of the gamma ray [14]. An example of such a scintillation detector is the gamma counter Wallac 1480 Wizard 3'' (Perkin Elmer), which is used at ETH Hönggerberg, Zürich. The Wallac 1480 Wizard has the capacity to measure high energy samples up to 2000keV. Its detector consists of thallium-activated sodium iodide crystals surrounded by lead for an optimal shielding from outside radioactivity [16].

The gamma counter is used for the activity determination of tissue samples after *ex vivo* organ sampling.

1.3.3. Autoradiography using Phosphor Imager Plates

The Fujifilm Imager plate (IP) used at ETH Höggerberg, Zürich, is a reusable, two-dimensional sensor for the detection of ionizing radiation energy. The so-called phosphors in use for the storage of the energy are photo-sensitive barium bromofluoride (BaFBr) crystals doped with bivalent europium to serve as the luminescence center. The Fuji BAS5000 (Bio-imaging analyzer system) phosphor imager is used for the readout of the stored radiation energy on the IP. The BAS5000 possesses a confocal laser and light-collecting optics. High resolution and sensitivity derive from a pixel size of 25 μ m and a dynamic range of up to five orders of magnitudes. The unit of the measured energy is given as photo stimulated luminescence (PSL) [17].

Autoradiography using the Fujifilm IP and the Fuji BAS5000 phosphor imager is the method of choice for the measurement of activity in tissue slices of specific organs of interest which can subsequently be stained histochemically. Quantitative *ex vivo* autoradiography analyses are well suited for cross-correlations with *in vivo* PET data.

1.3.4. Small Animal PET

Noninvasive imaging modalities provide many opportunities for molecular diagnosis in clinics, e.g. early detection, “real time” monitoring of disease and investigating the efficacy of new drugs; the most sensitive techniques in this field being PET and single photon emission computed tomography (SPECT) [18]. Imaging technologies are more and more used in preclinical research. Non-invasive imaging methods like PET allow longitudinal follow-up studies where animals can be repeatedly used, for example to monitor disease progression or the efficacy of a therapeutic intervention. Such set-ups are considered to give more reliable results than the traditional control group approach. The main advantage of these techniques is the fact that each animal can be used as its own control, therefore reducing the number of animals required for a study, while increasing the accuracy of the arising results [1, 9, 19]. Furthermore, by application of the same methodology in the pre-clinical and clinical setting, the translation of preclinical results to clinics should be improved.

The development of dedicated PET scanners with high sensitivity and high resolution helped to establish PET imaging in preclinical research [20]. The resolution of clinical tomographs (4-

8mm) is not sufficient for the accurate visualization of activity distribution in the rodents [21, 22].

The resolution in PET is limited by the positron range of the applied radionuclide (0.64mm and 1.03mm in water for low energy radionuclides as ^{18}F or ^{11}C , respectively [5]) and by the slight divergence of the travel of the annihilation photons from colinearity [2, 19]. Nevertheless, the resolution of a PET scanner is mainly determined by the size of the detector units of the tomograph. Dedicated small animal scanners generally reach resolutions in the millimeter range (**Table 1.1**) [23-27]. Due to the smaller size of their volumetric units, the sensitivity of small animal PET scanners must be increased compared to human PET in order to reach sufficient signal-to-noise ratios (S/N ratio) [19]. It is suggested that the sensitivity of the system should reach at least 1% in order to achieve reliable results from region of interest (ROI) analysis, however, for pixel-to-pixel analysis, a minimum sensitivity of 3% is required [28].

At ETH Honggerberg, the dedicated eXplore Vista PET/CT (GE Healthcare) is used for rodent PET. The dual-scintillator phosphor sandwich (phoswich) detector modules provide depth-of-interaction (DOI) correction by locating the interaction site of each γ -ray to the center of one of the two scintillator types. The front ring layer consists of cerium-doped lutetium-yttrium orthosilicate (LYSO) crystals, whereas cerium-doped gadolinium orthosilicate (GSO) crystals are located in the rear layer. The scintillation light of each of the two phoswich types decays with a very characteristic light decay time (LYSO: 40ns; GSO: 60ns). The Vista detector module is created by a position-sensitive photomultiplier tube optically coupled to the GSO layer. The axial FOV of this scanner (4.8cm) is sufficient for a whole body mouse scan in two bed positions. Measurements can be performed with three energy windows, each with a characteristic scatter fraction and count rate linearity profile. The GE Healthcare eXplore VISTA-CT software provides the possibility of scatter and random corrections as well as CT-based attenuation correction [29]. Three energy windows are available to choose from for data acquisition: 100-700keV, 250-700keV and 400-700keV. Data reconstruction can be achieved either via 2-dimensional filtered back projection (2D FBP) algorithm or via 2-dimensional ordered subset expectation maximization (2D OSEM). **Table 1.1** shows an overview of small animal PET systems commercially available up to now [24-27, 30-32].

	GE Healthcare eXplore Vista PET/CT	Oxford Positron Systems quad-HIDAC	Siemens microPET Focus 120	Siemens Inveon	Bioscan nanoPET /CT	Sedecal Argus PET/CT
Scanner Geometry	Ring	4x4 Quadratic array modules	Ring	Ring	Ring	Ring
Detector	LYSO / GSO	Ar gas filled hole- containing lead modules	LSO	LSO	LYSO	LYSO/GSO
Transaxial FOV (cm)	6.7	17	-	10	9.4	8.0
Axial FOV (cm)	4.8	28	7.6	12.7	9.5	4.7
Ring Diameter (cm)	11.8	17	14.7	16.1	15	11.8
Spatial Resolution (mm)	<2.1	<1.2	<2.4	<2.0	<1.2	<1.5
ACS (%)	4.0 (250-700keV)	1	7.1 (250-750keV)	10 (250- 625keV)	8.3	>11

Table 1.1. Comparison of five different small animal PET systems in terms of scanner construction and performance. ACS: absolute central point source sensitivity; FOV: Field of view.

The national electrical manufacturers association (NEMA) provides guidelines for a detailed performance evaluation of PET scanners in order to allow direct and reliable comparison of different systems available. The NEMA NU4-2008 describes the standards for the evaluation of small animal PET scanner in terms of phantom construction, nuclide of choice, amount of radioactivity used, reconstruction applied and analysis of the resulting data [33].

1.4. Animal Models in Translational Research

It is widely accepted that the complexity of animal models is necessary for successful biomedical investigations as predictions for the human body [34]. Nevertheless, the use of animal models in preclinical research can be questioned in regard of the translation of results to the clinics. Investigations have shown that in different fields of research, clinical studies have been performed in parallel to ongoing preclinical experiments or they have been performed despite negative outcome of animal studies beforehand, implying that these animal studies were assumed irrelevant [35].

A selection of methodological problems in animal experimentation that can lead to invalid results and therefore a waste of laboratory animals and research funding are the following: use of disparate animal species/strains, variations in drug dosing schedules and regimen, lack of randomization in choice of animals for a study, lack of reporting of follow up, different environmental conditions (transport, temperature, additional drugs, microenvironment) and insufficient sample sizes leading to inadequate power of the study.

It is known that not only the genetic background but also the laboratory environment can impact the outcome of animal experiments [36]. Environmental factors influencing experimental results were found to be surrounding temperature [37], laboratory routines like blood sampling, transport within and between rooms and the entrance of a person into the animal room [38], housing density [39], use of filter tops on animal cages [40] or exposure to other species [41]. Parallel administration of drugs (e.g. anesthetics) can also have a great impact on the outcome of animal experimentation [37, 42]. Therefore, high standardization of environmental parameters is believed to improve the reproducibility of results and to keep the inter- and intra-study variability low [43-46].

Furthermore, the use of appropriate animal strains has a big impact on the experimental outcome; using inbred strains can lead to less variability of the test results and therefore reduce the number of animals required per test group in order to maintain an acceptable study power [45]. It is also well known that investigations of genetically modified mice are highly influenced by the genetic background of the mutant [47]. Nevertheless, highly standardized animal experiments might lead to idiosyncratic results, which bear the risk of not being valid externally and therefore scientifically useless [36, 48, 49]. This can be compared with the importance of knowing the

genetic background of a mutant animal: experimental outcome is valid only for the specific environmental conditions chosen and might be invalid under different settings. Würbel et al and Richter et al therefore suggest a “systematic variation of genetic and environmental backgrounds, instead of excessive standardization” in order to get a high external validity of results [49, 50]. This approach is opposed by van der Staay and colleagues [44], who were emphasizing the importance of standardization in order to not “reduce the chance of detecting meaningful interactive effects between genetic and environmental factors”. They further stated that standardization “prohibits variation at random”.

Another problem is bias not only in selection of animals and performance of the experiments, but also in publishing data. Common biases in research are the following: Selection bias, performance bias, detection bias, attrition bias and publication bias. These biases have to be minimized by proper randomization, blinding and following of the intention-to-treat (ITT) principle. Furthermore it is important to publish all relevant data in order to avoid overstatement of efficacy due to publishing bias.

1.5. Refinement and Standardization of Small Animal PET Experimentation

Research efforts in the field of small animal PET imaging have constantly been growing in recent years. The non-invasiveness of the methodology and its high sensitivity, allowing the detection of picomolar concentrations of a radioprobe in the tissue of interest are some of the advantages of this technique, which is considered translational to the clinical setting [1]. Key points in the success of such translational research are the standardization and refinement of experimental protocols as well as the accuracy and reproducibility of the resulting small animal PET data. Ideally, it should be possible to make inter-study comparisons of small animal PET data obtained at different research centers.

Literature reveals a broad variety of physiological, pharmacological and methodological influences on the PET tracer disposition and uptake into target tissue in small animals, in particular of [¹⁸F]FDG in mice and rats. One of the main differences of human and small animal PET is the requirement of anesthesia for the scanning of rodents. It is known that anesthetic agents can have a striking impact on [¹⁸F]FDG uptake to the brain [37, 51, 52] and indirectly on organ uptake in general, e.g. by causing hyperglycemia in the case of Ketamine/Xylazine [37,

52, 53]. High blood glucose levels can cause reduced [^{18}F]FDG uptake into organs of interest due to competition between glucose and its radiolabelled analogue [6, 54]. In clinical PET, patients are fasting up to 12h prior to a PET scan [55]. For laboratory animals Fueger and colleagues suggest an overnight fasting period for optimal [^{18}F]FDG organ uptake in laboratory animals [37].

Another concern is the injection volume of radiotracer into the animal. Generally, maximal volumes of 5mL/kg body weight can be intravenously injected as a bolus into rats and mice. For optimal count rate statistics, it is required that a small animal voxel shows a similar coincidence rate as a human voxel, which would require the injection of considerable volumes, depending on the specific activity of the tracer. In addition, animals are exposed to high doses of radiation [56]. For tracers with kinetics that do not underlay the saturation principle, Jagoda and co-workers stated that injection of human doses into a rat should not be a problem. High radiation doses in small animals nevertheless might have an impact on the physiology and therefore also the tracer distribution and kinetics. Administration of high doses might also prevent repeated measurements of the same animal [57].

For an optimal [^{18}F]FDG uptake into the organ of interest, the environmental temperature during the tracer uptake phase might also play a role, particularly in reducing uptake into brown fat of small animals [37].

1.6. Aims of the Thesis

The non-invasiveness and the translational characteristic of small animal PET offer a great opportunity for a more efficient and better preclinical investigation of biomedical processes. In order to maximize the benefit of this methodology, a profound reliability assessment of the acquired data is necessary. The main goal of this thesis was to analyze the physiological and experimental factors influencing PET tracer organ uptake in detail – with a focus on [^{18}F]FDG (as an example of a metabolic tracer) and [^{18}F]fallypride (as an example of a receptor ligand tracer). This analysis had to be adapted to the specific laboratory conditions at ETH Höggerberg, Zürich. In a first step, the inherent intra- and inter-animal variability of PET tracer distribution had to be determined in order to evaluate the impact of different experimental parameters on small animal PET data. It was important to investigate the influence of anesthesia, environmental temperature during uptake phase or tracer formulation under the standard conditions used in this laboratory. In a second step, the potential benefit of experimental standardization on preclinical small animal studies was assessed, as strict standardization might lead to the generation of idiosyncratic results with no external validity. This investigation was designed according to a study performed by Richter and co-workers in the field of behavioral neuroscience [50]. Furthermore, it was necessary to evaluate the detailed performance of the small animal PET scanner eXplore Vista PET/CT used at ETH Höggerberg, according to the dedicated standards published by the NEMA [33]. The aim of this evaluation was to determine an acquisition and data reconstruction protocol assuring maximal reliability of measured data, additionally allowing a direct comparison of the eXplore Vista with similar available systems. The thesis should provide optimal guidelines for the performance and evaluation of small animal PET experiments in order to achieve highest possible accuracy, reproducibility and translatability of preclinical PET data.

1.7. References

- [1] Nanni C, Rubello D, Fanti S. Role of small animal PET for molecular imaging in pre-clinical studies. *Eur J Nucl Med Mol Imaging*. 2007;34:1819-1822
- [2] Ter-Pogossian MM. Positron emission tomography. *J Med Syst*. 1982;6:569-577
- [3] Image taken from the website of the European Nuclear Society
<http://www.euronuclear.org/info/encyclopedia/betaplusdecay.htm>
- [4] Image taken from the website of the Forschungszentrum Jülich
http://www.fz-juelich.de/zel/zel_bildgebung_beschreibung/
- [5] Cal-Gonzalez J, Herraiz JL, Espana S, Desco M, Vaquero JJ, Udias. Positron range effects in high resolution 3D PET imaging. *IEEE Nucl Sci Symp Conf Rec*. 2009;2788-2791
- [6] Wahl RL, Henry CA. Serum glucose: effects on tumor and normal tissue accumulation of [¹⁸F]FDG in rodents with mammary carcinoma. *Radiology*. 1992;183:643-647
- [7] www.uniport.org
- [8] Mueckler M. Facilitative glucose transporters. *Eur J Biochem*. 1994;219:713-725
- [9] Cherry SR, Gambhir SS. Use of positron emission tomography in animal research. *ILAR J*. 2001;42:219-232
- [10] Mukherjee J, Yang Z-Y, Brown T, Lew R, Wernick M, Ouyang X, Yasillo N, Chen C-T, Mintzer R, Cooper M. Preliminary assessment of extrastriatal dopamine D₂ receptor binding in the rodent and non-human primate brains using the high affinity radioligand, [¹⁸F]fallypride. *Nucl. Med. Biol*. 1999;26:519-527

- [11] Missale C, Nash, SR, Robinson SW, Jaber M, Garon MG. Dopamine receptors: from structure to function. *Physiol Rev.* 1998;78:189-225
- [12] Antonini A, Schwarz J, Oertel WH, Pogarell O, Leenders KL. Long-term changes of striatal dopamine D₂ receptors in patients with Parkinson's disease: A study with positron emission tomography and [¹¹C]raclopride. *Mov Disord.* 1997;12:33-38
- [13] Christian BT, Narayanan T, Shi B, Morris ED, Mantil J, Mukherjee J. Measuring the in vivo binding parameters of [¹⁸F]Fallypride in monkeys using a PET multiple-injection protocol. *J Cereb Blood Flow Metab.* 2004;24:309-322
- [14] Kowalsky RJ., Falen SW. Radiopharmaceuticals in Nuclear Pharmacy and Nuclear Medicine, 2004, 2nd Edition, Washington DC: American Pharmacists Association
- [15] VDC-505 Bedienungshandbuch, Veenstra Instrumental, 2005
- [16] Wallac 1480 Wizard 3'' Gamma Counter, Instrument Manual (2004), Perkin Elmer
- [17] www.sb.fsu.edu
- [18] Ametamey SM, Honer M, Schubiger PA. Molecular imaging with PET. *Chem Rev.* 2008;108:1501-1516
- [19] Myers R., Hume S. Small animal PET. *Eur. Neuropsychopharmacol.* 2002;12:545-555
- [20] Cherry SR. Of mice and men (and positrons) – advances in PET imaging technology. *J Nucl Med.* 2006;47:1735-1745
- [21] Seemann MD. Human PET/CT scanner: feasibility for oncological *in vivo* imaging in mice. *Eur J Med Res.* 2004;9:468-472

- [22] Teräs M, Tolvanen T, Johansson JJ, Williams JJ, Knuuti J. Performance of the new generation of whole-body PET/CT scanners: discovery VCT. *Eur J Nucl Med Mol Imaging*. 2007;34:1683-1692
- [23] Schäfers KP, Reader AJ, Kriens M, Knoess C, Schober O, Schäfers M. Performance evaluation of the 32-module quadHIDAC small-animal PET scanner. *J Nucl Med*. 2005;46:996-1004
- [24] Missimer J, Madi Z, Honer M, Keller C, Schubiger A, Ametamey SM. Performance evaluation of the 16-module quad-HIDAC small animal PET camera. *Phys Med Biol*. 2004;49:2069-2081
- [25] Wang Y, Seidel J, Tsui BMW, Vaquero JJ, Pomper MG. Performance evaluation of the GE healthcare eXplore VISTA dual-ring small-animal PET scanner. *J Nucl Med*. 2006;47:1891-1900
- [26] Bao Q, Newport D, Chen M, Stout DB, Chatziioannou AF. Performance evaluation of the inveon dedicated PET preclinical tomograph based on the NEMA NU-4 Standards. *J Nucl Med*. 2009;50:401-408
- [27] Laforest R, Siegel S, Newport DF, Yap J. Performance evaluation of the microPET[®] – Focus-F120. *IEEE Trans Nucl Sci*. 2007;54:42-49
- [28] Meikle SR, Eberl S, Fulton RR, Kassiou M, Fulham MJ. The influence of tomography sensitivity on kinetic parameter estimation in positron emission tomography imaging studies of the rat brain. *Nucl Med Biol*. 2000;27:617-625
- [29] Vista-CT User Manual, Version 4.0, GE Healthcare, 2007
- [30] www.bioscan.org

- [31] Saha GB. Basics of PET imaging: Physics, chemistry and regulations. Springer Science and Business Media, 2010
- [32] www.sedecal.com
- [33] National Electrical Manufacturers Association (NEMA). Performance measurements of small animal positron emission tomographs. NEMA Standards Publication NU 4-2008. Rosslyn, VA: NEMA; 2008.
- [34] Knight A. Systematic reviews of animal experiments demonstrate poor human clinical and toxicological utility. *ATLA*. 2007;35:641-659
- [35] Pound P, Ebrahim S, Sandercock P, Bracken M B, Roberts I. Where is the evidence that animal research benefits humans? *BMJ* 2004;328:514-517
- [36] Crabbe JC, Wahlsten D, Dudek BC. Genetics of mouse behavior: interactions with laboratory environment. *Science*. 1999;284:1670-1672
- [37] Fueger BJ, Czernin J, Hildebrandt I, Tran C, Halpern BS, Stout D, Phelps ME, Weber WA. Impact of animal handling on the results of ¹⁸F-FDG PET studies in mice. *J. Nucl. Med.* 2006;47:999-1006
- [38] Balcombe JP, Barnard ND, Sandusky C. Laboratory routines cause animal stress. *J Am Assoc Lab Anim Sci*. 2004;43:42-51
- [39] Laber K, Veatch LM, Lopez MF, Mulligan JK, Lathers DMR. Effects of Housing Density on Weight Gain, Immune Function, Behavior, and Plasma Corticosterone Concentrations in BALB/c and C57BL/6 Mice. *J Am Assoc Lab Anim Sci*. 2008;47:16-23

- [40] Klempt M, Rathkolb B, Fuchs E, Hrabé de Angelis M, Wolf E, Aigner B. Genotype-specific environmental impact on the variance of blood values in inbred and F1 hybrid mice. *Mamm Genome*. 2005;14:93-102
- [41] Grootendorst J, de Kloet ER, Vossen C, Dalm S, Oitzl MS. Repeated exposure to rats has persistent genotype-dependent effects on learning and locomotor activity of apolipoprotein E knockout and C57Bl/6 mice. *Behav. Brain Res*. 2001;125:249-259
- [42] Matsumura A., Mizokawa S., Tanaka M., Wada Y., Nozaki S., Nakamura F., Shiomi S., Ochi H, Watanabe Y. Assessment of microPET performance in analyzing the rat brain under different types of anesthesia: comparison between quantitative data obtained with microPET and *ex vivo* autoradiography. *NeuroImage* 2003;20:2040-2050
- [43] Van Zutphen LFM, Baumans V, Beynen AC. Grundlagen der Versuchstierkunde: Gustav Fischer Verlag. 1995;93ff, 189ff
- [44] Van der Staay FJ, Steckler T. The fallacy of behavioral phenotyping without standardization. *Genes, Brain and Behavior*. 2002;1:9-13
- [45] Hau J, van Hoosier GL. Handbook of Laboratory Animal Science, 2nd edition, Vol. I, *CRC Press*, 2003
- [46] Festing MFW. Good experimental design and statistics can save animals, but how can it be promoted? *ATLA*. 1976;32:133-135
- [47] Hummel KP, Coleman DL, Lane PW. The influence of genetic background on expression of mutations at the diabetic locus in the mouse. *Biochemical Genetics*. 1972;7:1-13
- [48] Würbel H. Behaviour and the standardization fallacy. *Nature genetics*. 2000;26:263

- [49] Würbel H. Behavioural phenotyping enhanced – beyond (environmental) standardization. *Genes, Brain and Behavior*. 2002;1:3-8
- [50] Richter SH, Garner JP, Würbel H. Environmental standardization: cure or cause of poor reproducibility of animal experimentation? *Nature methods*. 2009;6:257-261
- [51] Balaban RS, Hampshire VA. Challenges in small animal noninvasive imaging. *ILAR J*. 2001;42:4203
- [52] Toyama H, Ichisea M, Liowa J-S, Vinesa DC, Seneca NM, Modella KJ, Seidel J, Green MV, Innisa RB. Evaluation of anesthesia effects on [¹⁸F]FDG uptake in mouse brain and heart using small animal PET. *Nucl Med Biol*. 2004;31:251-256
- [53] Lee K-H, Ko B-H, Paik J-Y, Jung K-H, Choe Y. S, Choi Y, Kim, B-T. Effects of anesthetic agents and fasting duration on [¹⁸F]FDG biodistribution and insulin levels in tumor-bearing mice. *J. Nucl. Med.* 46 (2005) 1531-1536
- [54] Ishizu K, Nishizawa S, Yonekura Y, Sadato N, Magata Y, Tamaki N, Tsuchida T, Okazawa H, Miyatake I, Kikuchi H, Konishi J. Effects of hyperglycemia on FDG uptake in human brain and glioma. *J Nucl Med*. 1994;35:1104-1109
- [55] Helal BO Merlet P, Toubert M-E, Franc B, Schwartz C, Gauthier-Koelesnikov H, Prigent A, Syrota A. Clinical impact of [¹⁸F]FDG PET in thyroid carcinoma patients with elevated thyroglobulin levels and negative ¹³¹I scanning results after therapy. *J Nucl Med*. 2001;42:1464-1469
- [56] Jogoda EM, Vaquero JJ, Seidel J, Green MV, Eckelmann WC. Experiment assessment of mass effects in the rat: implications for small animal PET imaging. *Nucl Med Biol*. 2004;31:771-779

- [57] Kung M-P, Kung HF. Mass effect of injected dose in small rodent imaging by SPECT and PET. *Nucl Med Biol.* 2005;32:673-678

2. Performance Evaluation of the eXplore Vista PET/CT

2. Performance Evaluation of the Dedicated Small Animal PET/CT Tomograph eXplore Vista According to the NEMA NU4-2008 Standards

2.1. Introduction

Small animal positron emission tomography (PET) is an important tool for the translation of preclinical study results to the clinical setting. Due to the small dimensions of rodent organs the development of high-resolution small animal PET scanners was particularly important. In the past few years, a number of dedicated small animal PET systems have become available, such as the GE Healthcare eXplore Vista PET/CT small animal scanner [1]. For an adequate comparison of the performance of such preclinical systems, the national electrical manufacturers association (NEMA) has published a guideline for performance tests describing the use of dedicated phantoms for small animal PET systems [2]. In this study, the dual-ring version of the eXplore Vista PET/CT tomograph was characterized for spatial resolution, sensitivity, image quality and scatter fraction according to NEMA NU4-2008 standards and by an additional test investigating the impact of radioactivity outside of the field of view (FOV) on the acquired data.

2.2. Material and Methods

The GE Healthcare eXplore Vista PET/CT is a small animal PET scanner providing the possibility of additional CT scanning of the investigated subjects. The dual-ring version with dual-scintillator phosphor sandwich (phoswich) detector modules provides depth-of-interaction (DOI) correction by locating the interaction site of each γ -ray to the center of one of two scintillator types. The front ring layer consists of cerium-doped lutetium-yttrium orthosilicate (LYSO) crystals and cerium-doped gadolinium orthosilicate (GSO) crystals are located in the rear layer. The scintillation light of each of the two phoswich types decays with a very characteristic decay time (LYSO: 40ns; GSO: 60ns). The Vista detector module consists of a position-sensitive photomultiplier tube optically coupled to the GSO layer. The axial FOV of this scanner (4.8cm) is sufficient for a whole body mouse scan in two bed positions. Measurements can be performed with three energy windows, each with a characteristic scatter fraction and count rate linearity profile. The GE Healthcare eXplore VISTA-CT software provides the

possibility of scatter and random corrections as well as CT-based attenuation correction [3]. A detailed characterization of the eXplore VISTA system was described elsewhere [1] and performed in adaption to the NEMA NU2-2001 standards for human PET systems.

2.2.1. Spatial Resolution

The determination of the spatial resolution was performed using a ^{22}Na point source, 34kBq, with 0.3mm active diameter, embedded in a Plexiglas disc of 25mm diameter (the NEMA NU4 describes a Plexiglas cubus embedding the ^{22}Na source). The source was measured at 0, 5, 10, 15 and 25mm radial offset to the center of the FOV (cFOV) and at 0.25x length of the FOV away from the cFOV along the z-axis. Acquisition time was 5min and the measurements were performed for all three energy windows available. Data reconstruction was performed using a 2D filtered back projection (FBP) and a 2D ordered subset expectation maximization (OSEM) algorithm. The spatial resolution was determined as the full width at half maximum (FWHM) in all directions of the point spread function at each radial offset position.

2.2.2. Axial Sensitivity Profile and Absolute Central Point Source Sensitivity (ACS)

For the determination of the system sensitivity, the same ^{22}Na point source was used as described in the section 2.2.1. The source was measured along the z-axis in increments of 0.5mm. Acquisition time was 10s (100-700keV), 30s (250-700keV) and 40s (400-700keV) to reach a prompt coincidence rate of 10000 counts according to NEMA standards [2]. A background true event rate was determined with no source in the scanner for the same acquisition time as the point source measurements. The background (bgr) corrected prompt coincidence count rate was plotted against the axial position along the full axial FOV. Data was reconstructed using a 2D FBP algorithm (Ramp filter) and a region of interest (ROI) analysis was performed including all pixels within a radius of 1cm from the hottest pixel. The background corrected counts per second (cps) values arising from this ROI analysis were plotted against the axial position in the scanner as well.

The absolute central point source sensitivity (ACS) was calculated as follows:

$$ACS = \frac{\text{Coincidence Rate (cps)} - \text{Bgr (cps)}}{A \text{ (Bq)} \cdot \text{Branching Ratio}} \cdot 100$$

The Branching ratio of ^{22}Na is 0.906.

2.2.3. Scatter Fraction and Count Rate Performance

A line source filled with [¹⁸F]fluoride solution embedded in a solid cylinder of high density polyethylene simulating a rat (5x15cm) or a mouse body (2.5x7cm) was acquired with the cylinders positioned in the axial and radial center of the FOV (according to the NEMA NU4). The source was placed at a radial offset of 10mm and 17mm from the center for the mouse and the rat phantom, respectively. Data was acquired for approximately 17h in list mode format with subsequent framing into 20min frames. Measurements were performed with all three available energy windows. Background measurements were performed with empty line sources for an acquisition time of 20min. The list-mode data were rebinned into 2D sinogram sets of 20min each by single slice rebinning (SSRB). For each sinogram (transaxial bin size: 0.3785mm; slice thickness: 0.775mm), pixels located farther than 8mm from the edge of the phantom were set to zero. The profile of each projection angle was shifted to align the peak pixels with the center pixel of the sinogram. A sum projection for each slice and each frame was produced by adding 128 angular projections.

According to the NEMA standards, random and scatter counts were estimated by drawing a 14mm band around the central pixel. All counts farther away than 7mm from the center, as well as the linear interpolation between the count values of the pixels at the edges of the 14mm band were considered random, scatter (R_{r+s}) and intrinsic counts (R_{int}). Counts above the interpolation line within the 14mm band were regarded as true coincidences (R_t). Intrinsic counts were estimated from the background sinogram.

The scatter fraction for each slice was first determined for the final acquisitions j' , which showed count rate loss and random events below 1% of the event rate. It can be assumed that for these acquisitions the random event rate is negligible. The scatter fraction per slice (SF_i) was calculated as follows:

$$SF_i = \frac{\sum_{j'} R_{r+s,i,j'}}{\sum_{j'} R_{tot,i,j'}}$$

The random event rate ($R_{r,i,j}$) was calculated as follows:

$$R_{r,i,j} = R_{tot} - \left(\frac{R_{t,i,j}}{1 - SF_i} \right)$$

The scatter event rate ($R_{s,i,j}$), which was needed to calculate the scatter fraction, was determined as follows:

$$R_{s,i,j} = R_{tot,i,j} - R_{t,i,j} - R_{r,i,j} - R_{int,j}$$

The scatter fraction was calculated by dividing the scatter event rate by the sum of true and scatter event rate:

$$SF_j = \frac{R_{s,j}}{R_{t,j} + R_{s,j}}$$

The noise equivalent count (NEC) rate was determined by dividing the square of the true rate $R_{t,i,j}$ by the total count rate ($R_{tot,i,j}$).

$$R_{NEC} = \frac{R_{t,i,j}^2}{R_{tot,i,j}}$$

The system event rates were calculated by summing the individual event rates per slice and frame and plotted against the total activity (MBq) in the phantom.

2.2.4. Image Quality

The NEMA NU4 “image quality phantom” is a 50mm long, 30mm diameter cylinder from polymethylmethacrylate consisting of three parts: The fillable uniformity chamber (30mm long, 30mm diameter) enclosing two smaller, fillable cylinders (15mm long, 10mm outer diameter, 1mm wall thickness), which are attached to the lid and serve as containers of cold matter (non-radioactive water and air) and a third compartment consisting of a solid cylinder (20mm long, 30mm diameter) containing 5 fillable rods drilled through at a distance of 7mm of the cylinder center. The rod diameters are 1, 2, 3, 4 and 5mm, respectively. The phantom was filled with a start activity of 8.42MBq and images were acquired until the activity had decayed to 2.70MBq. This activity range covers the average amount of activity which is generally present in test animals at the scan start of *in vivo* PET scans. The NEMA guidelines suggest filling the phantom with 3.7MBq or with the amount of radioactivity which is generally applied in an average mouse study. Acquisitions time was 20min according to the NEMA NU4 and all three available energy windows (100-700keV, 250-700keV and 400-700keV) were investigated in an alternating fashion. Subsequent to the PET scans, a CT scan was performed with the radiographic source operated at 100 μ A and 40kV. CT data was reconstructed using the Feldkamp algorithm. PET

data was reconstructed by a 2D FBP algorithm (Ramp filter) and by a 2D OSEM (16 subsets, 2 iterations) algorithm with and without scatter, random and CT based attenuation correction. Image analysis was performed for all three phantom parts according to the NEMA NU4. In the center of the uniformity chamber, a volume of interest (VOI) of 22.5mm diameter and 10mm length was defined manually and the average concentration, the maximum and minimum values and the percentage standard deviation (%SD) were determined. In the rod region, the image slices covering the central 10mm length of the rods were averaged to obtain a single image slice of lower noise. Circular ROIs with twice the physical diameter of the individual rods were manually drawn around each rod. The maximum value of each of these ROIs was determined and divided by the mean value obtained in the uniformity test giving the recovery coefficient (RC) for each rod size. The RC can be defined as the measured radioactivity in a region divided by the true radioactivity (Keyes et al). In the center of the water- and air-filled non-radioactive compartments, cylindrical VOIs (7.5mm long and 4mm diameter) were defined and the ratio of the mean in each cold region to the mean of the hot uniform area was reported as spillover ratio (SOR).

2.2.6. Activity Outside of the Field of View

Due to the rather restricted size of the axial FOV of the eXplore VISTA (4.8cm), whole body acquisitions of test animals cannot be achieved within one bed position. Depending on the body distribution pattern of the applied tracer, a certain amount of radioactivity is located outside of the FOV. The impact of radioactivity outside of the FOV on the count rate was determined in static scans of an Eppendorf tube filled with 1mL [¹⁸F]fluoride solution of approx. 7MBq at the beginning of the measurement. The Eppendorf tube was positioned in the cFOV and measured for 5min, alternatively with no activity adjacent to the FOV or with an Eppendorf next to the FOV filled with a) double activity as in the FOV, b) 5 times the activity of the measured sample and c) 10 times the activity of the measured sample. The data was reconstructed using a 2D OSEM (16 subsets, 2 iterations) algorithm with scatter and random correction and the images were evaluated by a ROI analysis to determine a volume of approximately 1mL. The prompt coincidence rate and the count rate statistics (counts/sec/mL) of each acquisition with an Eppendorf tube was plotted against the true activity (MBq) in the Eppendorf tube at the start of the acquisition.

2.3. Results

2.3.1. Spatial Resolution

Figure 2.1 shows the spatial resolution of the 2D FBP (**A**) and 2D OSEM (**B**) reconstructed images of the ^{22}Na point source in radial (x), tangential (y) and axial (z) direction. The resolution in all three dimensions did not depend on the energy window chosen for data acquisition. Therefore, the values presented in **Figure 2.1** correspond to the average over all nine measurements, independent of the energy window. In the cFOV, the resolution was below 1.8mm and 0.9mm FWHM for FBP and OSEM reconstructed images, respectively. For both reconstruction types and all dimensions, the resolution was below 2.0mm within the central 2cm diameter FOV.

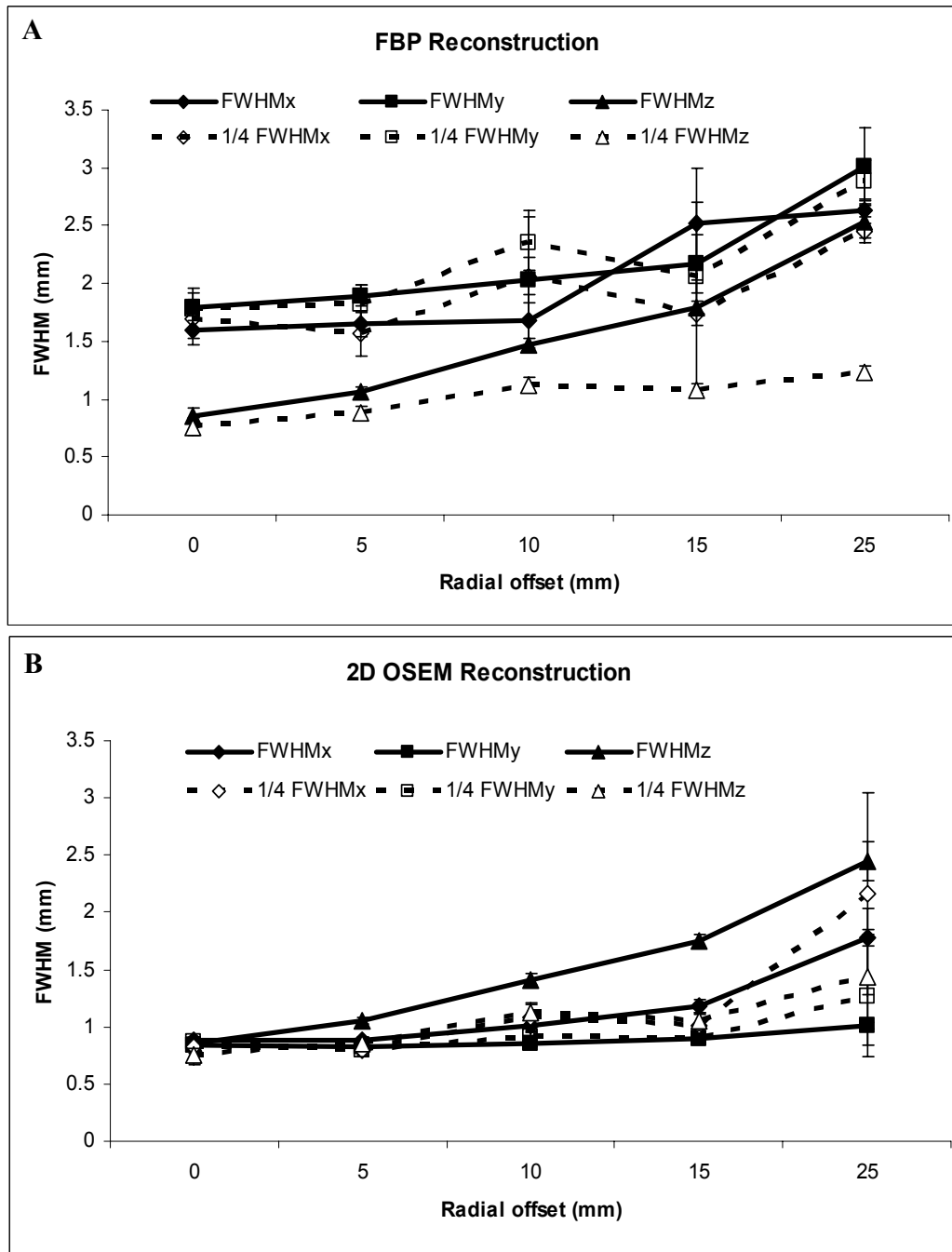


Figure 2.1. Resolution of reconstructed images (FWHM) of the eXplore Vista PET/CT system as a function of radial offset of the FOV. **A)** Axial, radial and tangential resolution for FBP reconstructed images. **B)** Radial (x), tangential (y) and axial (z) resolution for 2D OSEM reconstructed images. Solid lines correspond to offset positions in relation to the cFOV and dotted lines correspond to offset positions in relation to 1/4 of the axial FOV. n=9 acquisitions were performed per position (3 acquisitions per energy window).

2.3.2. Sensitivity

The absolute sensitivity of the point source measurement was plotted against the source position along the z-axis, as illustrated in **Figure 2.2**. The reason for the small bumps in the sensitivity profile is the small gap between the two detector rings of this dual-ring scanner [1]. The highest ACS (5.9%) was determined for the energy window 100-700keV. ACS values for 250-700keV and 400-700keV were 4.2% and 2.3%, respectively.

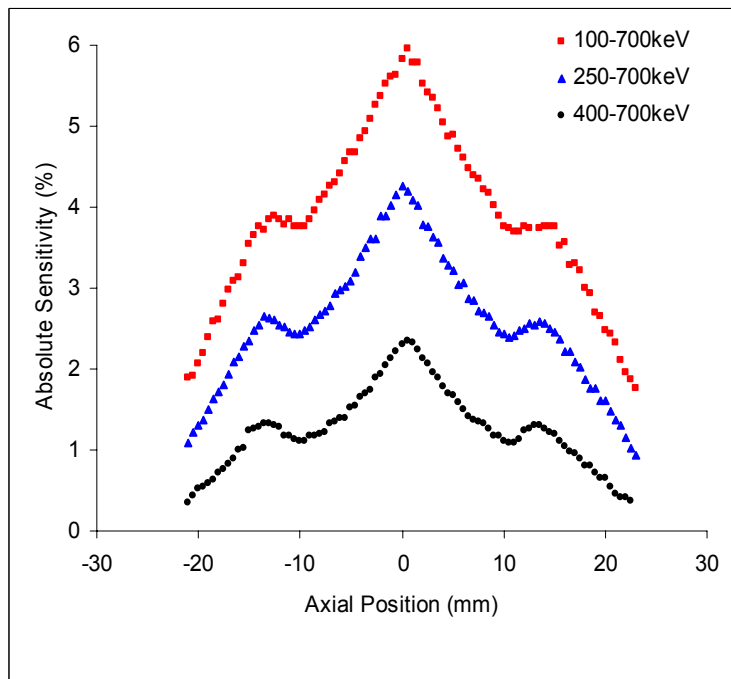


Figure 2.2. Absolute sensitivity profiles of the eXplore Vista PET/CT for all three energy windows as a function of ^{22}Na point source position along the z-axis.

2.3.3. Scatter fraction and Count Rate Performance

The scatter fractions for rat- and mouse-sized phantoms are listed in **Table 2.1**. The data show clearly that the bigger size of the rat phantom leads to almost a doubling of SF compared to the smaller mouse phantom.

Scatter fraction (SF) (%)	Mouse phantom	Rat phantom
100-700 keV	33.7	62.8
250-700 keV	25.6	42.4
400-700 keV	16.7	26.7

Table 2.1. SF for rat- and mouse sized phantoms over all three energy windows.

The event rate plots for total event, trues, randoms, scatter and NEC are depicted in **Figure 2.3**. Due to a system protection mechanism, it was not possible to measure higher activity than approximately 15MBq. This mechanism prevented the determination of the peak values for the described event rates. Nevertheless, the curves show how the individual event rates contribute to the total rate for mouse and rat phantoms. For the mouse phantom measured at 250-700keV, the scatter and random count rates correspond to 25% and 3% of the total count rate, respectively, whereas for the rat phantom, scatter and random rate were increased to 38% and 12% of the total rate (**Figure 2.3**). These values correspond well with the SF values determined for both phantom types (**Table 2.2**). The NEC rates for mouse and rat phantoms corresponded to 52% and 26% of the total count rate, respectively.

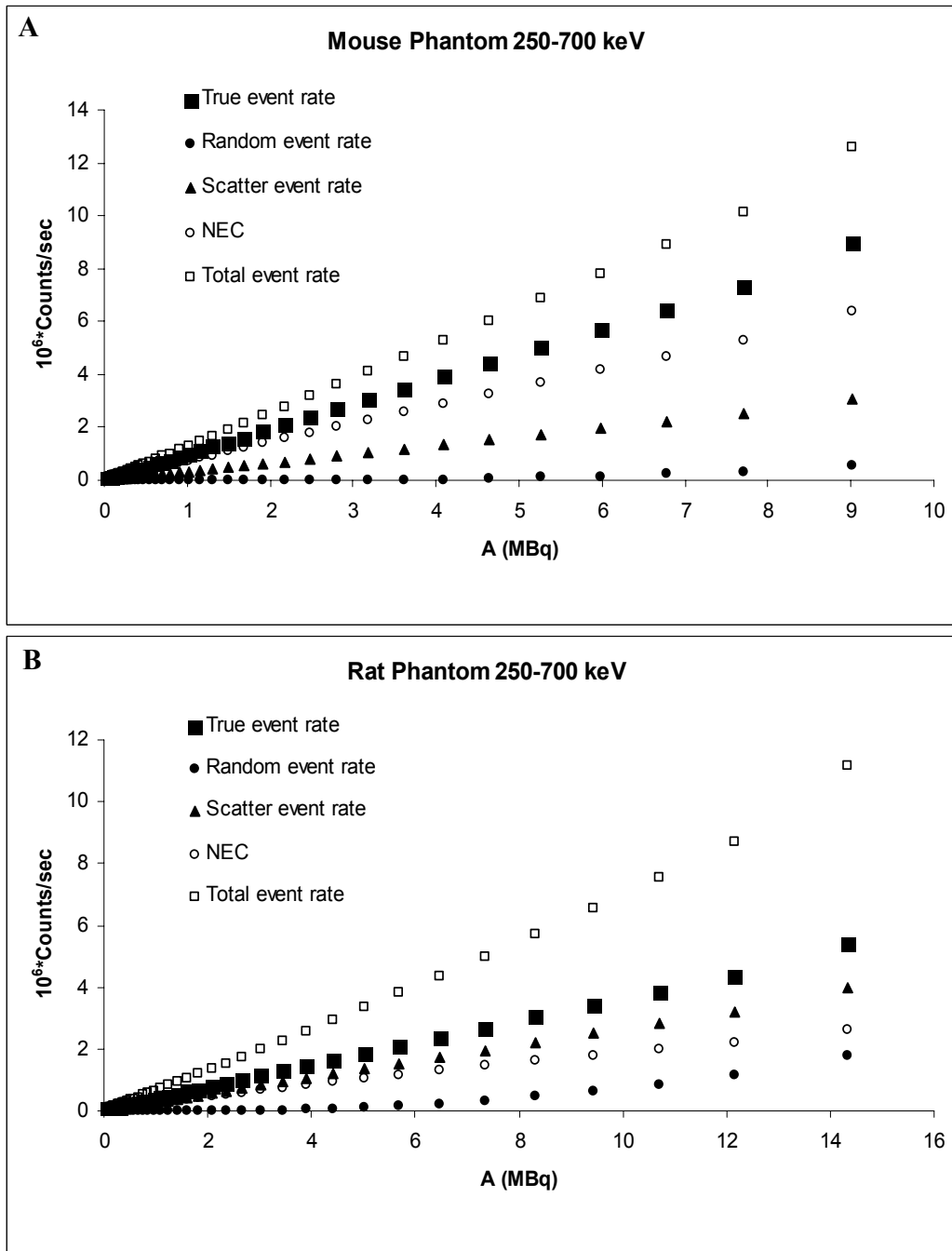


Figure 2.3. Event rates plotted against total activity in the measured phantom at an energy window of 250-700keV. A) Mouse phantom, B) Rat phantom.

2.3.4. Image Quality

Representative images of the NEMA image quality phantom are shown in **Figure 2.4**. An overview over all three compartments (uniformity chamber, rod compartment and spill-over compartment) is depicted in **Figure 2.4A**. The uniformity profile of the transversal uniformity chamber slice (**B**) is shown in **Figure 2.4C**. On the transversal slice of the rod compartment (**D**) the smallest rod (diameter 1mm) is hardly visible compared to the four rods with larger diameter.

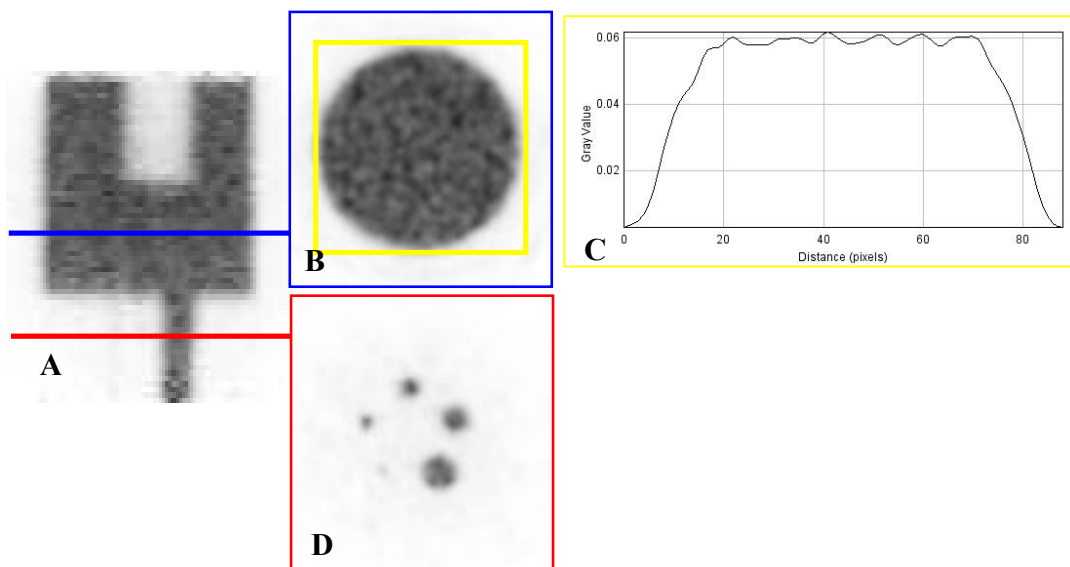


Figure 2.4. Representative coronal slice of the NEMA image quality phantom (**A**); a transversal view of the uniformity compartment (**B**) with corresponding profile across the slice (**C**), as well as a transversal slice of the rod compartment (**D**). The phantom was filled with 8.42MBq [^{18}F]fluoride solution and images were reconstructed by 2D OSEM algorithm including attenuation, scatter and random correction.

The uniformity, expressed as %SD of the averaged measured activity concentration within the uniformity compartment, was $7.4\pm 0.9\%$ for 2D OSEM reconstructed images and $13.6\pm 1.8\%$ for FBP reconstructed images, respectively ($P < 0.001$, **Figure 2.5**). There was a clear trend towards increased uniformity (decrease of %SD) with increasing activity. The energy window chosen for the image acquisition and the correction type (attenuation, scatter or random correction) applied during reconstruction did not impact the image uniformity.

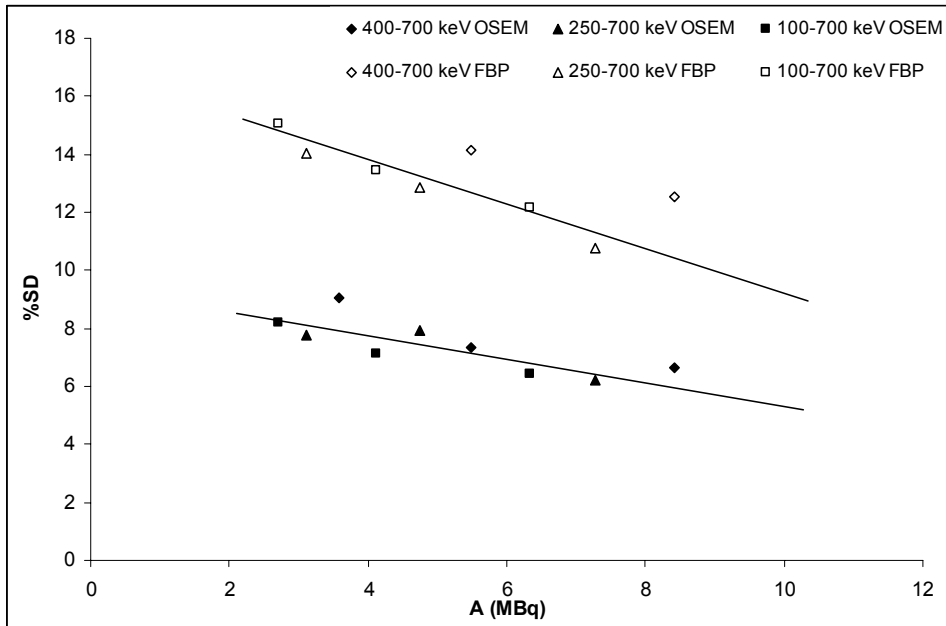


Figure 2.5. %SD of the averaged radioactivity concentration within the uniformity compartment of the image quality phantom reconstructed with 2D OSEM and FBP.

The RC indicates how much of the radioactivity effectively present in a certain region can be detected or recovered in the reconstructed image. The RCs for all 5 rods and both reconstruction methods are shown in **Figure 2.6**. The 2D OSEM method clearly leads to higher RCs than the FBP algorithm (24% higher in average over the rods of 2, 3, 4 and 5mm diameter). It was shown that attenuation correction was mainly responsible for the high RC values that were reached even for a rod diameter of 2mm (1.1 for 2D OSEM images and 0.6 for FBP images). Scatter and random correction did not have an impact on RC values (**Figure 2.6**). Uncorrected 2D OSEM reconstructed data gave RC values which were in a comparable range to FBP reconstructed data corrected for attenuation, scatter and random (**Figure 2.6**).

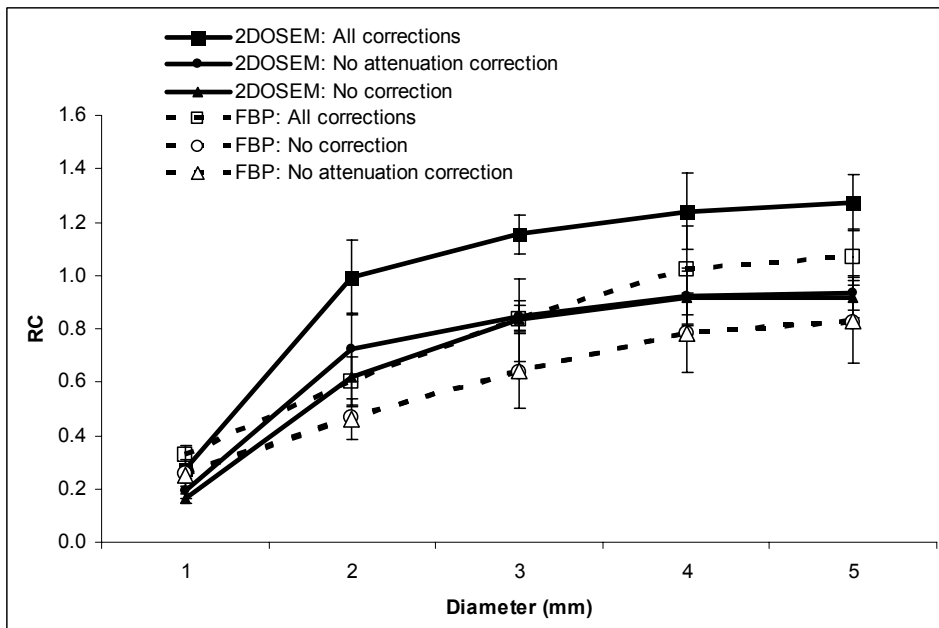


Figure 2.6. RCs for all 5 rods of the image quality phantom reconstructed with 2D OSEM (solid curves) and FBP (dotted curves) and corrected for attenuation, scatter and random (■); scatter and random (●) or none of the three (▲).

The SOR describes how the radioactivity concentration within a certain region is affected by radioactivity located in a neighboring region. The SOR was $15.5 \pm 1.4\%$ for the water-filled compartment and $14.6 \pm 1.3\%$ for the air-filled compartment after 2D OSEM reconstruction with attenuation, scatter and random correction. For the FBP reconstructed images corrected for attenuation, scatter and random, the SOR was $11.6 \pm 1.8\%$ and $11.3 \pm 1.5\%$ for the water- and air-filled compartments, respectively. For images reconstructed with scatter and random correction or no correction, the SOR for water was in a similar range as the SOR after attenuation correction ($13.8 \pm 1.8\%$ for 2D OSEM and $8.2 \pm 2.8\%$ for FBP after scatter and random correction; $14.9 \pm 2.1\%$ for 2D OSEM and $9.6 \pm 2.6\%$ for FBP without correction). However, for images not corrected for attenuation, the SOR for the air-filled compartment was approximately twice as high as the SOR for the water-compartment. Generally, SOR values for FBP reconstructed images were significantly lower than the ones arising from 2D OSEM data ($P < 0.001$).

2.3.5. Activity Outside of the Field of View

Due to the rather short axial FOV of the eXplore Vista PET (4.8cm) whole body scans of mice or rats cannot be achieved within one bed position. Therefore, during *in vivo* studies a certain amount of radioactivity is located outside of the FOV. Depending on the position of the animal within the FOV, this amount can be quite high. In order to determine the impact of activity located outside of the FOV during acquisition, an Eppendorf tube filled with a [¹⁸F]fluoride solution was positioned in the cFOV and scanned alternating with and without additional activity next to the FOV.

Analysis of the prompt coincidence rate clearly showed that amounts of radioactivity of approximately five times the dose located in the FOV in immediate vicinity to the FOV led to an overestimation of the detected prompt coincidence rate of more than 30% (**Figure 2.7A**). By reconstruction this overestimation was rectified; although it seemed that for high amounts of radioactivity outside of the FOV (e.g. 5 to 10 times as much as in the FOV), an underestimation of activity in the FOV (~10%) occurred (**Figure 2.7B**).

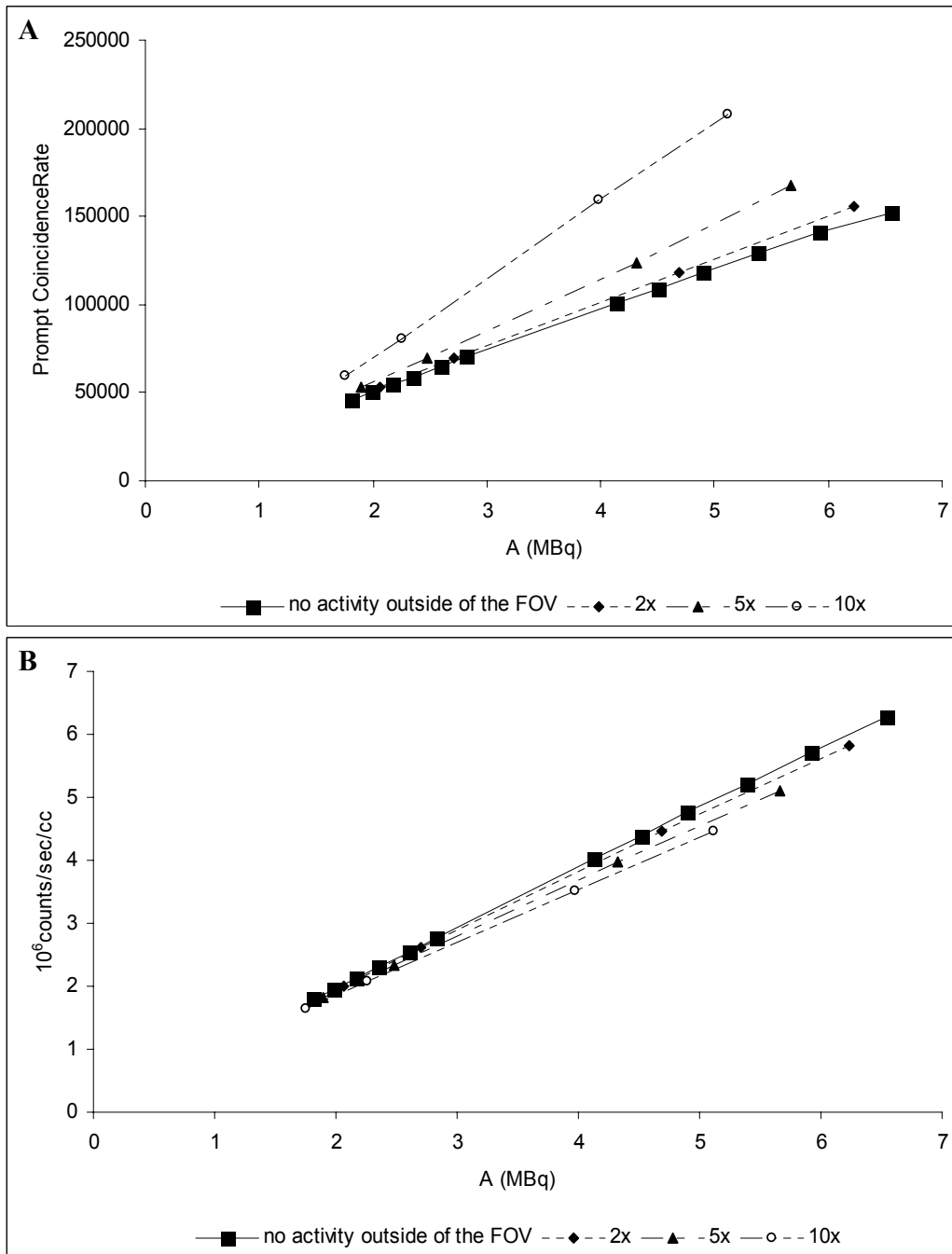


Figure 2.7. PET study to estimate the impact of activity located outside of the FOV on the acquired data. **A)** Prompt coincidence rate vs. activity in the FOV. **B)** Count rate statistics after reconstruction vs. activity in the FOV.

2.4. Discussion

The evaluation of the dual-ring version of the eXplore Vista PET/CT from GE Healthcare according to the NEMA standards for performance measurements of small animal PET tomographs suggests its suitability for reliable and semi-quantitative PET imaging of small animals. The data obtained in this study are in agreement with previous analyses of this scanner type [1, 4, 5]. Spatial resolution for FBP reconstructed data was better than 3.0mm FWHM in all determined dimensions and at all investigated locations of the FOV and better than 2.0mm FWHM in the central 2cm-diameter of the FOV. 2D OSEM reconstructed images showed superior spatial resolution, which was better than 2.5mm in all dimensions and all positions and better than 1.4mm within the central 2cm-diameter. This is in good accordance to Wang and co-workers who reported resolutions of better than 2.1mm in the whole FOV and better than 1.7mm in the central 2cm-diameter. The dedicated small animal tomographic systems manufactured by Siemens achieve spatial resolutions in a comparable range with better than 2.0mm in the central 4cm of the FOV (Inveon, [6, 7]), 2.4mm (microPET Focus 120, [8, 9]) and 2.6mm (microPET R4, [10]) in the central 2cm of the FOV. The quad-HIDAC small animal PET camera (Oxford Positron Systems) was reported to achieve the best spatial resolution in comparison with other small animal PET systems with a constantly high resolution of 1.1-1.2mm within the central 12cm of the FOV [11, 12]. The detector material of the 16 module quad-HIDAC consists of lead layers embedding the high-density avalanche chambers (HIDAC) [12, 13]. The resolution is determined by the size of the holes drilled into the lead (0.4mm diameter) rather than by the crystal size of the detector material, as it is the case for the tomographic systems developed by GE and Siemens with a crystal size of 1.45x1.45mm and 1.51x1.51mm for the eXplore Vista and the Inveon, respectively [1, 7], which may be one of the reasons for the superior resolution of the quad-HIDAC. The volumetric resolution determined for the eXplore Vista PET/CT was better than 2.5mm³ in the cFOV for FBP reconstructed data, which is well correlating with the 3.0mm³ after FBP reconstruction reported by Wang et al [1]. The spatial resolution of the scanner was independent of the energy window chosen for data acquisition.

The scanner sensitivity profile confirmed the very characteristic pattern for this type of tomograph presented earlier by Wang and co-workers and Espana and colleagues [1, 5]. The two bumps at an approximate distance of ¼FOV distance from the cFOV to both directions arise

from the small gap between the two detector rings of the dual-ring version of this scanner model. Absolute central point source sensitivity (ACS) was 5.9% (100-700keV), 4.2% (250-700keV) and 2.3% (400-700keV), depending on the energy window chosen. These results correspond well with the data found in the literature [1, 4, 5]. Wang et al reported 6.5%, 4.0% and 2.1% for the three energy windows, respectively [1]; Spinelli et al. found 5.9%, 3.9% and 2.2%. Espana reported an ACS value of 2.1% for an energy window of 250-700keV [4, 5]. Deviations between the ACS values of this and previous studies were in an acceptable range of $\pm 10\%$ and might be explained by the fact that the studies by Wang et al. and Espana et al. were not performed with exactly the same type of phantoms as they are described in the NEMA NU 4-2008 (e.g. ^{18}F vs. ^{22}Na) [1, 5]. For the small animal PET scanners from Siemens, the peak sensitivities reported were 10% (250-625keV) and 7.1% (250-750keV) for the Inveon and the microPET Focus 120 scanner, respectively [7, 8], which is substantially higher than the sensitivity of the eXplore Vista from GE Healthcare. The increased sensitivity of the Siemens systems might arise from the shorter attenuation length of the lutetium orthosilicate (LSO) crystals compared to the LYSO crystals used for the eXplore Vista (2.0cm vs. 1.169cm [14]). Nevertheless, the ACS of 4.3% of the 250-700keV window seems sufficiently high for reliable *in vivo* studies, as it has been proposed by Myers et al that the sensitivity of small animal scanners should reach at least 1% to achieve a an acceptable signal-to-noise ratio [15]. Even the HIDAC system with an ACS of around 1% therefore provides sufficient sensitivity [13, 12].

Count rate measurement did not result in peak value determination due to the automatic abortion of acquisition at activity doses higher than approximately 15MBq in the FOV. As the average small animal PET experiment at ETH Honggerberg does not require the injection of higher doses than 15MBq, it is assured that the acquired data are in the linear range of the system. The SFs for mouse-sized phantoms were in high correlation with the values reported by Wang et al and by Espana et al [1, 5]. For the three energy windows SF was 33.7% (100-700keV), 25.6% (250-700keV) and 16.7% (400-700keV). Wang and colleagues found SFs of 33.0%, 26.6% and 18.9% for the three energy windows, respectively [1], and Espana and co-workers reported values of 33%, 27% and 19% [5]. The deviation between values of the smallest energy window was in an acceptable range of 11%, and might be explained by the fact that the studies by Wang and colleagues and Espana and co-workers were not performed using exactly the same protocol as described in the NEMA NU 4-2008 (off axis positioning of the line source was slightly different)

[1, 5]. For the rat-sized phantoms, the differences between the data generated in this study and the data reported by Wang et al and Espana et al are even more striking: 62.8% (100-700keV), 42.4% (250-700keV) and 26.7% (400-700keV), compared to 48.3%, 37.0% and 29.2%, respectively, found by Wang et al. [1]. The values reported by Espana et al were 48%, 37% and 29% for all three energy windows, respectively [5]. The line source position difference in the rat phantoms of the individual studies was bigger than the difference in the mouse phantom; this might be the reason for the higher deviation of the results between this study and the ones by Wang and colleagues. The SF values reported by Bao et al. for the Inveon scanner from Siemens were substantially smaller; for the energy window of 350-625keV a SF of 7.8% and 17.2% were achieved for mouse- and rat-sized phantoms, respectively [7]. The SFs reported for the microPET Focus 120 are comparable with the ones of the Inveon [8]. For a mouse-sized phantom SFs of 8.2% (350-650keV) and 12.3% (250-750keV) were determined. The rat-sized phantom SFs were 17.6% and 26.3% for the two energy windows, respectively. For the quad-HIDAC, a mouse-sized phantom SF of 29% was reported for an energy window of 200-700keV [12], which is slightly higher than the one determined for the eXplore Vista. Possibly, the high energy resolution of the eXplore Vista crystals (26% and 33% for the LYSO and GSO crystals, respectively [1]) helps to reduce the detection of scattered events more efficiently than the HIDAC. It might also be possible that the lead detectors of the HIDAC contribute more to the amount of scattered events [11] than the crystal detectors of the eXplore Vista.

The NEMA uniformity study of the eXplore Vista showed that the 2D OSEM reconstruction resulted in better uniformity of images with only 7.4% deviation compared to 13.6% for FBP reconstructed images. The applied corrections (scatter, random and attenuation) and the energy windows chosen did not impact the image uniformity. 2D OSEM reconstructed uniformity for the eXplore Vista was in a comparable range with the one determined for the Inveon scanner (5.29%) and the microPET Focus 120 (6.24-8.8%) [7, 16]. Generally, it was found that with decreasing amount of radioactivity the uniformity was decreasing, which is explained by the reduced count rate performance leading to increased image noise.

RC values were crucially increased after attenuation correction. In the case of 2D OSEM reconstructed images, RCs exceeded 1 for all rod sizes >2mm diameter after attenuation, scatter and random correction compared with a RC 0.94 for a rod size of 5mm diameter with scatter and random correction only. For FBP reconstructed images, the RCs after attenuation, scatter and

random correction were in a similar range as the ones of the scatter and random corrected 2D OSEM data. These findings are in line with the results of Bahri and colleagues who stated that 2D OSEM reconstruction produced the highest RCs, whereas FBP reconstruction using a Ramp filter produced the lowest [16]. Moreover, the RCs determined for FBP reconstructed images were comparable to those reported for the Inveon and the microPET Focus 120 [6, 16]. For 2D OSEM reconstructed images, the results determined for the eXplore Vista were similar to the RCs resulting from the MAP reconstructed data of the Inveon [6].

SOR values determined in the air- and water-filled compartments with the eXplore Vista amounted to 11-15% for 2D OSEM and FBP reconstructed data in water and air and turned out to be high compared to the ones reported for the Inveon (-0.6-1.7% [7] and 1-6% [6]) and the microPET Focus 120 (-16.3-4.5% [16]). Attenuation correction was found to have a crucial impact on the SOR determined in the air-filled compartment. Uncorrected images or scatter and random corrected images resulted in similar SOR values. The SORs for air were approximately twice as high as the ones for water. Attenuation correction reduced the SOR values for air of approximately half, such that the SORs for water and air were brought to a comparable range. The SOR did therefore no longer depend on the cold material after attenuation correction. Generally, it can be stated that FBP reconstruction resulted in lower SOR values (25-40%, $P < 0.001$) for water- and air-filled compartments.

The impact of radioactivity located outside of the FOV was investigated due to the rather restricted axial FOV of the eXplore Vista PET/CT of 4.8cm, which does not allow a whole body mouse scan within one bed position. Depending on the body region of interest, it might happen that considerable amounts of activity are located in very close vicinity to this region but outside of the FOV. In this study, it was shown that the clearly overestimated prompt coincidence rate due to activity outside of the field of view was accounted for during the reconstruction process. For very high doses in close vicinity to the FOV (approximately 5 to 10 times the activity located in the FOV), there was even an underestimation of counts obtained after reconstruction. By investigating the activity distribution of several standard tracers in mice, it was found that such high amounts of activity are normally not located outside of the FOV during animal studies. Generally, for standard tracers like [^{18}F]FDG, which distribute all over the animal body, there are approximately the same amounts of radioactivity found in the upper abdominal region with the head as in the lower abdominal region. For example, total counts from the bladder were

approximately equal to the total counts from the heart and the head region including brain and Harderian glands (data not shown).

2.5. Conclusion

The eXplore Vista PET/CT tomograph from GE Healthcare is a dedicated preclinical PET system for the accurate imaging of small animals with high resolution and high sensitivity. The NEMA NU4-2008 standards allow a direct comparison with other dedicated small animal PET systems and it was shown that the eXplore Vista achieved competitive results. It is suggested to acquire small animal PET data with the eXplore Vista in the middle energy window of 250-700keV, which guarantees a sufficiently high sensitivity at high resolution and moderate scatter fraction. The 2D OSEM reconstruction algorithm seems to be superior compared to the FBP algorithm, resulting in increased RCs and higher uniformity. Application of scatter and random correction seems advisable due to the rather high SF. In the future, it might be worthwhile to investigate how the possibility of the 3D-OSEM reconstruction accounts for even better performance of the eXplore Vista PET/CT.

2.6. References

- [1] Wang Y, Seidel J, Tsui BMW, Vaquero JJ, Pomper MG. Performance evaluation of the GE Healthcare eXplore VISTA Dual-ring small-animal PET scanner. *J Nucl Med.* 2006;47:1891-1900
- [2] National Electrical Manufacturers Association (NEMA). Performance measurements of small animal positron emission tomographs. NEMA Standards Publication NU 4-2008. Rosslyn, VA: NEMA; 2008
- [3] Vista-CT User Manual, Version 4.0, GE Healthcare, 2007
- [4] Spinelli AE, D'Ambrosio D, Pettinato C, et al. Performance evaluation of a small animal PET scanner. Spatial resolution characterization using 18F and 11C. *Nucl Instrum Methods Phys Res A.* 2007;571:215-218
- [5] Espana S, Herraiz JL, Vicente E, et al. Validation of PeneloPET against two small animal PET scanners. *IEEE.* 2007;M18-382
- [6] Diesselhorst JA, Brom M, Laverman P, et al. Image-quality assessment for several positron emitters using the NEMA NU 4-2008 Standards in the siemens inveon small-animal PET scanner. *J Nucl Med.* 2010;51:610-617
- [7] Bao Q, Newport D, Chen M, Stout DB, Chatziioannou AF. Performance evaluation of the inveon dedicated PET preclinical tomograph based on the NEMA NU-4 Standards. *J Nucl Med.* 2009;50:401-408
- [8] Laforest R, Siegel S, Newport DF, Yap J. Performance evaluation of the microPET[®] – Focus-F120. *IEEE Trans Nucl Sci.* 2007;54:42-49

- [9] Kim JS, Lee JS, Im KC, Kim SJ, et al. Performance measurement of the microPET Focus 120 Scanner. *J Nucl Med.* 2007;48:1527-1535
- [10] Knoess C, Siegel S, Smith A, et al. Performance evaluation of the microPET R4 PET scanner for rodents. *Eur J Nucl Med Mol Imaging.* 2003;30:737-747
- [11] Schäfers KP, Reader AJ, Kriens M, Knoess C, Schober O, Schäfers M. Performance evaluation of the 32-module quadHIDAC small-animal PET scanner. *J Nucl Med.* 2005;46:996-1004
- [12] Missimer J, Madi Z, Honer M, Keller C, Schubiger A, Ametamey SM. Performance evaluation of the 16-module quad-HIDAC small animal PET camera. *Phys Med Biol.* 2004;49:2069-2081
- [13] Jeavons AP, Chandler RA, Dettmar CAR. A 3D HIDAC-PET camera with sub-millimeter resolution for imaging small animals. *IEEE Trans Nucl Sci.* 1999;46:468-473
- [14] Vallabhajosula S. Molecular imaging: radiopharmaceuticals for PET and SPECT. Springer-Verlag Heidelberg. 2009;p64
- [15] Myers R, Hume S. Small animal PET. *Eur Neuropsychopharmacol.* 2002;12:545-555
- [16] Bahri MA, Plenevaux A, Warnock G, Luxen A, Seret A. NEMA NU4-2008 image quality performance report for the microPET Focus 120 and for various transmission and reconstruction methods. *J Nucl Med.* 2009;50:1730-1738

3. Reproducible Small Animal PET

3. Comparison of Standardization and Heterogenization Approaches Towards Reproducible Small Animal PET Data

3.1. Introduction

Small animal positron emission tomography (PET) is a frequently used methodology to investigate murine models of healthy and diseased states. Preclinical PET has been revolutionized with the development of dedicated small animal PET scanners [1-3]. Non-invasive imaging methods like PET are considered to give more reliable results in longitudinal follow-up studies where animals can be used as their own control compared to studies where test and control animals are not identical [1, 4]. Additionally, strict standardization of experimental parameters is believed to reduce variability within test groups and to increase reliability of animal experiments [5, 6]. Nevertheless, recent investigations on mouse behavior revealed that the rate of false positive outcome was significantly higher under standardized conditions compared to an approach investigating pseudo-heterogenized groups [7]. Standardization proved to decrease the reproducibility of results among test groups. It is therefore suggested to heterogenize test groups in a controlled manner in order to increase external validity of results [7-10]. On the other hand, only standardization of test groups guarantees the detection of environmental influences on experimental outcome [6].

In this study, two representatives of different PET tracer categories were investigated as exemplary tracers. The glucose analogue, [¹⁸F]FDG, is the most frequently used PET tracer in the clinic and a “metabolic” tracer. Previous studies in the field of small animal PET have shown that the following experimental parameters crucially impact biodistribution of [¹⁸F]FDG: anesthetic agents, carrier gas, fasting, ambient temperature and injection type [11-16]. The dopamine D₂ receptor ligand [¹⁸F]fallypride {(S)-N-[(1-allyl-2-pyrrolidiny)methyl]-5-(3-¹⁸F-fluoropropyl)-2,3-dimethoxybenzamide} is a representative of a radioligand binding reversibly to a site on a neurotransmitter receptor. [¹⁸F]Fallypride shows excellent binding properties (high affinity and selectivity) and imaging characteristics for the visualization of the dopamine D₂ receptor subtype [17-19].

The inherent variability of [¹⁸F]FDG and [¹⁸F]fallypride organ uptake within and between individual animals was assessed using a highly standardized protocol. Moreover, experimental

factors were determined, which might essentially impact the outcome of [¹⁸F]FDG and [¹⁸F]fallypride rodent studies and therefore may require strict standardization. For example, ethanol is often required for tracer formulation and its potential impact as a vehicle on tracer distribution and elimination is not well characterized. Finally, the benefit of standardization over heterogenization on variability of [¹⁸F]FDG biodistribution was evaluated for an experimental setting with varying parameters: age, gender and cage occupancy.

3.2. Materials and Methods

3.2.1. Animal Preparation

Healthy animals were purchased from Charles River, Germany. The investigated strains were NMRI mice, C57Bl/6J mice and Crl:CD(SD) rats with gender, age and group size as listed in **Table 3.1**.

Animal care and experimental procedures were performed in accordance with and approved by the Swiss Federal Veterinary Office. Animals were kept in standard cages (groups of 2-13 animals per cage) in a Scantainer (Scanbur, Denmark) equipped with a filter cover. Ambient temperature was set to 23°C and air humidity was between 50 and 85%. Free access to food (Alleinfuttermittel for rats and mice, KLIBA NAFAG, Switzerland) and water was allowed throughout all experiments. A light-dark cycle of 12h (dark phase: 6pm - 6am) was maintained throughout all studies. Animal monitoring and cage changes were performed weekly by the experimenter or a professional animal care taker. Experiments were started between 7 and 9am involving two experimentators.

Strain	n	Anesth. Protocol			Temp. control	10% EtOH	Gender		Age			Cage density	
		Control (6min)	40min	60min	33°C	yes	m	f	5 weeks	7-10 weeks	14 weeks	n=2/cage	n=13/cage
SD rats	6	x					x						
SD rats	7		x				x						
SD rats	7			x			x						
NMRI mice	8		x				x			x			
NMRI mice	8		x		x		x			x			
NMRI mice	8		x			x	x			x			
NMRI mice	8		x		x	x	x			x			
NMRI mice	10		x				x		x			x	
NMRI mice	10		x				x				x	x	
NMRI mice	11		x				x		x				x
NMRI mice	11		x				x				x		x
NMRI mice	9		x					x	x			x	
NMRI mice	8		x					x			x	x	
NMRI mice	11		x					x	x				x
NMRI mice	12		x					x			x		x

Table 3.1. Test parameters of individual experiments. Three main experiments were performed, investigating: a) impact of anesthetic protocols (yellow) b) influence of ambient temperature and 10% ethanol in the tracer solution (orange) c) effect of gender, age and cage occupancy of test animals (grey).

3.2.2. Radiotracer Application

[¹⁸F]FDG was obtained from the commercial [¹⁸F]FDG production of the University Hospital Zurich in batches of 1-2GBq/mL.

The radiosynthesis of [¹⁸F]fallypride was performed according to the protocol of Mukherjee et al. [14]. The radioligand was produced in batches of 500-5000MBq, with activity concentrations of 500–2000MBq/mL and specific activities between 54 and 260GBq/μmol at the end of synthesis. Radiotracer injection into rats was performed using the Vasofix[®]Braunüle[®] (Braun AG) catheter. Tail vein injections of ~15MBq [¹⁸F]FDG in 300μL physiological NaCl solution (Braun AG) were followed by rinsing the catheter with 150μL physiological NaCl solution. In mice, ~15MBq [¹⁸F]FDG in 100μL physiological NaCl solution were directly injected into the tail vein. Likewise, [¹⁸F]fallypride was injected into mice via direct tail vein injection of 100μL. In order to keep the injected cold mass constant, decreasing radioactive doses of [¹⁸F]fallypride were

injected over each test day (between 18 and 2MBq). Over all studies, the injected cold mass of [¹⁸F]fallypride was between 20 to 130ng corresponding to 1.5-9.0nmol/kg body weight.

3.2.3. Small Animal PET Imaging

All PET experiments were performed at the Animal Imaging Center, Center for Radiopharmaceutical Sciences at ETH Zurich using the dedicated 36-module eXplore Vista-PET/CT tomograph (GE Healthcare) with a maximum resolution of higher than 2mm full width at half maximum (FWHM) and a field of view (FOV) with an axial length of 48mm and a diameter of 67mm [20]. Animals underwent one bed position scans with the brain in the center of the FOV or two bed positions for whole body scans.

a) Static PET scanning protocol

Animals were restrained and injected 30min ([¹⁸F]FDG) and 20min ([¹⁸F]Fallypride) before scan start. The urinary bladder was emptied by pressing the lower abdomen before induction of anesthesia 10min before scan start and animals were then fixed on the bed of the scanner. Isoflurane was used as anesthetic agent of choice with oxygen/air (50%/50%) as carrier gas. Data were acquired from 30-60min post injection (p.i.) for [¹⁸F]FDG emission scans and from 20-60min p.i. for [¹⁸F]fallypride emission scans (energy window 250-700keV). Images were reconstructed using a 2D OSEM algorithm (2 iterations, 16 subsets) with scatter and random correction, no attenuation correction was performed. Voxel size of reconstructed images was 0.3875x0.3875x0.775mm³.

b) Dynamic PET scanning protocol

Animals were anesthetized and an injection catheter (Vasofix[®]Braunüle[®] (Braun AG), 22G, 0.9x25mm) was placed in a lateral tail vein and rinsed with 100μL Heparin solution (Heparin-Na (Bichsel AG, Switzerland), 25000 I.E./5mL) before animals were positioned on the scanner bed. Tracer injection and PET scan start were performed simultaneously. Data was acquired from 0-60min p.i. for [¹⁸F]FDG emission scans in the list mode format (energy window 250-700keV). Data were split into two time frames of 30min each and images were reconstructed as described above. For dynamic scanning protocol only the second 30min frame was further investigated. Reconstructed images were inspected in coronal, sagittal and horizontal planes throughout the reconstructed volume. Region of interest (ROI) analysis was performed with the biomedical image quantification software PMOD (Pmod Technologies Ltd, Adliswil Switzerland) [21].

ROIs were drawn manually using whole brain for [¹⁸F]FDG studies and striatum for [¹⁸F]fallypride studies. Tracer uptake was quantified as standardized uptake value (SUV) by normalizing the average activity concentration (counts/sec/mL) of each volume of interest (VOI) to the injected dose per body weight (MBq/kg).

3.2.4. Quantification of *ex vivo* Tissue Uptake

Subsequent to PET imaging, animals were euthanized by decapitation at approximately 61min p.i. Organs were collected, the wet weights were determined and organs were measured by classical gamma counting (Wallac 1480 Wizard, Perkin Elmer). Radiotracer uptake was expressed as percentage of injected dose per g tissue normalized to the body weight of the animals (norm. %ID/g) and calculated as follows: organ activity (counts per minute)·100/[injected dose (counts per minute)·organ weight (g)]/body weight (kg).

3.2.5. Measurement of Physiological Parameters

Body temperature of all animals under isoflurane anesthesia was monitored using a rectal temperature sensor. A stream of warm air was blown through the scanner tube to avoid hypothermia during anesthesia and to keep body temperature constantly between 35 and 37°C. Depth of anesthesia monitoring was achieved by sensing the breath rate with an abdominal breathing belt (rats) or by visual breath rate counting (mice). The breath rate was kept constant at a rate of ~60 breaths per minute (bpm) by adjustment of anesthesia.

3.2.6. Assessment of Test-Retest Variability of [¹⁸F]FDG Whole Brain and [¹⁸F]Fallypride Striatum Uptake

Three static PET scanning experiments were performed for each individual animal of a group to assess the variability between brain scans of the same animal (intra-animal variability) and scans of different individuals (inter-animal variability). Between scans, animals underwent one week of recovery. [¹⁸F]FDG scans were performed with SD rats (male, 200-300g, n=6-7) and [¹⁸F]fallypride scans with NMRI mice (male, 34-39g, n=7) and C57Bl/6J mice (male, 18-26g, n=7). Variability of tracer uptake to brain (¹⁸F]FDG) or striatum (¹⁸F]fallypride) was calculated as coefficient of variation (COV), corresponding to the relative standard deviation of the mean.

3.2.7. Influence of Experimental Parameters on [¹⁸F]FDG and [¹⁸F]Fallypride Biodistribution

To determine the impact of different experimental parameters on [¹⁸F]FDG biodistribution, animals underwent static or dynamic PET scanning. Animals were sacrificed by decapitation at 61min p.i., organs were collected and measured by classical gamma counting (Wallac 1480 Wizard, Perkin Elmer).

Individual test parameters of experiments are listed in **Table 3.1**.

a) Anesthetic protocols (male SD rats, 220-280g, n=6)

The impact of anesthetic protocols on [¹⁸F]FDG organ uptake was investigated by applications of isoflurane anesthesia of different duration (0-61min p.i. for dynamic PET scanning, 20-61min p.i. for static PET scanning and 55-61min p.i. as control conditions).

b) Temperature (male NMRI mice, 18-46g, n=8)

Animals underwent a static PET scanning protocol. Temperature control during [¹⁸F]FDG uptake phase (0-20min p.i.) was achieved by placing the animal under an infrared lamp subsequent to tracer injection. The temperature at the position of the animal was 33°C. Control animals were kept in the same room at 23°C.

c) EtOH in the administered tracer solution ([¹⁸F]FDG: male NMRI mice, 18-46g, n=8; [¹⁸F]fallypride: male C57Bl/6J mice, 20-25g, n=8)

[¹⁸F]FDG or [¹⁸F]fallypride were injected in physiological saline solution containing 10% of EtOH (v/v). This amount corresponds to a blood concentration of approximately 4‰ ethanol for a mouse of average size. Tracer solutions injected to control animals did not contain 10% EtOH. Experimental handling and data collection and interpretation were performed in a blinded fashion.

3.2.8. Analysis of Standardization vs. Pseudo-Heterogenization

Investigation of the benefit of standardization over heterogenization of test groups was performed according to the study of Richter and co-workers (**Figure 3.1**) [7]. Static [¹⁸F]FDG whole body scans were performed with eight groups of NMRI mice under different standardized conditions. Animals were sacrificed subsequent to the PET scan (61min p.i.), 19 organs were collected and measured by classical gamma counting. The data of all 4x8 animals of each gender

3.2.9. Statistical Analysis

Figures show mean±SD, unless stated otherwise. Differences among experimental groups in SUVs and %ID/g values of the various tissues investigated were statistically evaluated by analysis of variance (ANOVA) and subsequent post hoc Tukey tests for comparisons of three or more groups and by two-tailed student's t-tests for comparisons of two groups. Statistical significance was set at the 95% level and Bonferroni correction was applied where required. All statistical analyses were performed using the computer software SPSS 15.0 version for Windows (SPSS-inc. Chicago, Illinois, 1994).

3.3. Results

3.3.1. Test-Retest Variability of [¹⁸F]FDG Brain Uptake and Striatal Uptake of [¹⁸F]Fallypride

Brain and striatum uptake variability of [¹⁸F]FDG and [¹⁸F]fallypride were determined in highly standardized test-retest studies. Test-retest variability (COV) of [¹⁸F]FDG brain uptake was calculated from brain SUVs of one group of animals scanned three times with one week recovery between scans. The study was performed with two independent batches of animals to determine inter-study variability. The different variability types are illustrated in **Figure 3.2A**. Inter- and intra-animal variability of [¹⁸F]FDG brain uptake did not differ significantly, 8±2% (inter-animal COV) compared to 10±4% (intra-animal COV) for the first study and 14±7% (inter-animal COV) compared to 21±10% (intra-animal COV) for the second study. By trend, intra-animal variability was greater than inter-animal variability. Repetition of the test-retest set-up resulted in an inter-study variability of 10±6% for [¹⁸F]FDG brain uptake. The difference in [¹⁸F]FDG brain uptake of the second test days of the two studies proved to be significant (16 and 24%, P<0.05, **Figure 3.2B**).

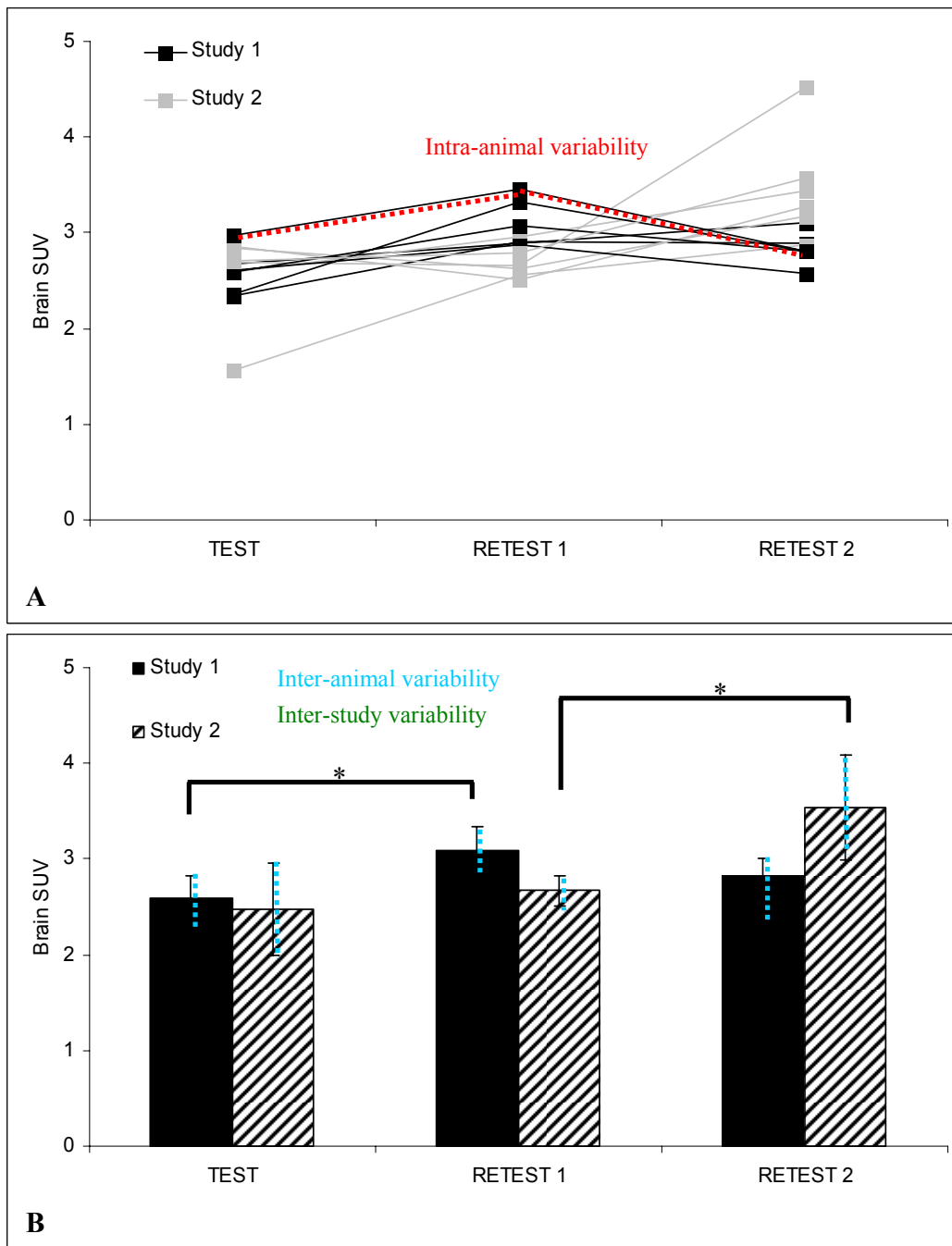


Figure 3.2. **A)** Different types of variability of [¹⁸F]FDG brain uptake in male Crl:CD(SD) rats (n=6). Each data point corresponds to the [¹⁸F]FDG brain SUV of one individual animal. Intra-animal variability: the variability between three brain scans of one individual (indicated in red). **B)** Column bar representation of the data from **A)**. Inter-animal variability: the variability between brain scans of different individuals acquired on the same test day (represented by the SD, indicated in blue). Inter-study variability: the variability of [¹⁸F]FDG brain scans between two independent test groups acquired under exactly the same experimental conditions (indicated in green). *P<0.05.

Inter- and intra-animal variability of [^{18}F]fallypride striatum uptake did not differ significantly, $16\pm 4\%$ (inter-animal COV) compared to $23\pm 8\%$ (intra-animal COV) for C57Bl/6J mice and $11\pm 4\%$ (inter-animal COV) compared to $9\pm 8\%$ (intra-animal COV) for NMRI mice. Likewise, [^{18}F]fallypride striatum uptake between individual test days did not differ significantly, whereas NMRI mice tended to accumulate more [^{18}F]fallypride in the striatum than C57Bl/6J mice; on the third test day, the difference was significant (**Figure 3.3**). Strain differences also occurred concerning accumulation of [^{18}F]fallypride in the eye region. The very high [^{18}F]fallypride accumulation in the eye region observed in C57Bl/6J mice was due to a non-blockable uptake or binding to the retina (unpublished results from autoradiography experiments). This phenomenon was not observed in NMRI mice, [^{18}F]fallypride accumulation in the eye region was in the background range, comparable with cerebellum uptake (**Figure 3.3**).

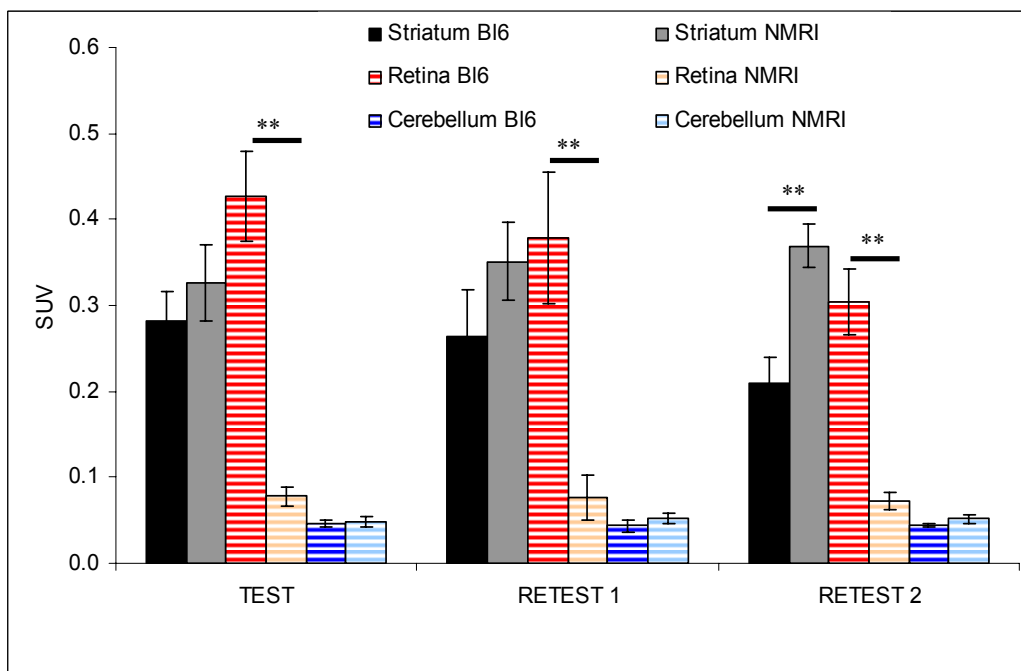


Figure 3.3. [^{18}F]Fallypride uptake to striatum, retina and cerebellum (expressed as SUV). Solid: striatum; red striped: retina; blue striped: cerebellum. NMRI mice (light colors): $n=6$; C57Bl/6J mice (dark colors): $n=7$. *** $p < 0.001$.

3.3.2. Impact of Experimental Parameters on [¹⁸F]FDG and [¹⁸F]Fallypride Tissue Distribution

Experimental parameters such as type of anesthetic agent and ambient temperature of the animal during tracer uptake proved to influence [¹⁸F]FDG tissue distribution crucially [11]. In this study, the impact of duration of isoflurane anesthesia, ambient temperature (33°C vs. 23°C) during the first 20min of [¹⁸F]FDG uptake and the addition of 10% ethanol to the administered [¹⁸F]FDG and [¹⁸F]fallypride solution was investigated. Extreme differences in ambient temperature and ethanol concentration were chosen to determine whether strict standardization of these parameters is necessary to achieve reliable results with variabilities in a range as described in section 3.3.1.

The anesthetic protocol (static vs. dynamic) had a significant impact on [¹⁸F]FDG uptake in several organs. [¹⁸F]FDG brain uptake of animals anesthetized during the whole tracer uptake phase (dynamic protocol) was reduced by 27% compared to animals investigated under static conditions (P<0.01). The static protocol resulted in a 17% reduction of brain uptake compared to the control group which was not scanned (short anesthesia of 6min for humane decapitation; P<0.01). [¹⁸F]FDG muscle uptake showed a similar pattern as brain uptake with highest uptake under control conditions (P<0.01). Contrary to these findings, [¹⁸F]FDG blood concentration was lowest in the control and highest in the “dynamic” test group (P<0.01), as shown in **Table 3.2A**. Control of ambient temperature (33°C) during the first 20min after [¹⁸F]FDG injection resulted in 40% decreased [¹⁸F]FDG brown fat tissue uptake compared to control animals at room temperature or animals with 10% ethanol co-administration at room temperature (not significant). Furthermore, animals receiving 10% ethanol showed a 34% decrease in muscle uptake compared with the temperature controlled test group (P<0.05). [¹⁸F]FDG brain uptake was not significantly influenced by an increased ambient temperature or 10% ethanol administration (**Table 3.2B**). *Ex vivo* biodistribution of [¹⁸F]fallypride was not significantly influenced by 10% ethanol in the administered tracer solution. Nevertheless, there was a trend towards increased [¹⁸F]fallypride accumulation in the striatum under ethanol conditions (16%, not significant, **Table 3.2C**). Gender and age of test animals proved to significantly impact [¹⁸F]FDG uptake to certain peripheral organs, but not to the brain. Male animals accumulated 18% more [¹⁸F]FDG in the liver (P<0.05) and 21% less [¹⁸F]FDG in their reproductive organs (P<0.01) than females. More than double the amount of [¹⁸F]FDG was accumulated in the fat of

females compared to males ($P < 0.01$), whereas [^{18}F]FDG blood concentration was 33% higher in males ($P < 0.01$, **Table 3.2D**). Older animals accumulated 13% less [^{18}F]FDG in their bone marrow ($P < 0.05$) and 28% more [^{18}F]FDG in their Harderian glands (HG) ($P < 0.01$) compared to younger mice. The number of animals per cage did not impact [^{18}F]FDG organ distribution. The potential influence of combined effects of two or three of the investigated parameters was excluded by performance of a 3-way ANOVA where no significant differences due to multiple parameters were confirmed.

Influence of experimental parameters on tissue distribution of [¹⁸F]FDG or [¹⁸F]Fallypride expressed as norm. %ID/g (mean±SD)				
A) Anesthetic protocol: [¹⁸F]FDG				
	<i>Brain</i>	<i>Muscle</i>	<i>Blood</i>	
Control	0.31±0.04	0.066±0.026	0.015±0.006	
Dynamic	0.19±0.04**	0.028±0.006**	0.051±0.009**	
Static	0.26±0.02**	0.04±0.006**	0.033±0.004**	
B) Ambient temperature / 10% EtOH: [¹⁸F]FDG			C) 10% EtOH: [¹⁸F]Fallypride	
	<i>Brown fat tissue</i>	<i>Muscle</i>	<i>Striatum</i>	
Control (23°C)	0.30±0.18	0.097±0.038	0.25±0.03 (n.s.)	
33°C	0.18±0.07 (n.s.)	0.119±0.016*	-	
r.t. / 10% EtOH	0.37±0.14	0.08±0.023*	0.28±0.03 (n.s.)	
33°C / 10% EtOH	0.40±0.19	0.089±0.018	-	
D) Gender: [¹⁸F]FDG				
	<i>Liver</i>	<i>Blood</i>	<i>Fat</i>	<i>Reproductive organs</i>
Female	0.018±0.005	0.01±0.003	0.024±0.015	0.052±0.017
Male	0.022±0.006*	0.015±0.005**	0.011±0.009**	0.041±0.009**
E) Age: [¹⁸F]FDG				
	<i>Bone</i>	<i>Harderian gland</i>	<i>Urine</i>	
5 Weeks	0.097±0.016	0.45±0.12	3.4±2.3	
14 Weeks	0.084±0.022*	0.63±0.22**	1.9±1.1*	

Table 3.2. **A)** Influence of anesthesia duration on [¹⁸F]FDG distribution. *Ex vivo* biodistribution of [¹⁸F]FDG in Crl:CD(SD) rats (male), n=6. Control: anesthesia from 55-61min p.i.; dynamic: anesthesia from 0-61min p.i.; static: anesthesia from 20-61min p.i. **P<0.01 for comparison with control condition. **B)** Influence of ambient temperature and ethanol application on [¹⁸F]FDG distribution. *Ex vivo* biodistribution of [¹⁸F]FDG in NMRI mice (male) under control conditions, ambient temperature control between 0-20min p.i., 10% ethanol in the administered tracer solution (10µl ethanol) and a combination of the two; n=8. *P<0.05 for comparison between conditions indicated in grey. **C)** Influence of ethanol in the tracer solution on [¹⁸F]fallypride distribution. *Ex vivo* biodistribution of [¹⁸F]fallypride in C57Bl/6J mice (male), n=8. Comparison of mice receiving 10% ethanol in the administered tracer solution (corresponding to 10µl ethanol) with control animals. **D)** Influence of gender, age and cage occupancy on [¹⁸F]FDG biodistribution. *Ex vivo* biodistribution of [¹⁸F]FDG in male and female NMRI mice (n=38 for males, n=44 for females). *P<0.05, **P<0.01. **E)** *Ex vivo* biodistribution of [¹⁸F]FDG in 14 weeks and 5 weeks old NMRI mice (n=40 for old animals and n=42 for young animals). *P<0.05, **P<0.01 for comparisons between male and female or 5 and 14 weeks old animals, respectively.

3.3.3. Standardization vs. “Pseudo-Heterogenization”

According to the study of Richter and co-workers, it was investigated whether strict standardization of experimental test groups in small animal [¹⁸F]FDG PET might lead to reduced reproducibility of results compared to heterogenized test groups [7]. Therefore, [¹⁸F]FDG organ uptake was determined in eight test groups. Each group was strictly standardized to the parameters gender, age and cage occupancy (**Figure 3.1**). Gender differences of [¹⁸F]FDG uptake in 19 different organs were determined by comparing pairs of groups only differing in gender. Inter- and intra-group variability (COV) of [¹⁸F]FDG tissue uptake was determined and compared with the results from the “pseudo-heterogenized” set-up (**Figure 3.1**). The intra-group [¹⁸F]FDG tissue uptake COVs were 17% greater for heterogenized groups compared with standardized groups (P<0.01). On the other hand, the variability between different test groups was 13% smaller for the heterogenized set-up (P<0.05) as shown in **Table 3.3**.

	Standardized	Heterogenized
Inter-group variability (COV)	32±2%	28±2%*
Intra-group variability (COV)	31±1%	35±1%**

Table 3.3. Influence of standardization and heterogenization on [¹⁸F]FDG organ uptake variability. Inter- and intra-group variability of [¹⁸F]FDG uptake for all organs measured (mean of COVs±SEM of standardized groups vs. COVs±SEM of heterogenized groups, in %). *P<0.05, **P<0.01.

The false positive rate of standardized and “pseudo-heterogenized” results was determined by comparison with “true” gender differences of [¹⁸F]FDG organ uptake resulting from pooled data of the same gender. It was investigated whether strict standardization leads to increased false positive rates of results. Standardized test groups produced a false positive rate of 9±5% (mean±SEM), whereas heterogenized test groups resulted in 2±3% false positives (not significant, **Figures 3.4A**). Because of the significantly lower false negative rate of the standardized set-up compared to the heterogenized study (63% vs. 100%, P<0.05, **Figures 3.4B**), the significance level α of the pseudo-heterogenized set-up was adapted from 0.05 to 0.38 in order to achieve a comparable study power for both set-ups (power: 37%). The recalculated

(using the adapted α) false positive rate of heterogenized samples was $6\pm 6\%$ compared to $9\pm 5\%$ for the standardized ones (not significant, **Figures 3.4A**).

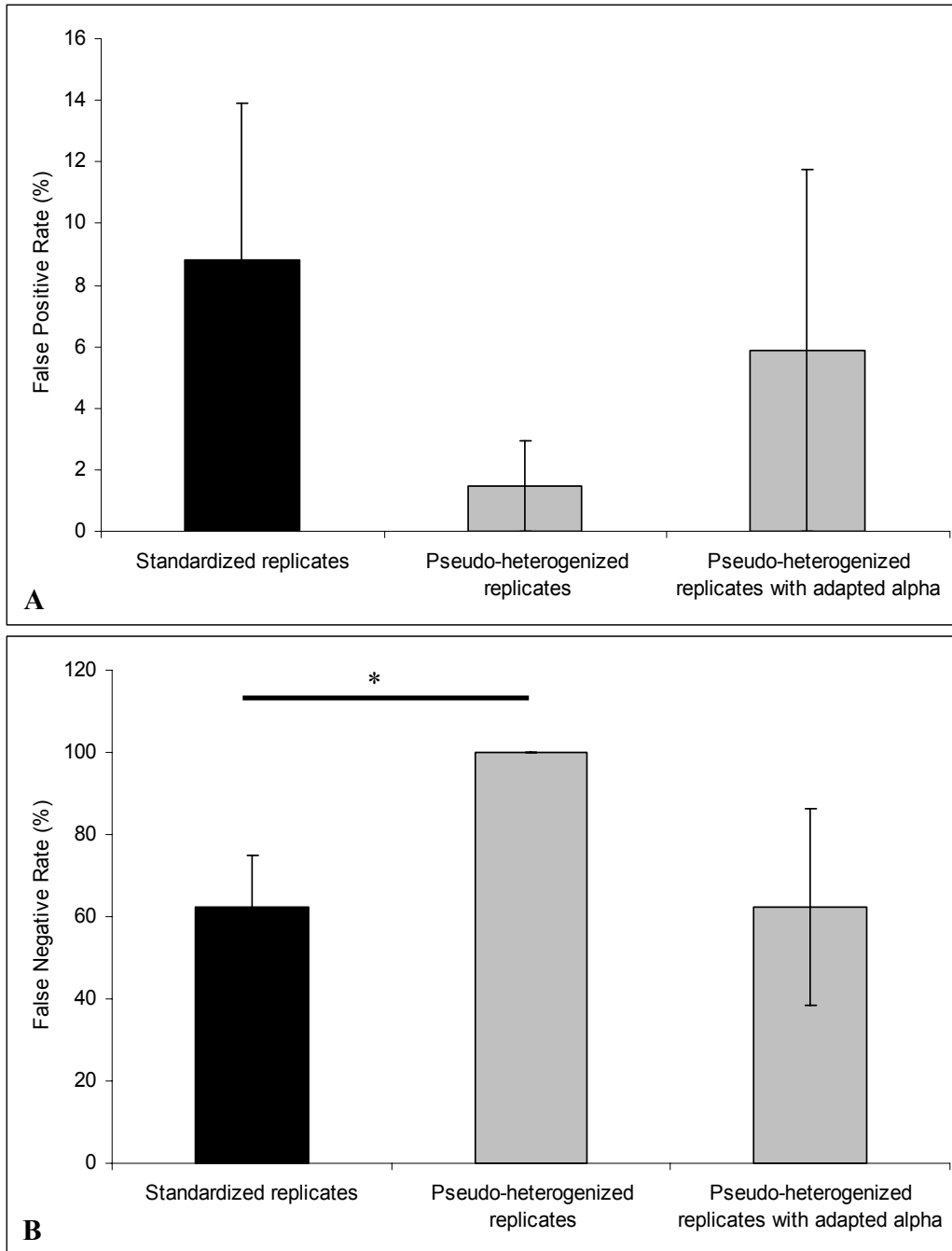


Figure 3.4. Data analysis for false positive and false negative rates. Comparison of false positive (**A**) and false negative (**B**) rates between the standardized set-up (black) and the pseudo-heterogenized set-up (grey). For heterogenized groups, α was adapted from 0.05 to 0.38 in order to achieve the same study power as in the standardized set-up. $n=4$, $*P<0.05$, error bars: \pm SEM.

3.4. Discussion

The reproducibility of [^{18}F]FDG rat brain PET scans was not found to be improved by measuring animals repeatedly. The variability of the brain uptake of [^{18}F]FDG and of the striatal accumulation of [^{18}F]fallypride between scans of the same animal compared to scans of different individuals was higher than the by trend (not significant). Furthermore, measuring the same group of animals repeatedly produced significantly different brain SUVs on different test days. The reason for this might be related to the fact that these animals have already experienced radiotracer injection, anesthesia and general experimental handling, which might impact the metabolism of individual animals. In addition, animals were one week older at the time point of the retest. The most plausible explanation, however, would be that the determined significances are false positives, as it is known that strict standardization leads to a clear increase of the false positive rate [7]. It therefore seems advisable to use heterogenized experimental conditions in order to avoid high false positive rates. Controlling heterogenized conditions is very important, as certain parameters might crucially impact study outcome. It is thus advisable to standardize such parameters to reach a satisfactory study power.

Several parameters with a potential impact on [^{18}F]FDG biodistribution were investigated. Of all tested parameters, anesthetic protocols proved to influence [^{18}F]FDG brain uptake most. Therefore, it is suggested to standardize anesthetic protocols to produce reliable small animal [^{18}F]FDG brain PET data. Results revealed that anesthesia duration was inversely proportional to [^{18}F]FDG brain uptake, which is presumably due to a decreased cerebral metabolic glucose rate (CMR_{gluc}) under isoflurane anesthesia [22]. These results confirm similar findings of isoflurane impact on [^{18}F]FDG brain uptake described before [11, 12, 14]. [^{18}F]FDG muscle uptake showed a similar decrease with anesthesia duration. This effect is most probably due to the lack of motion during anesthesia. On the other hand, blood content was clearly higher, the longer the duration of anesthesia; this effect might arise from reduced [^{18}F]FDG brain and muscle uptake.

Experimental parameters like ambient temperature, gender and age significantly altered [^{18}F]FDG uptake to liver, fat tissue, HG, bone marrow as well as [^{18}F]FDG urine content. The reduced brown fat tissue uptake of [^{18}F]FDG at an increased ambient temperature is in correlation to the findings of Fueger and co-workers [11]. In this study, mice were kept at ambient temperatures of thermoneutrality, which is between 30 and 34°C for mice. In the

thermoneutrality zone, brown fat dependent thermoregulation does not take place. While it is obvious that increased ambient temperature during [^{18}F]FDG uptake leads to a decreased brown fat uptake compared to animals kept at room temperature, the impact of age on bone marrow and Harderian gland uptake is less apparent. It seems that young animals have an increased glucose turn-over rate in bone marrow. [^{18}F]FDG fat tissue uptake was higher in females compared to males, which can be explained by a higher generation of fat deposits in females. Blood concentration of [^{18}F]FDG and [^{18}F]FDG liver uptake was higher in males, suggesting a higher metabolic activity of the liver and a slower blood clearance compared to females.

An ethanol concentration of 10% in the tracer solution did not impact [^{18}F]FDG or [^{18}F]fallypride tissue distribution significantly. Nevertheless, [^{18}F]fallypride striatum uptake was increased in animals receiving ethanol compared with control animals (16%, not significant). This trend supports the hypothesis that the rate of metabolic transformation of [^{18}F]fallypride might be slowed down under acute ethanol conditions. It was assumed that [^{18}F]fallypride is metabolized via an oxidative process in the liver. Acute ethanol administration is known to induce hypoxia in the liver [23] and is therefore believed to impact the enzyme capacity of oxygenating enzymes. Ethanol was therefore expected to slow down the degradation process of [^{18}F]fallypride, a low extraction compound, resulting in altered uptake characteristics in its target organs (mainly striatum). Varying contents of ethanol in the [^{18}F]fallypride solution might therefore lead to increased variability of striatum uptake, which may be considered for an optimal tracer formulation.

It was previously reported that over-night fasting was beneficial for small animal [^{18}F]FDG study outcome, due to reduced competition of glucose with [^{18}F]FDG for cellular uptake [11, 16, 24, 25]. For this study, it was assumed that fasting of animals might conduce twofold positively to the outcome. Besides increasing the overall organ uptake of [^{18}F]FDG, it was expected that the variability of blood glucose levels of individual animals would be reduced crucially and a relatively uniform low concentration reached. This was assumed to reduce intern [^{18}F]FDG uptake variability to target organs. However, it was shown that fasting did not lead to reduced blood glucose levels or to reduced variability of blood glucose concentration (data not shown). One reason for this might be the short fasting duration of only four hours that was used to fulfill the regulations of the authorities. These findings superseded a dedicated experiment to study the influence of blood glucose levels on [^{18}F]FDG organ uptake.

As expected, the standardization study according to a protocol by Richter and co-workers revealed that strict standardization of test groups resulted in decreased intra-group variability; but increased inter-group variability [7]. This suggests that the low intra-group variability does not necessarily correspond to low inter-group variability as generally assumed [5, 6]. The significantly higher false positive rate under standardized conditions reported by Richter and colleagues were not confirmed, most probably due to the small scale of this study (four group comparisons per standardized and heterogenized set-up in this study vs. 18 group comparisons per set-up in the study of Richter and co-workers). Nonetheless, the results revealed a clear trend towards affirmation of the findings by Richter et al [7].

This study also showed that the variability of [^{18}F]FDG tissue uptake is strongly dependent on the tissue of interest. Brain uptake was rather stable with a variability ranging from 6-16%, whereas the variability of [^{18}F]FDG concentration in blood and the HG was in a range of 20-40%. Considering this high variability for [^{18}F]FDG organ uptake, it is advisable to perform sample size calculations prior to experiments to avoid exclusion of effects due to unsatisfactory study power.

3.5. Conclusion

Small animal PET studies should be designed with care, taking into account that using animals as their own control does not necessarily increase reliability of results. Considering the high inevitable variability of [^{18}F]FDG organ uptake, it is important to perform detailed sample size calculations prior to a study. Furthermore, experimental parameters which do not impair tracer distribution significantly (e.g. ambient temperature, housing conditions, gender and age of animals) are suggested to be varied in a controlled manner to produce results with maximal external validity. In the future, it would be worthwhile to perform studies involving different small animal PET centers to investigate closer on external validity of results.

3.6. References

- [1] Nanni C, Rubello D, Fanti S. Role of small animal PET for molecular imaging in pre-clinical studies. *Eur J Nucl Med Mol Imaging*. 2007;34:1819-1822
- [2] Cherry SR. Of mice and men (and positrons) – advances in PET imaging technology. *J Nucl Med*. 2006; 47:1735-1745
- [3] Ametamey SM, Honer M, Schubiger PA. Molecular imaging with PET. *Chem Rev*. 2008;108:1501-1516
- [4] Cherry SR, Gambhir SS. Use of positron emission tomography in animal research. *ILAR Journal*. 2001;42:219-232
- [5] Van Zutphen LFM, Baumans V, Beynen AC. *Grundlagen der Versuchstierkunde*: Gustav Fischer Verlag. 1995;93ff, 189ff
- [6] Van der Staay FJ, Steckler T. The fallacy of behavioral phenotyping without standardization. *Genes, Brain and Behavior*. 2002;1:9-13
- [7] Richter SH, Garner JP, Würbel H. Environmental standardization: cure or cause of poor reproducibility in animal experiments? *Nature Methods*. 2009;6:257-261
- [8] Crabbe JC, Wahlsten D, Dudek BC. Genetics of mouse behavior: interactions with laboratory environment. *Science*. 1999;284:1670-1672
- [9] Würbel H. Behavioural phenotyping enhanced – beyond (environmental) standardization. *Genes, Brain and Behavior*. 2002;1:3-8
- [10] Paylor R. Questioning standardization in science. *Nature Methods*. 2009;6:253

- [11] Fueger BJ, Czernin J, Hildebranth I, et al. Impact of animal handling on the results of [¹⁸F]FDG studies in mice. *J Nucl Med*. 2006;47:999-1006
- [12] Toyama H, Ichise M, Liow J-S, et al. Evaluation of anesthesia effects on [¹⁸F]FDG uptake in mouse brain and heart using small animal PET. *Nucl Med Biol*. 2004;31:251-256
- [13] Flores JE, McFarland LM, Vanderbilt A, Ogasawara AK, Williams S-P. The effects of anesthetic agent and carrier gas on blood glucose and tissue uptake in mice undergoing dynamic [¹⁸F]FDG-PET imaging: sevoflurane and isoflurane compared in air and in oxygen. *Mol Imaging Biol*. 2008;10:192-200
- [14] Woo S-K, Lee TS, Kim KM, et al. Anesthesia condition for [¹⁸F]FDG imaging of lung metastasis tumors using small animal PET. *Nucl Med Biol*. 2008;35:143-150
- [15] Matsumura A, Mizokawa S, Tanaka M, et al. Assessment of microPET performance in analyzing the rat brain under different types of anesthesia: comparison between quantitative data obtained with microPET and *ex vivo* autoradiography. *NeuroImage*. 2003;20:2040-2050
- [16] Wahl RL, Henry CA, Ethier SP. Serum glucose: effects on tumor and normal tissue accumulation of 2-[¹⁸F]fluoro-2-deoxy-D-glucose in rodents with mammary carcinoma. *Radiology*. 1992;183:643-647
- [17] Mukherjee J, Yang Z-Y, Das MK, Brown T. Fluorinated benzamide Neuroleptics-III. Development of (S)-N-[(1-allyl-2-pyrrolidinyl)methyl]-5-(3-[¹⁸F]fluoropropyl)-2,3-dimethoxybenzamide as an improved dopamine D₂ receptor tracer. *Nucl Med Biol*. 1995;22:283-296
- [18] Mukherjee J, Yang Z-Y, Brown T, et al. Preliminary assessment of extrastriatal dopamine D-2 receptor binding in the rodent and nonhuman primate brains using the high affinity radioligand, ¹⁸F-fallypride. *Nucl Med Biol*. 1999;26:519-527

- [19] Honer M, Brühlmeier M, Missimer J, Schubiger PA, Ametamey SM. Dynamic Imaging of Striatal D₂ Receptors in Mice Using Quad-HIDAC PET. *J Nucl Med.* 2004;45:464-470
- [20] Wang Y, Seidel J, Tsui BMW, Vaquero JJ, Pomper MG. Performance evaluation of the GE Healthcare eXplore VISTA Dual-ring small-animal PET scanner. *J Nucl Med.* 2006;47:1891-1900
- [21] Mikolajczyk K, Szabatin M, Rudnicki P, Grodzki M, Burger C. A JAVA environment for medical image data analysis: initial application for brain PET quantification. *Med Inform.* 1998;23:207–214
- [22] Cucchiara RF, Theye RA, Michenfelder JD. The effects on canine cerebral metabolism and blood flow. *Anesthesiology.* 1974;40:571-574
- [23] Arteel GE, Raleigh JA, Bradford BU, Thurman RG. Acute alcohol produces hypoxia directly in rat liver tissue *in vivo*: role of Kupffer cells. *Am J Physiol.* 1996;271:G494-500
- [24] Ishizu K, Nishizawa S, Yonekura Y, et al. Effects of hyperglycemia on FDG uptake in human brain and glioma. *J Nucl Med.* 1994;35:1104-1109
- [25] Lindholm P, Minn H, Leskinen-Kallio S, Bergmann J, Ruotsalainen U, Joensuu H. Influence of the blood glucose concentration on FDG uptake in cancer – A PET study. *J Nucl Med.* 1993;34:1-6

4. Retro-ocular PET Tracer Accumulation

4. Characterization of Retro-ocular PET Tracer Accumulation in Rodents

4.1. Introduction

Positron emission tomography (PET) is a non-invasive functional imaging methodology for diagnosis of cancer and diseases of the central nervous system (CNS). Small animal PET gained increasing impact in preclinical research mainly due to the recent development of dedicated small animal PET scanners with increased spatial resolution of less than 2mm [1, 2]. Due to the better resolution of these systems it became possible to localize high accumulations of various PET tracers in the retro-ocular region of test animals like mice and rats, whereas earlier reports located these hotspots in the frontal brain area to intra-cranial accumulation [3-5]. To date, there is no consensus about the responsible organ for this kind of retro-ocular PET tracer accumulation. Some authors assumed the intra-orbital lachrymal glands to be responsible [3, 5-7] but by far the most publications assigned these hot spots to the so-called Harderian gland (HG) [4, 8-10]. The HG is named after Johann Jacob Harder who discovered and described it first in 1694 in the red deer [11, 12]. The glands are present in a variety of species: most mammals, birds, amphibian and reptiles, but not in humans [12, 13]. It is known that they are sites of production for lipids, indols and porphyrins [13, 14], but their physiological function is not yet understood. Several possible functions are suggested in literature: lubrication of the cornea, photoprotection, thermoregulation, function in the immune system, pheromone secretion and functions in aggression and social behaviour [12, 14, 15]. The gland is rather large, sometimes even larger than the eye itself, covering most of the posterior surface of the eyeball [12].

Besides the fact that many PET tracers tend to accumulate strongly in the retro-ocular area of small animals, remarkable differences of the retro-ocular accumulation pattern depending on the investigated animal strain have been observed. For example, the metabolic tracer [^{18}F]FDG and the receptor ligand tracer [^{18}F]fallypride seem to accumulate differently in various mouse and rat strains. Albino rat strains like Wistar and Sprague Dawley (SD) showed higher [^{18}F]FDG accumulation in retro-ocular regions compared to the brain, whereas Brown Norway (BN) rats seemed to accumulate more [^{18}F]FDG in the brain [16]. On the other hand, the pigmented mouse strain C57Bl/6J showed more [^{18}F]fallypride uptake in the retro-ocular area than in its main

target organ striatum, whereas the albino strain NMRI did not accumulate any [^{18}F]fallypride in the eye region (**Figure 4.1**).

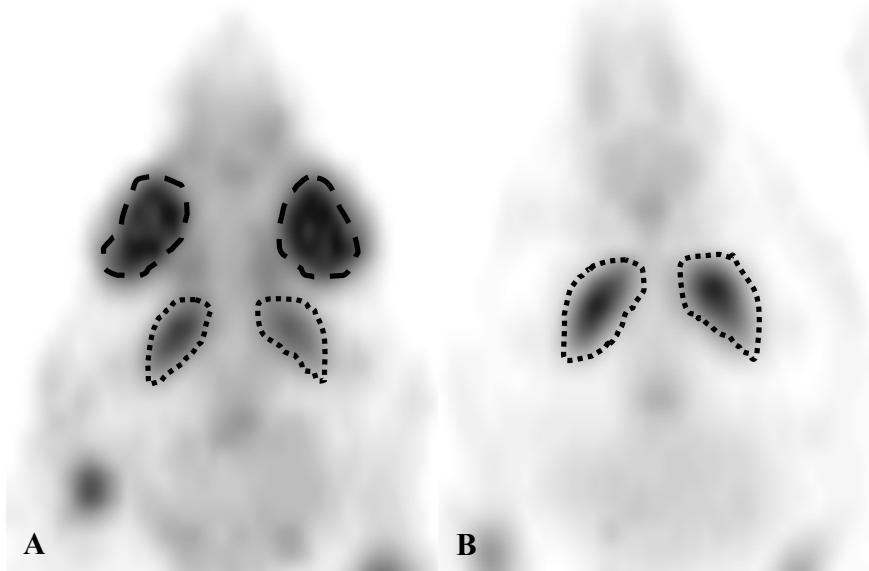


Figure 4.1. MIPs of [^{18}F]fallypride brain PET images of a C57Bl/6J mouse (**A**) and a NMRI mouse (**B**). Dotted lines encircle the striatum location; interrupted solid lines encircle the retro-ocular area. Injected dose: 7MBq (C57Bl/6J mouse) and 11MBq (NMRI mouse), static scan under isoflurane anesthesia from 20-60min post injection.

In this study, the tissue responsible for retro-ocular PET tracer accumulations was determined exemplarily for the exemplary tracers [^{18}F]FDG, a metabolic tracer, and [^{18}F]fallypride, a reversible neurotransmitter receptor ligand. Furthermore, the nature of this retro-ocular PET tracer accumulation was characterized in detail and strain differences were assessed.

4.2. Material and Methods

4.2.1. Animal Preparation

Animals were purchased from Charles River Germany. The investigated strains were NMRI mice (male, 20–49g, n=12, two batches), C57Bl/6J mice (male, 20-40g, n=13, two batches), Crl:WI rats (male, 200-350g, n=4, one batch) and BN/Crl rats (female, 150-250g, n=4, one batch).

Animal care and experimental procedures were performed in accordance with and approved by the Swiss Federal Veterinary Office. Animals were kept in standard cages (groups of 2-6 animals per cage) inside a Scantainer (Scanbur, Denmark) equipped with a filter cover. Ambient temperature was set to 23°C and air humidity was between 50 and 85%. Free access to food (Alleinfuttermittel for rats and mice, KLIBA NAFAG, Switzerland) and water was allowed throughout all experiments except if stated otherwise. A light-dark cycle of 12h (dark phase: 6pm - 6am) was maintained through all studies. Animal monitoring, as well as cage changes was performed weekly by the experimenter or a professional animal care taker. Experiments were started between 7 and 9am involving two experimentators.

4.2.2. Radiotracers

[¹⁸F]FDG was obtained from the commercial [¹⁸F]FDG production of the University Hospital Zurich in batches of 1-2GBq/mL. The radiosynthesis of [¹⁸F]fallypride was performed according to the protocol of Mukherjee et al [17]. The radioligand was produced in batches of 500-5000MBq, with activity concentrations of 500–2000MBq/mL and specific activities between 54 and 260GBq/μmol at the end of synthesis.

4.2.3. Radiotracer Injection

Radiotracer injection into rats was performed with the Braunüle[®] (Vasofix) catheter: tail vein injections of ~15MBq [¹⁸F]FDG in 300μL physiological NaCl solution (Braun AG) were followed by rinsing of the catheter with 150μL physiological NaCl solution.

Mice were injected directly into the lateral tail vein. Injected doses of [¹⁸F]FDG were approximately 15MBq in 100μL physiological NaCl solution. For [¹⁸F]fallypride injections, the injected cold mass was kept constant, resulting in a decrease of injected radioactivity over time. The injection volume was adjusted to match injected volume of [¹⁸F]FDG and the injected masses over all studies were 1.5-9nmol/kg body weight or 20-130ng per animal.

4.2.4. Measurement of physiological parameters

Body temperature of all animals under isoflurane anesthesia was monitored using a rectal temperature sensor. A stream of warm air was blown through the scanner tube in order to avoid hypothermia during anesthesia. Body temperature was kept between 35 and 37°C.

Depth of anesthesia monitoring was achieved by sensing the breath rate with an abdominal breathing belt (rats) or by visual breath rate counting (mice). The breath rate was kept constant at ~60 breaths per minute (bpm) by adaption of anesthesia.

4.2.5. PET imaging / *ex vivo* biodistribution

PET experiments were performed at the Animal Imaging Center, Center for Radiopharmaceutical Sciences at the ETH Zurich using the dedicated 36-module eXplore Vista PET/CT tomograph (GE Healthcare) with a resolution of better than 2.1mm full width at half maximum (FWHM) [18]. All animals underwent a scan in one bed position with the brain in the center of the field of view (FOV, 48mm axially and 67mm in diameter).

Static PET scanning protocol:

The urinary bladder was emptied manually before induction of anesthesia. Ten minutes before scan start, animals were anesthetized using isoflurane with oxygen/air (50%/50%) as carrier gas and fixed on the animal bed of the scanner. The isoflurane concentration was adjusted to 2-5% in order to achieve a constant breath rate of ~60bpm. Data were acquired from 30-60min post injection (p.i.) for [¹⁸F]FDG emission scans and from 20-60min p.i. for [¹⁸F]fallypride emission scans (energy window 250-700keV). Blocking studies of [¹⁸F]fallypride were performed as described in section 2.5. 30min before tracer injection, animals received an intra peritoneal (i.p.) injection of either 1mg/kg haloperidol (Serva, dissolved as 0.33 mg/mL in NaCl solution (Braun AG) with 28% (m/v) hydroxypropyl-β-cyclodextrin (Aldrich) and 0.28% (v/v) DMSO) or

vehicle (NaCl solution with 28% (m/v) hydroxypropyl- β -cyclodextrin and 0.28% (v/v) DMSO) in volumes correspondingly). Images were reconstructed using a 2D OSEM algorithm (2 iterations, 16 subsets) with scatter and random correction (no attenuation correction). Voxel size of reconstructed images was $0.3875 \times 0.3875 \times 0.775 \text{mm}^3$. PET data were analyzed by visual inspection in coronal, sagittal and horizontal planes throughout the reconstructed volume. Region of interest (ROI) analysis was performed manually using the dedicated biomedical image quantification software PMOD (Pmod Technologies Ltd, Adliswil Switzerland) [19]. Manual ROI analysis guided by radioactivity accumulation was performed for the following organs: brain (whole brain for [^{18}F]FDG studies and striatum for [^{18}F]fallypride studies), HG and eye. Tracer uptake to each individual organ was quantified as standardized uptake value (SUV) by normalizing the average activity concentration of each volume of interest (VOI) to the injected dose per body weight.

Subsequent to the PET scan, animals were sacrificed by decapitation (at approx. 61min p.i.). Organs of interest were collected and activity concentrations were assessed by classical gamma counting (Wallac 1480 Wizard, Perkin Elmer). For *ex vivo* autoradiography measurements, brain, eye ball with the HG and the intra- and extra-orbital lachrymal glands were collected and embedded separately in Neg-50 Frozen Section Medium (Richard Allan Scientific). The tissue samples were frozen in 2-Methylbutan (Fluka) at -30 to -36°C . The frozen organs were cut into $20\mu\text{m}$ thick slices at -18°C using the Cryostat microtome HM 505N (Microm GmbH) and brought on microscopy slides of the type SuperFrost[®] (Menzel-Gläser). After air drying, the tissue slices were exposed to phosphor imager plates (BAS-MS imaging plates, Fujifilm) and the plates were subsequently read using the BAS5000 reader (Fuji).

Quantification of [^{18}F]FDG or [^{18}F]fallypride uptake to organs of interest was achieved by calculating the normalized %ID/g organ as follows: organ activity (counts per minute) \cdot 100 / [injected dose (counts per minute) \cdot organ weight (g)] / body weight (kg).

For [^{18}F]FDG studies the whole brain was investigated; for [^{18}F]fallypride studies the brain was further dissected into striatum, hippocampus, cortex, cerebellum, midbrain, brain stem. Furthermore HG, intra-orbital lachrymal gland, extra-orbital lachrymal gland and eye were analyzed.

Quantification of autoradiography slices was performed by ROI definition of all tissue slices and the activity concentration was calculated as PSL/pixel (PSL = Photo stimulated luminescence).

Activity concentrations normalized for injected dose per body weight of all ROIs of an individual organ were averaged and the activity concentration ratios between brain and eye glands (HG, intra- and extra-orbital lachrymal gland) were calculated.

4.2.6. *In vitro* Autoradiography using [¹⁸F]Fallypride

Tissue slices of brains and eye/HG of two animals per mouse strain (NMRI and C57Bl/6J) were obtained as described in section 2.5. The slices were adjusted to room temperature for approximately 30min and equilibrated in Tris-buffer (50mM Tris, 120mM NaCl, 5mM KCl, pH=7.4 at 37°C (HCl) + 0.1% (m/v) BSA for 10min according to a protocol of Mukherjee et al [17]. Incubation with [¹⁸F]fallypride ($K_d = 0.03\text{nM}$ for [¹⁸F]fallypride [17] Mukherjee et al. 1995) was performed under four different conditions. Per condition, two glass slides with two tissue cuts each were used. Specific binding was investigated at two different concentrations of [¹⁸F]fallypride, $17\times K_d$ and $1\times K_d$ in Tris-buffer + 0.1% (m/v) BSA. Haloperidol (Serva) was used as a blocking agent (10 μM). The slices were then incubated for 1h at 37°C. After incubation, the supernatant was discarded and the slices were washed in Tris-buffer (37°C) for 2x2min followed by a second washing step in millipore water (2x5s). 10 μL of each incubation solution on filterpaper fixed to glass slides were used as standards for later quantification. The slices were subsequently dried under a cold stream of air and exposed to phosphor imager plates (15min for $17\times K_d$ -samples and 35min for $1\times K_d$ -samples). The plates were subsequently read using the BAS5000 reader (Fuji).

4.2.7. Histology

Eosin and haematoxylin tissue staining was performed by placing slices into a haematoxylin solution (Gill Nr.1, Sigma Aldrich) for 12min, followed by a washing step under tap water for 10min. Washed slices were dipped into 60% ethanol for 30s and transferred to an eosin solution (0.2% (w/v) in 90% ethanol (v/v)) for 12s. Subsequently, the slices were washed in 60% ethanol, 70% ethanol, 80% ethanol and 90% ethanol (each step 30s) before they were kept in xylene (puriss p.a., Fluka) for a minimum of 10min. The stained and water-free tissue samples were mounted using Eukitt[®] (Fluka) and investigated with the Zeiss Axiovert 35 microscope (West Germany).

4.2.8. Statistical Analysis

Figures show mean±SD, unless stated otherwise. Differences among the experimental groups in the SUVs and norm.%ID/g of the various tissues investigated were statistically evaluated by analysis of variance (ANOVA) and subsequent post hoc tukey tests for comparisons of three or more groups and by two-tailed t-tests for comparisons of two groups. Statistical significance was set at the 95% level and Bonferroni correction was applied where required.

4.3. Results

4.3.1. Identification of the Responsible Tissue for Retro-ocular [¹⁸F]FDG and [¹⁸F]Fallypride Hotspots

In order to identify the responsible organ for the retro-ocular accumulation of [¹⁸F]FDG and [¹⁸F]fallypride, *in vivo* PET scanning, *ex vivo* tissue counting and *ex vivo* autoradiography was performed. Moreover, tissue slices (brain and eye glands) exposed to phosphor imager plates for autoradiography, were subsequently stained with eosin and haematoxylin, allowing a direct comparison of radioactivity distribution and histology. In a first series of experiments, the extra-cranial uptake of [¹⁸F]FDG in Wistar and SD rats was analyzed. [¹⁸F]FDG PET scans of Wistar and SD rats showed high retro-ocular accumulation (**Figure 4.2**).

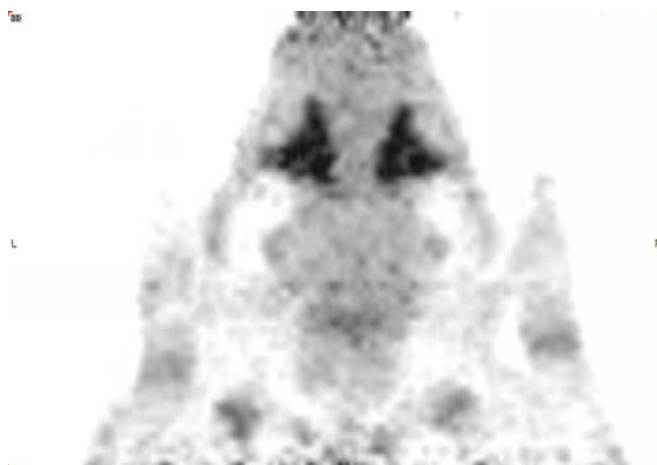


Figure 4.2. Maximum intensity projection (MIP) of a [¹⁸F]FDG PET head scan of a SD rat injected with 15MBq. Static PET scan under isoflurane anaesthesia was acquired from 30-60min post injection.

[¹⁸F]FDG accumulation in all three eye glands (HG, intra-orbital lachrymal gland and extra-orbital lachrymal gland) were quantified by *ex vivo* autoradiography and the gland with the highest [¹⁸F]FDG accumulation relatively to the brain was determined (**Figure 4.3**).

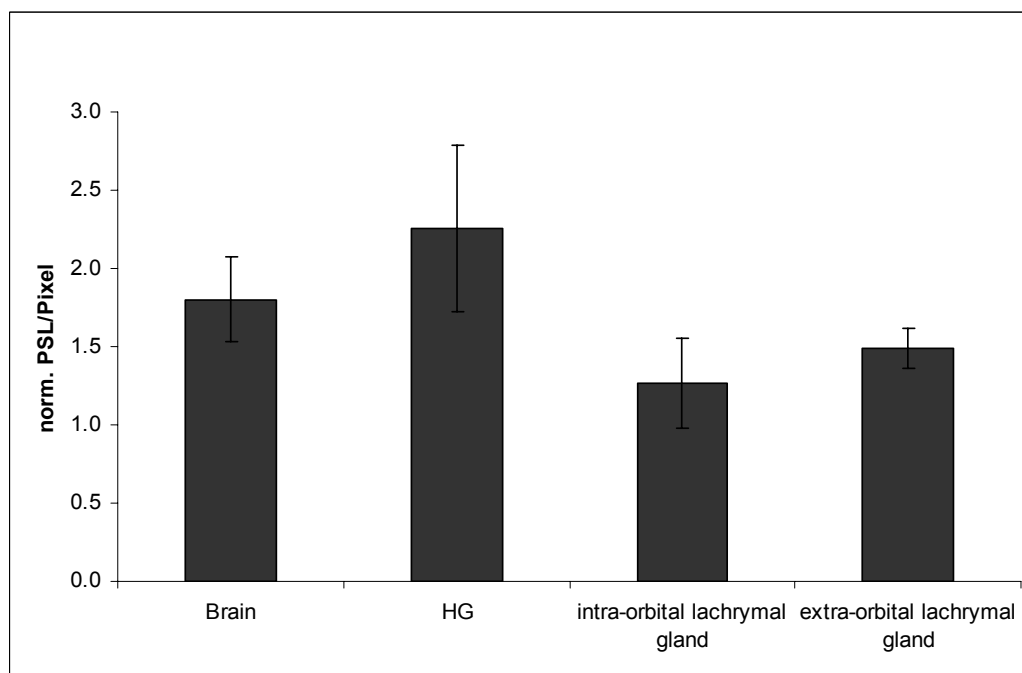


Figure 4.3. Quantification of *ex vivo* autoradiography of cranial and extra-cranial [¹⁸F]FDG uptake in a male Wistar rat injected with 50MBq (n=1). Error bars represent SD arising from n=12 slices per organ investigated.

Eosin/haematoxylin staining of the tissue slices subsequent to *ex vivo* autoradiography showed a very distinct tissue structure containing reddish-brown aggregations of pigment in the acini of the gland with the highest [¹⁸F]FDG uptake (**Figure 4.4.A**). This pigment accumulation is characteristic for the porphyrin producing HG [12, 14]. The tissue samples of the two remaining eye glands showed a very similar staining pattern relative to each other (**Figure 4.4.B** and **4.4.C**). Therefore, as the location of the extra-orbital lachrymal gland (**4.4.C**) was known, the intra-orbital lachrymal gland was identified as structure **4.4.B** (**Figure 4.4.B**).

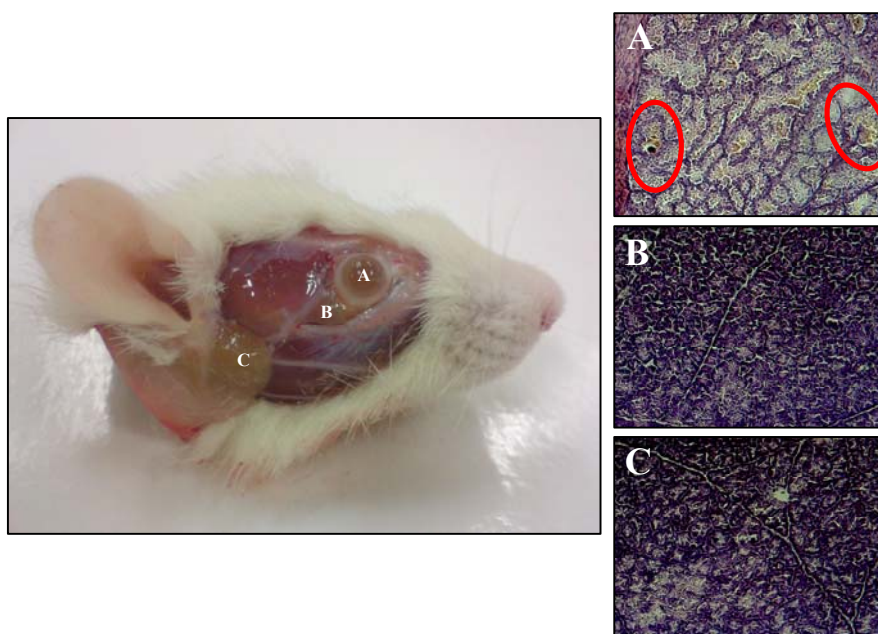


Figure 4.4. Eye gland anatomy and eosin/hematoxylin staining of tissue samples of a Crl:CD(SD) rat (male). **A)** Eye ball covering the HG **B)** intra-orbital lachrymal gland **C)** extra-orbital lachrymal gland. All slices were 20 μ m thick and stained with eosin/hematoxylin. Red circles indicate porphyrin aggregations in acini of the HG.

In a second series of experiments, the extra-cranial accumulation of [18 F]fallypride was investigated. [18 F]Fallypride, in contrast to [18 F]FDG, is a reversibly binding dopamine D₂/D₃ receptor ligand tracer, which showed high retro-ocular accumulation in pigmented mice (C57Bl/6J). The pattern of retro-ocular [18 F]fallypride on PET images appeared similar to the extra-cranial [18 F]FDG accumulation pattern in rats (**Figure 4.1A**). However, in contrast to the retro-ocular [18 F]FDG uptake in rats, quantitative [18 F]fallypride PET with subsequent *ex vivo* organ counting revealed that the HG was not the main source for the high retro-ocular uptake of [18 F]fallypride in C57Bl/6J mice. The eye rather than the HG was found to accumulate the highest concentration of [18 F]fallypride. This uptake was even 25% higher than the accumulation in the target tissue of [18 F]fallypride, the D₂ receptor-rich striatum ($P < 0.001$, **Table 4.1**).

<i>Ex vivo</i> Tissue counting	norm. %ID/g
Striatum	0.34 \pm 0.03
HG	0.27 \pm 0.03
Eye	0.41 \pm 0.03

Table 4.1. *Ex vivo* tissue distribution of [18 F]fallypride in C57Bl/6J mice (male, n=8).

To investigate the sub-structure of the mouse eye responsible for the high [^{18}F]fallypride accumulation, *ex vivo* autoradiography with subsequent eosin/haematoxylin staining of brain and eye/HG was performed. It was shown that mainly the retina was responsible for the strong accumulation of [^{18}F]fallypride in eyes of C57Bl/6J mice (**Figure 4.5**, *ex vivo* autoradiography).

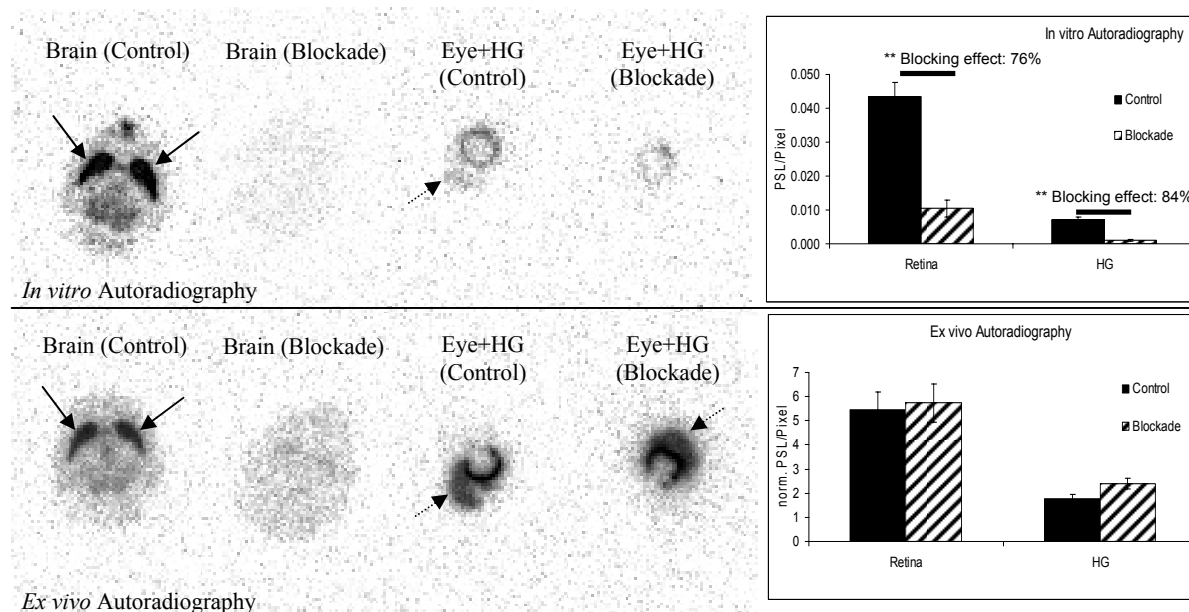


Figure 4.5. Comparison of *in vitro* and *ex vivo* [^{18}F]fallypride autoradiography of brain (striatum indicated by solid arrows) and eyes with HG (indicated by dotted arrows) using male C57Bl/6J mice, n=1/experiment. Haloperidol was used as a blocking agent to assess the specific or non-specific nature of tracer uptake. Quantitative accumulation of [^{18}F]fallypride is represented as column graphs. Error bars represent SD arising from n=6 slices per organ investigated. Data resulting from ROI analysis of *ex vivo* autoradiography were normalized to the injected dose per body weight. **P<0.01.

The high [^{18}F]fallypride accumulation in the retina compared to the striatum and the HG was unexpected, as the retina is not known to express D₂/D₃ receptors. Only D₄ receptors were previously reported to be expressed in the retina [20]. To exclude specific binding of [^{18}F]fallypride to dopamine receptors in the retina, blocking studies were performed using the dopamine-receptor ligand haloperidol (**Figure 4.5**) [21].

In vitro and *in vivo* / *ex vivo* blocking studies of [^{18}F]fallypride uptake in C57Bl/6J and NMRI mice using haloperidol confirmed the high specificity of [^{18}F]fallypride binding to the dopamine D₂ receptors in the striatum of both mouse strains. Binding of [^{18}F]fallypride was blocked by

more than of 95% ($P < 0.01$, **Figure 4.6**). However, the strong *in vivo* accumulation of [^{18}F]fallypride in the retina (eye) of C57Bl/6J mice could not be blocked, whereas the accumulation in the HG was partially blocked by 30% ($P < 0.05$, **Figure 4.6**). *In vitro* accumulation of [^{18}F]fallypride in the retina was negligible compared to the striatum (**Figure 4.5**, *in vitro* autoradiography); nevertheless, [^{18}F]fallypride *in vitro* binding to the retina was blocked by 76% under co-incubation conditions with haloperidol ($P < 0.05$, **Figure 4.5**). This result suggests that the ocular accumulation of [^{18}F]fallypride *in vitro* might arise from specific binding to D_4 receptors.

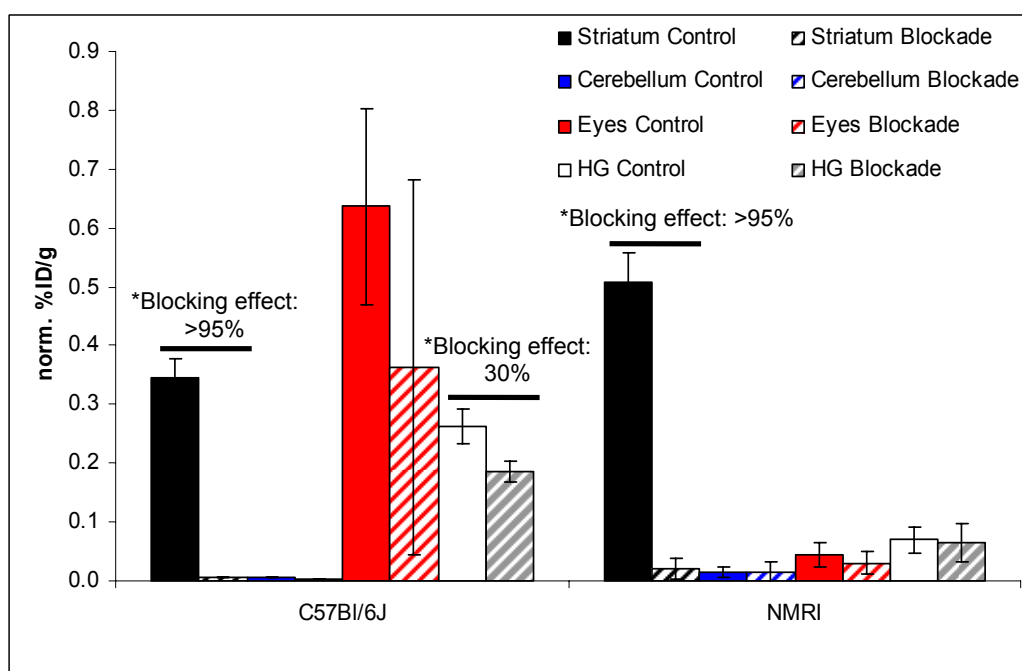


Figure 4.6. *Ex vivo* tissue distribution of [^{18}F]fallypride in C57Bl/6J and NMRI mice under control and haloperidol blocking conditions. $n=2$ /per group. $*P < 0.05$.

4.3.2. Strain Differences in Retro-ocular Tracer Uptake

For both investigated PET tracers, [^{18}F]FDG and [^{18}F]fallypride, strain differences in retro-ocular accumulation patterns were observed in PET images of mice and rats (**Figure 4.1**). These differences were investigated in more detail by performing *in vivo* PET experiments and *ex vivo* tissue counting using different rodent strains. *Ex vivo* tissue counting showed that the [^{18}F]FDG accumulation in both investigated rat strains, SD and BN, was higher in the HG compared to the brain. However, the relative distribution pattern between brain and HG was different in the two strains. SD rats accumulated 80% more [^{18}F]FDG in the HG compared to the brain, whereas the uptake difference between brain and HG was only 25% in BN rats (**Figure 4.6**).

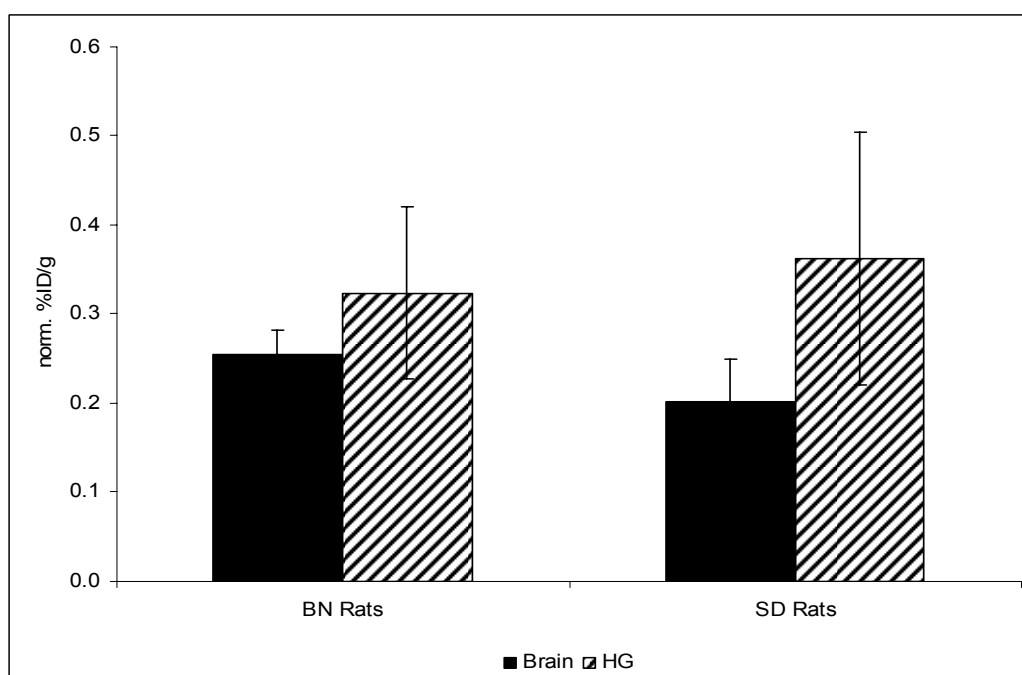


Figure 4.7. *Ex vivo* distribution of [^{18}F]FDG in brain and HG of BN and SD rats (n=3).

For the second tracer investigated, [^{18}F]fallypride, even more striking retro-ocular accumulation differences were observed between pigmented C57Bl/6J mice and NMRI albino mice (**Figure 4.1**). These strain differences of [^{18}F]fallypride distribution were quantitatively confirmed by *in vivo* PET experiments. [^{18}F]Fallypride striatum uptake (SUV) was 43% higher in NMRI mice than in C57Bl/6J mice ($P < 0.001$, **Figure 4.8**). [^{18}F]Fallypride accumulation in the retina of

C57Bl/6J mice was 30% higher than the striatum accumulation ($P < 0.001$, **Figure 4.8**), whereas in NMRI mice, retina uptake was 80% lower than the striatum uptake, most probably corresponding to non-specific binding comparable to uptake levels in the cerebellum ($P < 0.001$, **Figure 4.8**).

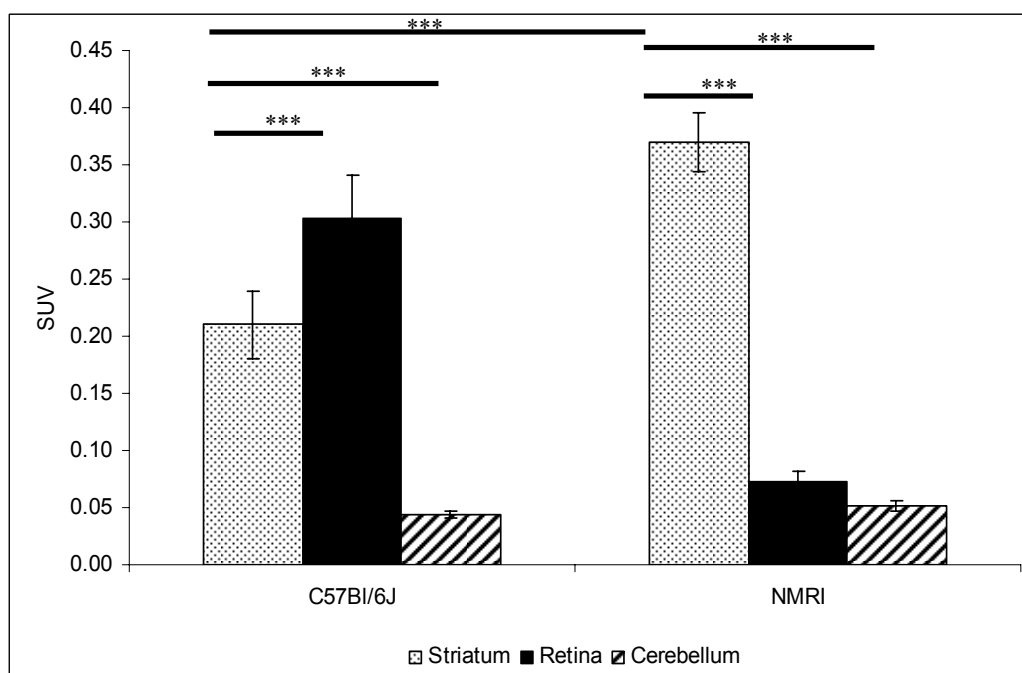


Figure 4.8. [^{18}F]Fallypride uptake to striatum, retina and cerebellum determined by ROI analysis of PET images. NMRI mice: $n=6$; C57Bl/6J mice: $n=7$. *** $P < 0.001$.

4.4. Discussion

The three periocular glands HG, intra-orbital lachrymal gland and extra-orbital lachrymal gland could be anatomically allocated in the rodent head by eosin/haematoxylin staining of gland slices. The relatively big triangularly shaped gland (approx. 20mg for a mouse of average size), filling most of the cavity behind the eyeball was identified as the HG. This tissue showed a very typical histochemical staining pattern with reddish-brown porphyrin aggregations in the glandular acini. The smaller eye gland located at the inner cantus of the eye showed a staining pattern very similar to the one of the extra-orbital lachrymal gland, suggesting that this small gland is the intra-orbital lachrymal gland.

By measuring [^{18}F]FDG uptake to eye glands and brain using PET, classical *ex vivo* tissue counting and *ex vivo* autoradiography, the HG proved to be the responsible organ for the strong retro-ocular accumulation of [^{18}F]FDG. The high [^{18}F]FDG HG accumulation is suggested to arise from high lipid metabolism rather than from ATP production [22]. To date, it is not known whether the uptake occurs via facilitative glucose transporters (GluTs). GluT1, which is responsible for glucose and [^{18}F]FDG transport across the blood brain barrier was not detected in HG tissue [23, 24]. Investigations on different uptake patterns in different rat strains did not reveal clear strain differences among SD and BN rat strains. In both strains, [^{18}F]FDG uptake to HG exceeded brain uptake. However, there was a trend that BN rats accumulated more [^{18}F]FDG in the brain in absolute terms than SD rats. Therefore, SD rats seemed to accumulate more [^{18}F]FDG in the HG relative to the brain than BN rats, which might be reflected on maximum intensity projection of the rat head.

At the first glance, head PET scans of C57Bl/6J mice injected with [^{18}F]fallypride show a very similar retro-ocular accumulation pattern as observed on [^{18}F]FDG images. Nevertheless, *ex vivo* tissue counting and autoradiography proved that the biggest part of [^{18}F]fallypride accumulation occurred in the retina and only a smaller, but still sizeable part of extra-striatal uptake of [^{18}F]fallypride was due to the HGs.

[^{18}F]Fallypride binding to the retina might be explained by the presence of the D₂-like dopamine D₄ receptors, which are widely present in the retina of rodents [20]. However, *in vitro* autoradiography showed only negligible binding of [^{18}F]fallypride to retina and HG of C57Bl/6J mice, which was blocked by 75-85% using the non-selective D₂ and D₄ receptor antagonist haloperidol ($P < 0.01$) [21]. It is therefore suggested, that this modest binding of [^{18}F]fallypride is specific due to D₄ receptors. On the other hand, haloperidol treatment did not have a blocking effect on [^{18}F]fallypride accumulation in the retina of C57Bl/6J mice *in vivo*. This very strong retinal accumulation observed in *in vivo* PET images cannot arise from specific binding of [^{18}F]fallypride to dopamine D₄ receptors, since it clearly exceeds the extent of this specific binding determined *in vitro*. This pronounced uptake is therefore considered to be non-specific, as it is not possible to block the accumulation by haloperidol. Furthermore, the high retro-ocular accumulation of [^{18}F]fallypride was only observed in C57Bl/6J mice. PET images of NMRI mice did not show retro-ocular hotspots, suggesting that high accumulation of [^{18}F]fallypride in the retina *in vivo* is restricted to pigmented animals. This effect might arise from an accumulation of

[¹⁸F]fallypride to melanin. It has been shown earlier that lipophilic substances, like certain anaesthetic agents (e.g. pentobarbital with a logP=2.11 [25]) bind to melanin in the retina of pigmented animals [26], leading to reduced sensitivity of pigmented animals to such anaesthetics [27].

A series of brain PET tracers proved to accumulate non-specifically in the HGs of preclinical rodent models, e.g. [¹⁸F]FDEGPECO, [¹⁸F]PECMO, [¹⁸F]FECNT, [¹¹C]raclopride, [¹¹C]MPEP and [¹¹C]verapamil [3, 28-31]. Each of these tracers shows lipophilic physicochemical properties (logP = 0.9-2.7), which is necessary for successful crossing of the blood-brain-barrier [32, 33]. PET tracers with more hydrophilic characteristics, i.e. [¹⁸F]NMe-FHBT, hydrophilic bombesins and folate analogues, generally showed negligible HG accumulation (data not shown). This might lead to the conclusion that the HG, which is a site for lipid synthesis, accumulates and stores lipophilic substances. It might also be possible that lipophilic substances bind to the porphyrin pigments in the HG of rodents, similar as they seem to bind to melanin in the retina.

The close vicinity of the frequently observed retro-ocular hotspots in PET images could have a negative impact on data quantification due to spill-over and partial volume effects. A study performed by Fukuyama and co-workers in 1998 investigated the effect of [¹⁸F]FDG HG uptake on the measurement of cerebral metabolic rate of glucose (CMRGlc) by small animal PET. They found that the frontal lobe CMRGlc was slightly overestimated due to the HGs but still within a permissible range [8]. With the new generation of high-resolution small animal PET scanners, spill-over and partial volume effects due to high tracer uptake in the HG should not affect quantification of PET brain data, since the spatial resolution of dedicated scanners has been further improved since 1998, when Fukuyama and co-workers performed their study.

4.5. Conclusion

The organ responsible for the high retro-ocular accumulation of [^{18}F]FDG was identified as the HG. The receptor ligand tracer [^{18}F]fallypride on the other hand, showed very high non-specific *in vivo* accumulation in the retina of C57Bl/6J mice. Therefore, PET images need to be interpreted and quantified with care with regard to retro-ocular accumulation of PET tracers. Apparently, the HG is not always the only reason for extra-cranial PET tracer accumulation. Other tracers which are known to accumulate in the retro-ocular region of rodents turned out to be tracers typically used for brain imaging ($\log P > 1$), suggesting a non-specific accumulation of rather lipophilic substances in pigment-containing tissues *in vivo*. The uptake mechanism of PET tracers to the HG and the further processing of such tracers within the gland remain to be investigated in more detail.

4.6. References

- [1] Cherry SR. Of mice and men (and positrons) – advances in PET imaging technology. *J Nucl Med.* 2006; 47:1735-1745
- [2] Chatziioannou AF. Molecular imaging of small animals with dedicated PET tomographs. *Eur J Nucl Med.* 2002;29:98-114
- [3] Honer M, Hengerer B, Blagoev M, Hintermann S, Waldmeier P, Schubiger PA, et al. Comparison of [¹⁸F]FDOPA, [¹⁸F]FMT and [¹⁸F]FECNT for imaging dopaminergic neurotransmission in mice. *Nucl Med Biol.* 2006;33:607-614
- [4] Kuge Y, Minematsu K, Hasegawa Y, Ymaguchi T, Mori H, Matsuura H, et al. Positron emission tomography for quantitative determination of glucose metabolism in normal and ischemic brains in rats: an insoluble problem by the Harderian glands. *J Cereb Blood Flow Metab.* 1997;17:116-120
- [5] Myers R, Hume S. Small animal PET. *Eur Neuropsychopharmacol.* 2002;12:545-555
- [6] Myers R. The biological application of small animal PET imaging. *Nucl Med Biol.* 2001;28:585-593
- [7] Uchida H, Okamoto T, Ohmura T, Shimizu K, Satoh N, Koike T, et al. A compact planar positron imaging system. *Nucl Instrum Methods Phys Res A.* 2004;516:564-574
- [8] Fukuyama H, Hayashi T, Katsumi Y, Tsukada H, Shibasaki F. Issues in measuring glucose metabolism of rat brain using PET: the effect of Harderian glands on the frontal lobe. *Neuroscience letters.* 1998;255:99-102
- [9] Fueger BJ, Czernin J, Hildebranth I, Tran C, Halpern S, Stout D, et al. Impact of animal handling on the results of [¹⁸F]FDG studies in mice. *J Nucl Med.* 2006;47:999-1006

- [10] Brammer DW, Riley JM, Kreuser SC, Zasadny KR, Callaham MJ, Davis MD. Harderian gland adenectomy: a method to eliminate confounding radio-opacity in the assessment of rat brain metabolism by [¹⁸F]fluoro-2-deoxy-D-glucose positron emission tomography. *J Am Assoc Lab Anim Sci.* 2007;46:42-45
- [11] Hillenius WJ, Phillips DA, Rehorek SJ. “A new lachrymal gland with an excretory duct in red and fallow deer” by Johann Jacob Harder (1964): English translation and historical perspective. *Ann Anat.* 2007;189:423-433
- [12] Payne AP. The Harderian gland: a tercentennial review. *J Anat.* 1994;185:1-49
- [13] Albert DM, Frayer WC, Black HE, Massicotte SJ, Sang DN, Soque J. The Harderian gland: its tumors and its relevance to humans. *Trans Am Ophthalmol Soc.* 1986;84: 321–341
- [14] Buzzell GR. The Harderian gland: perspectives. *Microsc Res Tech.* 1996;34:2-5
- [15] Payne AP. The Harderian gland: its biology and role in porphyrin synthesis. *Molec Aspects Med.* 1990;11:145-152
- [16] Ametamey SM, Honer M, Schubiger PA. Molecular imaging with PET. *Chem Rev.* 2008;108:1501-1516
- [17] Mukherjee J, Yang Z-Y, Das MK, Brown T. Fluorinated benzamide Neuroleptics-III. Development of (S)-N-[(1-allyl-2-pyrrolidinyl)methyl]-5-(3-[¹⁸F]fluoropropyl)-2,3-dimethoxybenzamide as an improved dopamine D₂ receptor tracer. *Nucl Med Biol.* 1995;22:283-296
- [18] Wang Y, Seidel J, Tsui BMW, Vaquero JJ, Pomper MG. Performance evaluation of the GE Healthcare eXplore VISTA Dual-ring small-animal PET scanner. *J Nucl Med.* 2006;47:1891-1900

- [19] Mikolajczyk K, Szabatin M, Rudnicki P, Grodzki M, Burger C. A JAVA environment for medical image data analysis: initial application for brain PET quantification. *Med Inform.* 1998;23:207–214
- [20] Patel S, Chapman KL, Marston D, Hutson PH, Ragan CI. Pharmacological and functional characterization of dopamine D₄ receptors in the rat retina. *Neuropharmacology.* 2004;44:1038-1046
- [21] Jentsch JD, Taylor JR, Redmond DE, Elsworth JD, Youngren KD, Roth RH. Dopamine D₄ receptor antagonist reversal of subchronic phencyclidine-induced object retrieval/detour deficits in monkeys. *Psychopharmacology.* 1999;142:78-84
- [22] Watanabe M. An autoradiographic, biochemical and morphological study of the Harderian gland of the mouse. *J Morphol.* 1980;163:349-365
- [23] Mueckler M. Facilitative glucose transporters. *Eur J Biochem.* 1994;219:713-725
- [24] Takebe K, Nio-Kobayashi J, Takahashi-Iwanaga H, Yajima T, Iwanaga T. Cellular expression of a monocarboxylate transporter (MCT1) in the mammary gland and sebaceous gland of mice. *Histochem Cell Biol.* 2009;131:401-409
- [25] Sawada H, Jinno K. Capillary electrophoretic separation of structurally similar solutes in noncross-linked poly(acrylamide-co-N-isopropylacrylamide) solution. *Electrophoresis.* 1997;18:2030-2035
- [26] Buschke, W. Die Hautdrüsenorgane (Hardersche Drüsen, Inguinaldrüsen, Präputialdrüsen, Analdrüsen, Kaudaldrüsen, Kieferdrüsen) der Laboratoriumsnagetiere und die Frage ihrer Abhängigkeit von den Geschlechtsdrüsen. *Cell Tissue Res.* 1993;18:217-143

- [27] Sisson DF, Siegel J, Westenberg IS. Are the differential effects of chloral hydrate on hooded rats vs. albino rats due to pigmentation or strain differences? *Pharmacol Biochem Behav.* 1989;39:665-670
- [28] Baumann CA, Mu LJ, Johannsen S, Honer M, Schubiger PA, Ametamey SM. Structure-activity relationships of fluorinated (E)-3-((6-methylpyridin-2-yl)ethynyl)cyclohex-2-enone-O-methyloxime (ABP688) derivatives and the discovery of a high affinity analogue as a potential candidate for imaging metabotropic glutamate receptors subtype 5 (mGluR5) with positron emission tomography (PET). *J Med Chem.* 2010;53:4007-4017
- [29] Lucatelli C, Honer M, Salazar J-F, Ross TL, Schubiger PA, Ametamey SM. Synthesis, radiolabeling, in vitro and in vivo evaluation of [¹⁸F]FPECMO as a positron emission tomography radioligand for imaging the metabotropic glutamate receptor subtype 5. *Nucl Med Biol.* 2009;36:613-622
- [30] Pellegrino D, Ciccetti F, Wang X, Zhu A, Yu M, Saint-Pierre M, et al. Modulation of dopaminergic and glutamatergic brain function: PET studies on parkinsonian rats. *J Nucl Med.* 2007;48:1147-1153
- [31] Kuntner C, Bankstahl JP, Bankstahl M, Stanek J, Wanek T, Stundner G, Karch R, Brauner R, Meier M, Bing X, Müller M, Löscher W, Langer O. Dose-response assessment of tariquidar and elacridar and regional quantification of P-glycoprotein inhibition at the rat blood-brain barrier using (R)-[¹¹C]verapamil PET. *Eur J Nucl Med Mol Imaging.* 2010;37:942-953
- [32] Pinborg LH, Videbaek C, Ziebell M, Mackeprang T, Friberg L, Rasmussen H, et al. [³¹I]Epididepride binding to cerebellar dopamine D2/D3 receptors is displaceable: Implications for the use of cerebellum as a reference region. *NeuroImage.* 2007;34:1450-1453

- [33] Dishino DD, Welch MJ, Kilbourn MR, Raichle ME. Relationship between lipophilicity and brain extraction of [¹¹C]-labeled radiopharmaceuticals. *J Nucl Med.* 1993;31:656-671

5. Conclusion and Future Perspectives

5. Conclusion and Future Perspectives

Small animal PET is a complex methodology, which gained increasing impact in the recent years especially due to the development of dedicated small animal PET systems. To date, there are still remarkable challenges regarding instrumentation, data evaluation and experimentation, which need to be overcome in order to achieve fully quantitative and reliable small animal PET data. A detailed performance evaluation of the dedicated small animal scanner eXplore Vista according to the NEMA NU4-2008 guidelines showed competitive performance with comparable devices described in literature (Inveon, Siemens; microPET Focus 120, Siemens; 16module quad-HIDAC, Oxford Positron Systems, 32module quad-HIDAC; Oxford Positron Systems; NanoPET, Bioscan; LabPET, Gamma Medica). Data acquisition is suggested to be performed using the middle energy window of 250-700keV in order to achieve minimal scatter fraction at maximal sensitivity. For data reconstruction, the 2D OSEM algorithm is recommended, as it leads to superior spatial resolution and uniformity of images compared to the FBP algorithm. Performance of scatter and random correction is crucial in order to account for the rather high scatter fraction which was detected. Despite the high quality of the data acquired by this dedicated machine, absolute quantification of data remains challenging. Even with application of scatter, random and CT-based attenuation correction, the complete recovery of radioactivity present in a certain region of interest is strongly dependent on the dimension of the radioactivity distribution, as it was shown that the smaller the radioactive area the smaller the recovery coefficient (RC). In the case of the eXplore Vista PET/CT at ETH Honggerberg, Zurich, the reliability of CT-based attenuation correction is still questionable, as the recovery coefficient for areas with more than 3mm diameter resulted in RCs greater than 1 after 2D OSEM reconstruction, indicating an overestimation of radioactivity for these particular ROIs. Furthermore, partial volume effects remain a limiting factor for absolute quantification of very small regions; and last but not least, the physical limitations of spatial resolution due to positron range and the deviation of the two gamma rays after annihilation from co-linearity, will also affect absolute quantification of PET data. However, there are promising efforts undertaken to correct for positron range. For example, the introduction of positron range profile kernels for various PET nuclides into a 3D-OSEM reconstruction algorithm proved to increase spatial resolution of the eXplore Vista by 0.2mm. It might be stated, that correction for positron range

and deviation from co-linearity during the reconstruction process seem to be the only options to further increase spatial resolution of PET images and subsequently reduce partial volume effects. In the future, it seems therefore worthwhile to investigate the potential positive impact of the 3D OSEM reconstruction algorithm on the performance of the eXplore Vista PET/CT, particularly on the spatial resolution which might be crucially reduced and image quality which might be increased compared to the application of 2D reconstruction algorithms.

In addition to the detailed analysis of the instrumental aspects of small animal PET, investigations on the impact of experimental parameters on the reliability of small animal PET data suggested that the currently applied methodology is robust. In the case of [^{18}F]FDG, duration of isoflurane anesthesia was the only parameter which significantly affected the accumulation of [^{18}F]FDG in the brain as the main target organ in healthy rats. Therefore, it is advised to strictly standardize anesthetic protocols for small animal [^{18}F]FDG PET experiments. Impact of anesthesia and other experimental parameters on [^{18}F]FDG uptake to peripheral organs like muscle or bone marrow have to be assessed prior to experimental performance on their relevance for the particular study. For [^{18}F]FDG brain uptake studies, the relatively low uptake e.g. to muscle can be neglected such that parameters with a significant impact on muscle uptake do not need to be strictly standardized in order to guarantee reliable results on brain uptake of [^{18}F]FDG. In accordance with the findings of Richter and colleagues, there is strong evidence that introducing systematic heterogenization might increase the external validity and reliability of results. However, this heterogenization needs to be introduced with care, as the impact of experimental parameters can be crucially different for various types of PET tracers. For example, ethanol content in the administered tracer solution did not affect [^{18}F]FDG brain uptake, whereas a strong tendency towards increased accumulation of the receptor tracer [^{18}F]fallypride in its target organ striatum was determined under the same condition. Therefore, it seems that administration of [^{18}F]fallypride solutions with varying ethanol content might crucially increase the inter-experimental variability of [^{18}F]fallypride data, which in turn might negatively impact on the reliability and comparability of data acquired on different test days. These findings suggest that tracer formulation of radiopharmaceuticals with pharmacokinetics that might be affected by formulation additives, such as ethanol, should be strictly standardized to avoid impaired reliability of experimental outcome. Preliminary tests to assess potential effects of such additives might help to decide about the usefulness of strictly standardized formulation

protocols. Such an assessment or estimation of experimental parameters with a potential impact on tracer distribution is suggested to be performed prior to each small animal PET study with the goal of group difference identification. Furthermore, it is highly recommended to perform group size calculation prior to *in vivo* PET experiments in order to assure that the optimal number of animals is used per test group, which guarantees the reliable identification of differences between two groups without wasting animal lives and resources. Group size calculations require an estimation of experimental variability prior to the calculation. Therefore, it is suggested to perform preliminary tests for the estimation of data variability. For long-term follow-up studies in which animals are investigated repeatedly, the preliminary assessment of the intra-animal variability is most relevant. As it has been shown that intra-animal variability in tissue uptake of both investigated surrogate tracers was not lower than the inter-animal variability, the number of animals per group might not be reduced compared to the traditional set-ups using separate groups of animals per investigated time point. In the future, it seems useful to determine the reliability and the external validity of small animal PET results under standardized and heterogenized conditions by involving different PET centers in one study. The first step for such a set-up would presumably be the development of standard test series to achieve direct comparability of data acquired using different small animal PET systems. Such standard series seem to be necessary even if two centers are using PET systems with very comparable performance according to the NEMA standards. Even though the NEMA guidelines provide relative comparability between the performances of various small animal PET scanners, they do not allow absolute comparison of semi-quantitative results.

Despite the remaining problems of absolute quantification, semi-quantitative results (SUVs) arising from small animal PET data acquisitions seem reliable and well suited for the characterization of new potential radiopharmaceuticals and for follow-up small animal PET studies.

Curriculum Vitae

- 2007-2010** Ph.D. studies, Institute of pharmaceutical sciences, ETHZ
“Refinement and standardization of small animal PET scanning experimentation and analysis”
Center for Radiopharmaceutical Sciences of ETHZ, PSI and USZ, Prof. Dr. P.A. Schubiger
- 2004-2007** Diploma studies, chemical biology, ETHZ
Diploma thesis: *“Developing a new method for the study of glycosyl phosphatidylinositide (GPI) biosynthesis in vitro”*
Semester work: *“Synthesis of mannans for the α -(1→6)-mannosyl-transferase of *M.tuberculosis* and the construction of lipoarabinomannan (LAM)”*
Laboratory for organic chemistry (LOC) ETHZ,
Prof. Dr. P.H. Seeberger
- 2002-2004** Undergraduate studies: biology, chemistry oriented; ETHZ
- 03-06/2002** Language studies in Cork, Ireland
Cambridge Certificate in Advanced English (CAE)
- 09/2001-03/2002** Internship in the laboratory for water quality control,
Stadtwerke St.Gallen

Presentations

Scientific Talks

- SGNM, Geneva 2009: *“Impact of anesthesia on FDG tissue uptake in small animal PET imaging”* M. Kehl, M. Honer, C. Keller, P.A. Schubiger, S.M. Ametamey
- “Doktorandentag”, Institute for pharmaceutical science, ETHZ 2009: *“Refinement and Standardization of small animal PET scanning experimentation and data analysis”* M. Kehl, M. Honer, C. Keller, P.A. Schubiger, S.M. Ametamey
- AGRR, Dresden 2009: *“Inter- & intra-animal variability in small animal PET: an attempt towards reproducible and standardized rodent PET imaging”* M. Kehl, M. Honer, C. Keller, P.A. Schubiger, S.M. Ametamey

Poster Presentations

- CIMST Symposium, ETHZ 2008: *“Refinement and standardization of small animal PET scanning experimentation and data analysis”* M. Kehl, M. Honer, S. Baumann, C. Keller, V. Uhlendorf, P.A. Schubiger, S.M. Ametamey
- SGNM, St.Gallen 2008: *“Refinement and standardization of small animal PET scanning experimentation and data analysis”* M. Kehl, M. Honer, S. Baumann, C. Keller, V. Uhlendorf, P.A. Schubiger, S.M. Ametamey
- ZNZ Symposium, ETHZ 2008: *“Impact of different anesthetic protocols on FDG organ uptake in small animal PET scanning experiments and ex vivo tissue sampling”* M. Kehl, M. Honer, C. Keller, P.A. Schubiger, S.M. Ametamey
- ZNZ Symposium, ETHZ 2010: *“PET tracer accumulation in the eye region of rodents”* M.I. Kehl, M. Honer, P.A. Schubiger, S.M. Ametamey
- EANM, Vienna 2010: *“Small Animal PET Imaging: Is Strict Standardization the Key to More Robust Data?”* M.I. Kehl, M. Honer, P.A. Schubiger, S.M. Ametamey